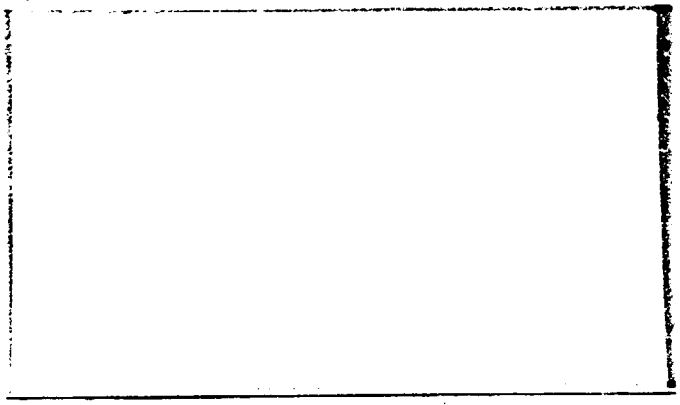

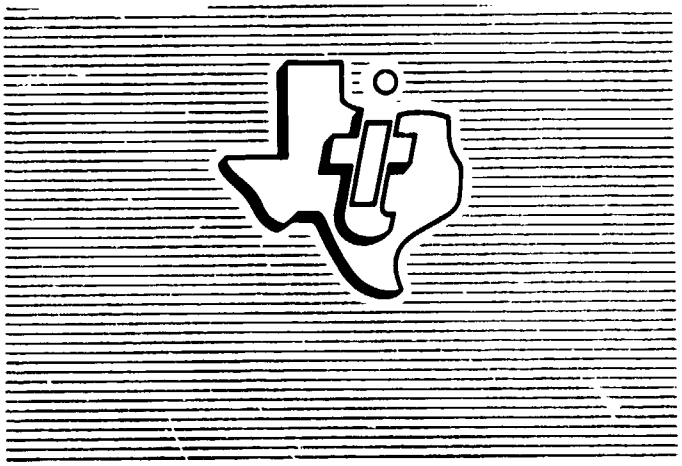

TEXAS INSTRUMENTS
INCORPORATED

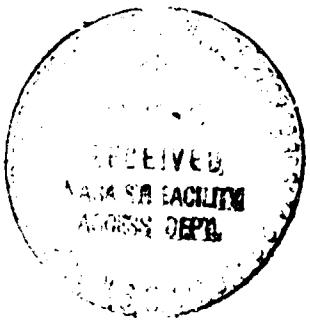

This Report Contains
TI INTERNAL DATA
Downgrade 13 March 1979

FINAL REPORT FOR SIMULTANEOUS, MULTIPLE, INDEPENDENTLY STEERED BEAM STUDY FOR AIRBORNE ELECTRONICALLY STEERABLE PHASED ARRAY (AESPA) PROGRAM

MAY 1978

Prepared for:

George C. Marshall Space Flight Center Alabama 35812

Contract No. NAS8-32627

Prepared by:

Equipment Group
Texas Instruments Incorporated
P.O. Box 226015
Dallas, Texas 75266

Report Number: EM 911-05-78

TEXAS INSTRUMENTS
INCORPORATED

TABLE OF CONTENTS

LIST OF ILLUSTRATIONS

LIST OF TABLES

TEXAS INSTRUMENTS INCORPORATED
EQUIPMENT GROUP
13500 North Central Expressway
P.O. Box 226015
Dallas, Texas 75266

May, 1978

FINAL REPORT FOR SIMULTANEOUS, MULTIPLE, INDEPENDENTLY STEERED BEAM STUDY FOR AIRBORNE ELECTRONICALLY STEERABLE PHASED ARRAY (AESPA) PROGRAM

SECTION I

INTRODUCTION

This report presents the results of a 9-month study program performed by Texas Instruments for NASA related to the Airborne Electronically Steerable Phased Array (AESPA) program (Contract No. NAS8-32627).

The purpose of the program was to develop design concepts for the formation of multiple, simultaneous, independently pointed beams for satellite communication links.

The effort in this report consists of tradeoffs of various approaches which were conceived as possible solutions to the problem. After the preferred approach was selected, a more detailed design was configured and has been presented as a candidate system that should be given further consideration for development leading to a preliminary design.

Criteria for the selection of the preferred concept were based on the following:

Power consumption

Complexity

Cost

Weight

Size

Reliability

Versatility (adaptability to other frequencies and more beams)

The concepts which will be discussed in this report are as follows:

Phased array

Butler matrix

Luneberg lens

Phased array with amplifiers

Butler matrix with amplifiers

Phase-amplitude steered multibeam array with amplifiers

Phase-amplitude steered multibeam reflective array with amplifiers

The AESPA program is a multiphased contract with various developmental tasks. The objectives of the AESPA program are:

To develop a highly reliable solid-state communication terminal system applicable to low- and high-altitude, reusable and/or permanently placed satellites

To provide high-gain electronic beamsteering without incurring a weight penalty

To develop a highly efficient modular antenna concept applicable to moderate apertures driven by fully duplexed, electronic transceiver modules

To extend these capabilities to Ku-band for high-data-rate payloads (with data rates up to 10^8 bits per second).

To better understand the series of tasks performed to date on this contract, a description of the phases of this program that either have been completed or are underway follows. The first phase of this program was to perform a preliminary design of a lightweight, high-gain, spaceborne communications array. This array includes simultaneous transmit and receive (2282 and 2101 MHz, respectively) and automatic acquisition and tracking of signal within a 60-degree cone from the array normal and provides for independent forming of the transmit and receive beams. Essential parameters in the system design were:

Light weight -- less than 50 pounds

High reliability – 30,000 hours mean time to failure

High efficiency – 60-percent antenna efficiency; 30-percent transmitter efficiency

High sensitivity -- 5-dB noise figure.

The first phase of the contract defined the mechanical design concept shown in Figure 1-1, as well as the system block diagram shown in Figure 1-2. This concept was verified through analytical and numerical studies in the first phase, and a final report was issued in April 1971 giving the results.

The results of the study indicated that development of three critical hardware areas was required to further verify the approach. As a result, a second phase (AESPA II) was started in April 1971 to design, construct, and test a lightweight, full-scale, 128-element antenna array; to develop and test an RF transmit manifold; and to develop and test a working electronics module containing duplexer, transmitter, receiver, and phase-shifter circuits. The 128-element antenna array is shown on the test mount in Figure 1-3. A quarter section of the RF distribution manifold, which is placed on the back of the 128-element antenna, is shown in Figure 1-4. One of the AESPA II prototype modules used in this array is shown in Figure 1-5.

During the development of the critical hardware for the S-band array, NASA's cognizant engineer, D. O. Lowrey, realized that additional development effort was required to allow this technology to be applied to the Ku-band link to be used for applications such as the Tracking and Data Relay Satellite System (TDRSS). As a result, the scope of the AESPA program was

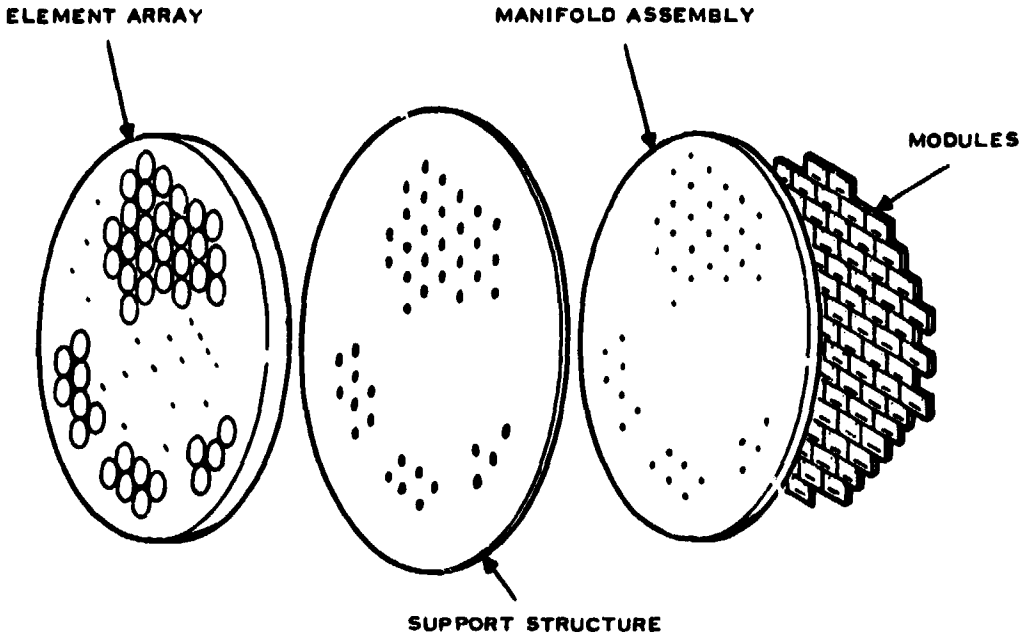

Figure 1-1. Array Assembly

increased to develop a series of diodes that could be used for power generation at those frequency bands. This program fostered the development of a gallium arsenide diode that can be used to generate power at frequencies from F- through J-band. The current and projected performance of these diodes is shown in Figure 1-6. The diode delivered to NASA under this contract is shown in Figure 1-7.

The next phase of the AESPA program (AESPA III) began in April 1972 and continued the critical component development undertaken in 1971. This phase includes the following line items:

Development of beamsteering logic

Construction of 12 additional modules incorporating phase trim and lower noise figure and capable of being hermetically sealed

Development of a dc and logic manifold

Study of a Ku-band electronically steerable antenna system.

The dc and logic manifold is shown during fabrication in Figure 1-8. The beamsteering logic is contained on two cards designed to be suitably packaged in the rear of the array. One card is shown mounted on the automatic checkout equipment in Figure 1-9. AESPA III was completed 3 April 1973 and included a final report for this contractual phase.

As a result of the accomplishments made on this contract, other NASA centers have become interested in both the modular antenna concept and the microwave integrated circuits developed for the AESPA module. Early in 1972, a presentation was made to the Pioneer Venus

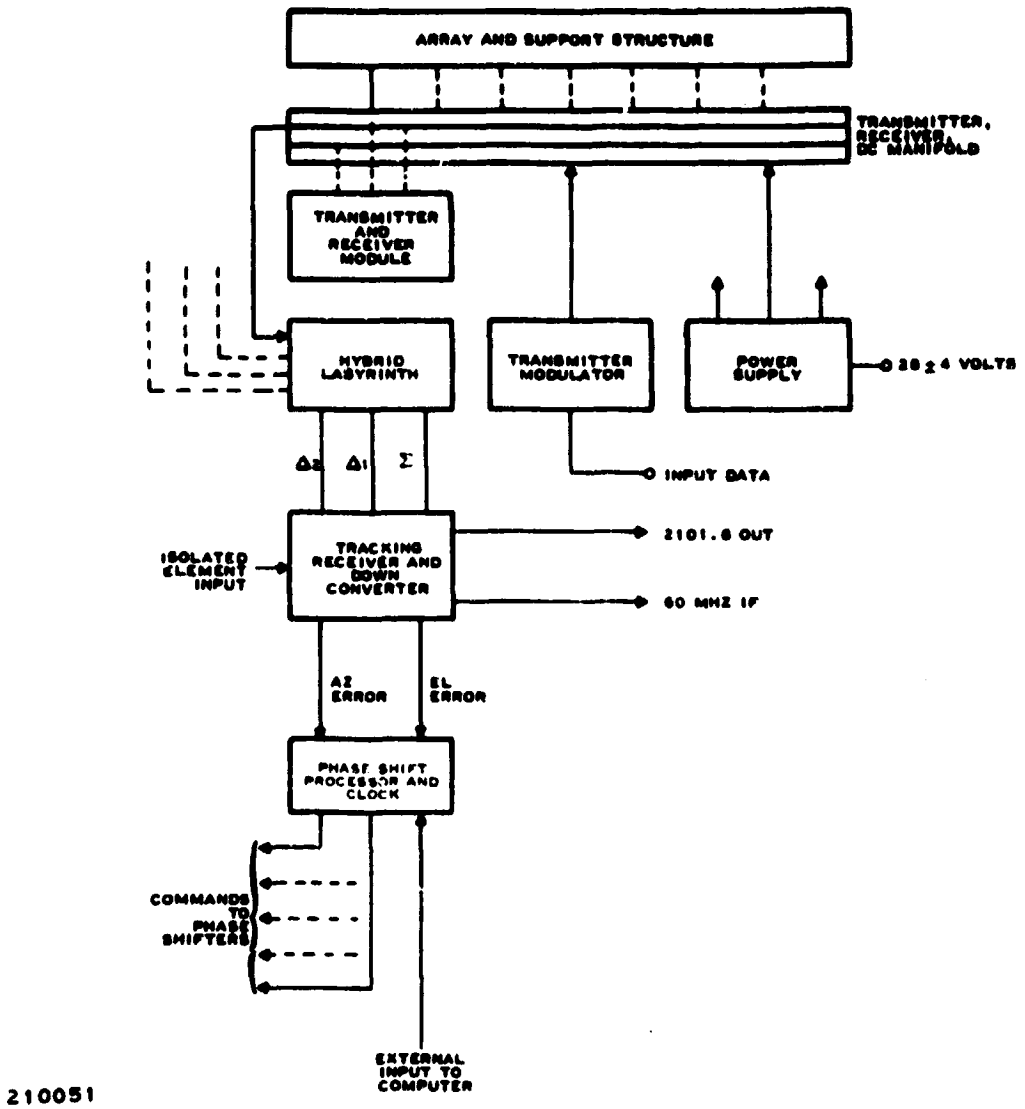

Figure 1-2. System Block Diagram

Orbiter study team on Texas Instruments efforts on Contract No. NAS8-25847. The study team thought that the active module concept held promise of an attractive design for an Electronically Despun Antenna (EDA) system for the Pioneer Venus Orbiter. As a result, in July 1972, Contract NAS2-1754 was formalized by NASA Ames Research Center (ARC) for Texas Instruments to study the application of the existing module developed on the AESPA contract (NAS8-25847) to power the three alternative antenna configurations shown in Figures 1-10 and 1-11. Figure 1-10 shows the concept of a separate high-gain electronically despun antenna placed on top of the spacecraft. Two similar configurations are shown in Figure 1-10: a 30-inch-diameter cylinder and a 48-inch-diameter cylinder. The 30-inch cylinder has 24 columns, each driven by an AESPA module. The 48-inch cylinder has 48 columns, each driven by an AESPA module.

Figure 1-3. 128-Active-Element Antenna

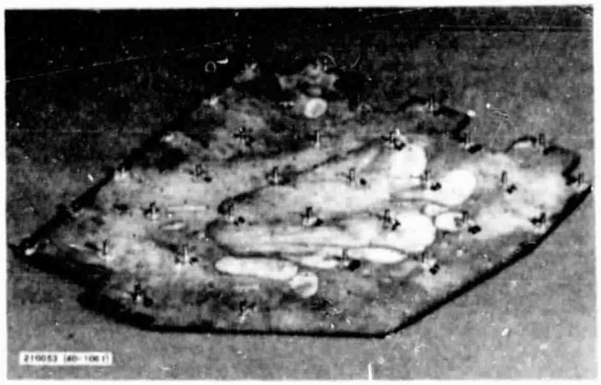

Figure 1-4. Manifold, Front View

Figure 1-11 shows an alternate configuration in which the antenna elements are integrated into the solar cell field on the outside diameter of the spacecraft, leaving the top of the spacecraft open for experiments. Since the Pioneer Venus Orbiter spacecraft is to be a low-cost spacecraft based upon existing developments, the use of the existing module developed on the AESPA program is a vital part of the electronically despun antenna design.

During the EDA study, it became apparent that the fully diplexed module developed on the AESPA program could be modified slightly to operate as a radar module because of the broadband nature of the receive circuits. It was recognized that there was a possibility that radar mapping of Venus could be performed by the electronically despun antenna simultaneously with the communications function. To determine the viability of this approach, ARC asked Texas Instruments to compare three approaches to the radar system for the Pioneer Venus Orbiter. These three approaches include:

- A fully integrated electronically despun antenna having a separate cylindrical aperture for communications, with radar capability over an approximate 45-degree sector of that cylinder
- A dedicated rectangular planar radar array using AESPA modules
- A mechanically steered reflector system.

During the study phase of AESPA III, the type of electronically steerable phased array to be used at J-band was investigated, and the use of the diodes in a power amplifier to derive the benefits of increased reliability/performance at J-band was considered.

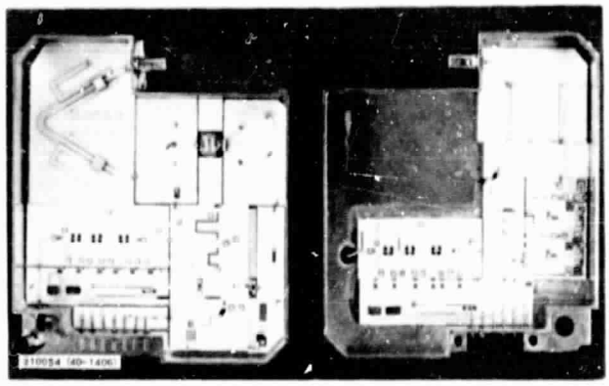

Figure 1-5. Prototype Module

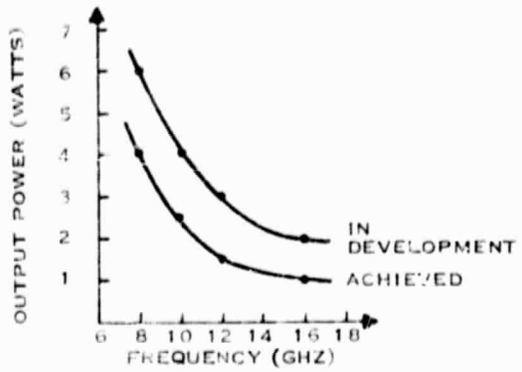

Figure 1-6. Diode Performance

210055

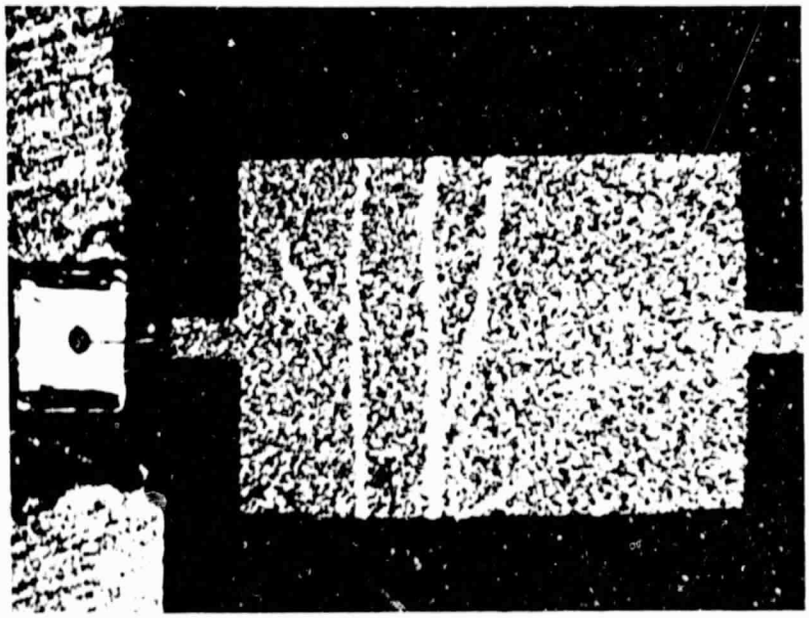

(B) DIODE PLACEMENT

Figure 1-7. Microstrip Circuit and Diode

During the fourth phase of the AESPA program, the following activities were accomplished:

Completion of the 48 AESPA module.

Completion of a 48-element transmit manifold

Completion of a 48-element receive manifold

Completion of a 48-element dc logic manifold

Completion of a study of a Ku-band electronically steered phased array.

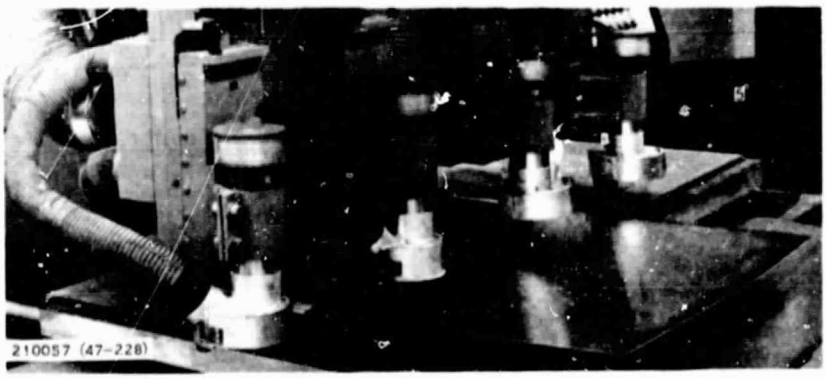

Figure 1-8. DC and Logic Manifold

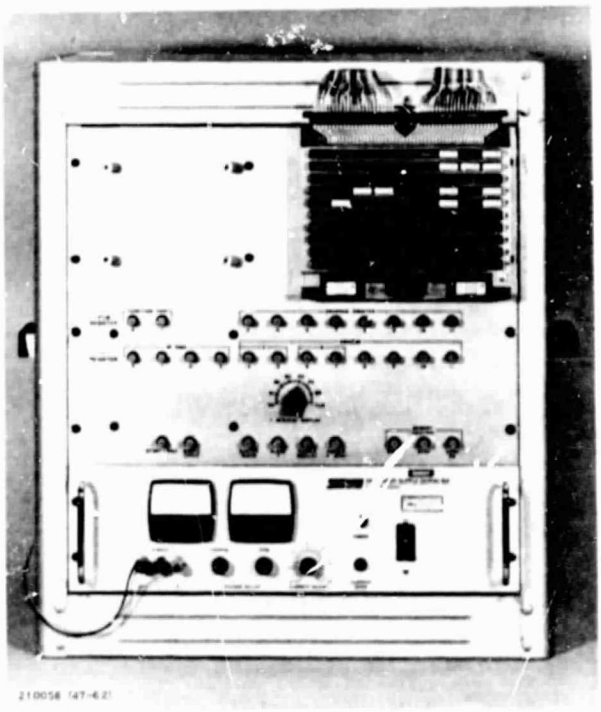

Figure 1-9. Beamsteering Logic

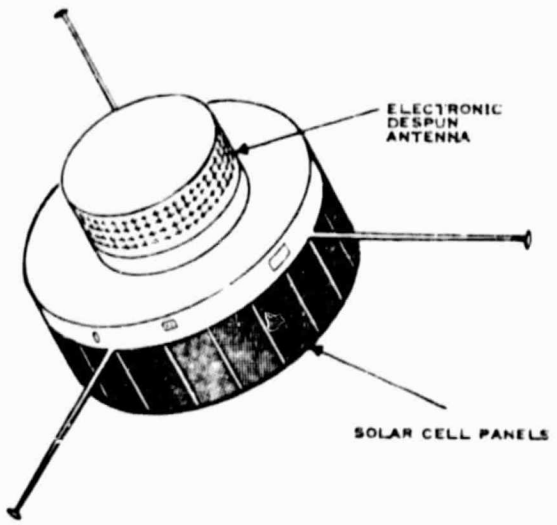

210059

Figure 1-10. Baseline System Concept

During this contract modification, Texas Instruments integrated and tested all previously completed components of the S-band array and began development of a J-band phase shifter. The results of the tests and progress on the phase-shifter development are covered in Final Report DM75-05-10 dated April 1975. Portions of the system completed at that point are shown crosshatched in the block diagram of Figure 1-12.

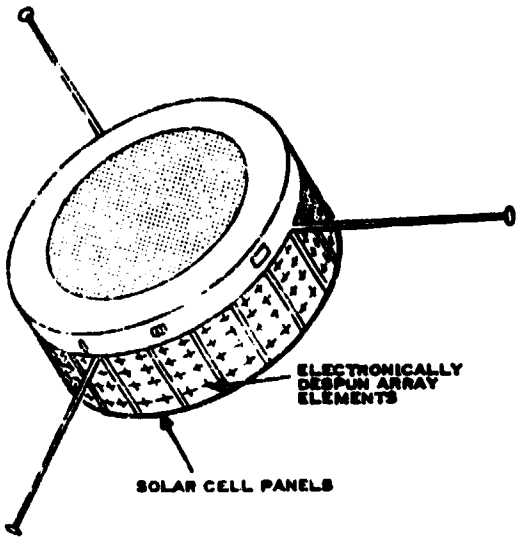

210060 **Figure 1-11. Spacecraft Integrated System**

Contract modification 9 was completed, during which Texas Instruments performed preliminary design studies, circuit design, and fabrication of the monopulse receiver section of the AESPA. A four-channel monopulse receiver was designed with a single difference channel breadboarded. This single channel contains most of the basic circuitry of the receiver and was used to demonstrate beamtracking capability. The results of this task, including test data showing performance of the circuitry, were presented in Final Report DM76-06-05.

A design study of the J-band aperture was completed under contract modification 10 along with an engineering model J-band phase shifter. Figure 1-13 is a photograph of the phase shifter developed during this part of the program. The array study covered three different configurations that could be developed to meet the AESPA performance levels, similar to those shown in Table 1-1 which were written for the S-band model. The three configurations studied were the flat-plate-fed array (transmissive array), the reflector-fed array (reflective array), and the constrained feed array. Of the three arrays, the transmissive and reflective designs were chosen as the best candidates on which to perform trade analyses to select the best configuration for further development.

The trade analysis was completed under Contract NAS8-32070 and the final results are covered in Report No. CD77-08-01 dated August 1977. The J-band array has the capability of simultaneous or separate transmission and reception of telecommunication signals. A trade analysis was performed on two antenna concepts, with a transmissive array selected as the preferred approach. Preliminary mechanical design was then performed on the transmissive array concept to complete the system definition. The phase shifter developed during the previous program was modified to meet the mechanical requirements in the transmissive array, and a microstrip dipole was designed and successfully integrated with this phase-shifter module. Figure 1-14 is a photograph of the J-band transmissive array phase-shifter module.

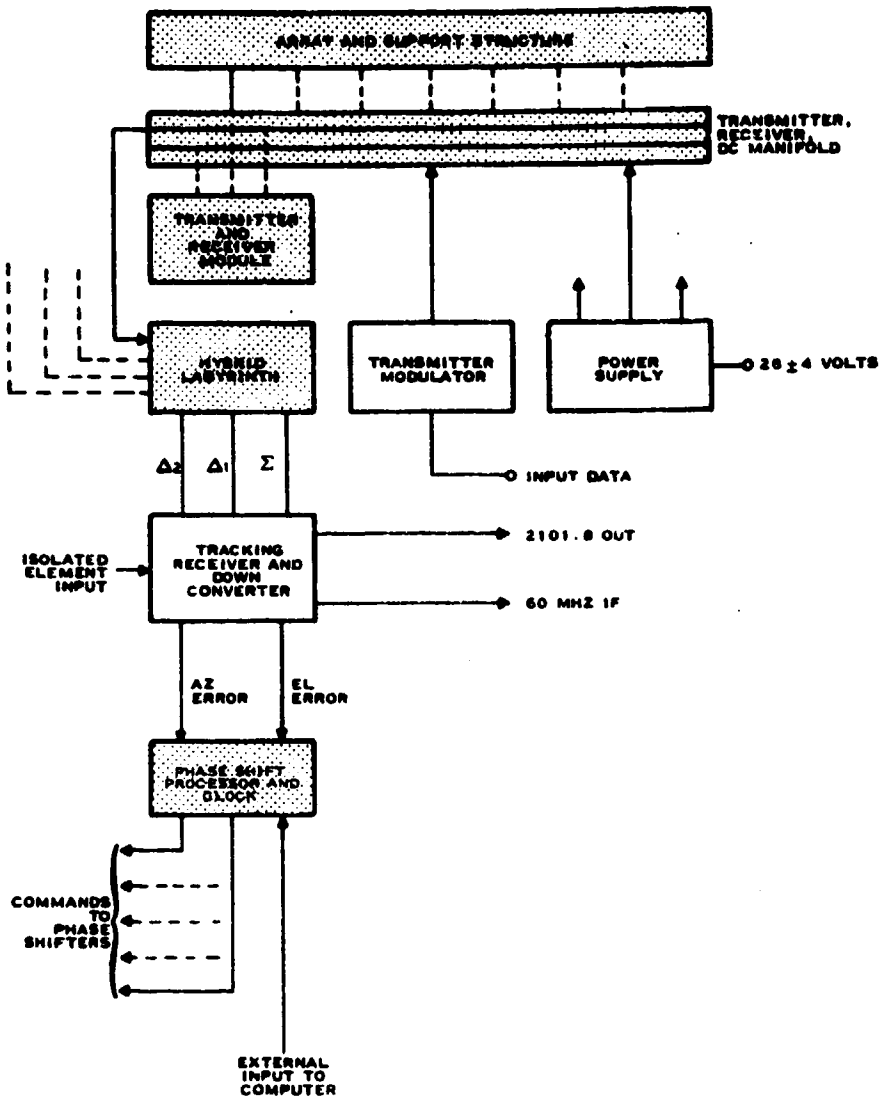

210061

Figure 1-12. System Block Diagram

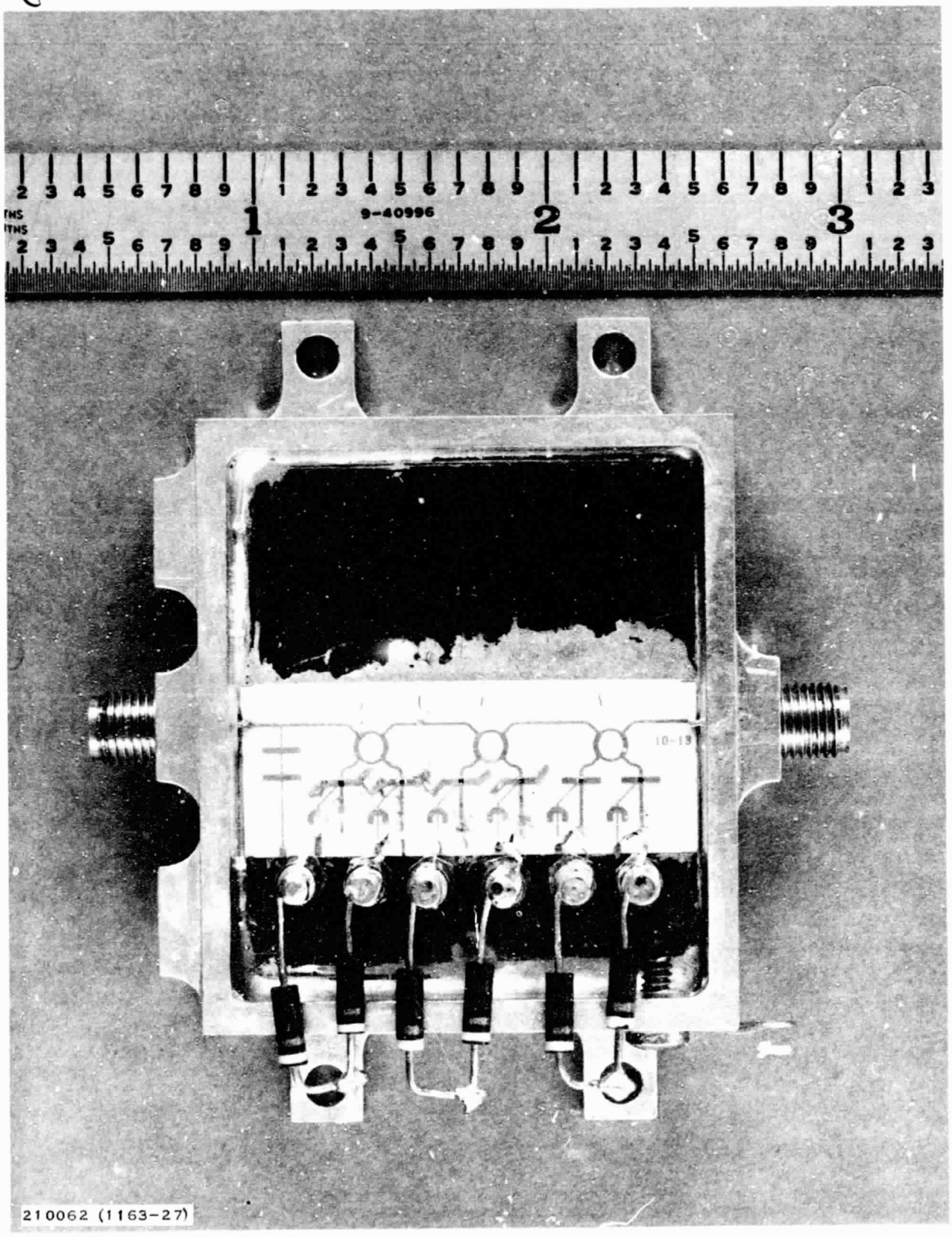

Figure 1-13. Microstrip Phase Shifter Prototype Design

TABLE 1-1. PERFORMANCE SPECIFICATIONS

Scan angle: 60 degrees from broadside (maximum)

Scan increments: <2.5 degrees

Transmit frequency: 2282.5 MHz

Transmit gain: 20 dB at maximum scan

Frequency stability: ±0.003 percent

Input impedance: 50 ±3 ohms

Power output: >25 watts at 2282.5 MHz

Polarization: right-hand circular (RHCP)

Antenna efficiency: 60 percent or greater at f_o

Beamwidth: 10 degrees (60 degrees from broadside)

Sidelobes: 12 dB below mainlobe at maximum scan

Grating lobe: suppressed below maximum scan

Bandwidth (transmitter): 30 MHz (minimum); 60 MHz (maximum)

VSWR: 1.5 maximum at any scan angle

Modulation (transmitter): FM

Modulation input impedance: 10,000 ohms ($0 < f < 200$ kHz)

Modulation distortion: down 35 and 45 dB for 2nd and 3rd harmonics, respectively, at 300 to 500 MHz with peak deviation of 50 kHz

Intermodulation distortion: down 40 dB

Deviation sensitivity: 200 ±10 kHz/rms volt

Deviation linearity: ±1 percent, $\Delta < 200$ kHz; ±2 percent, $\Delta < 500$ kHz

Carrier deviation: ±500 kHz

Frequency response (transmitter): ±1.5 dB with respect to 50 kHz, $0 < f < 500$ kHz

Random motion: 25 g for 5 minutes in each of three orthogonal planes

Acoustical noise: 50M 71810

RFI: MIL-I-6181D

Incidental FM: 8 kHz maximum

Incidental AM: 5 percent maximum

Protection: capable of open circuit, short circuit, or ±28 volts applied to modulation input

Receive frequency: 2101.8 MHz

Receiver bandwidth: minimum, 30 MHz; maximum, 60 MHz

Polarization: RHCP

Receive gain: 25 dB at maximum scan

Noise figure: 10 dB, maximum

Output frequencies: IF (60 MHz); baseband, 2101.8 MHz

Output impedance: 50 ±3 ohms

Aperture: 225 elements (maximum)

Operational modes: self-focusing, pointing-logic controlled, hybrid

Prime power source: 28 ±4 volts ($Z_o < 1$ ohm)

Conversion efficiency (dc to RF): > 10 percent

Grounding: 10^7 ohms isolation

Polarity reversal (28 V): no effect

Radius of curvature: ≅ 300 cm

Mounting: flush mount

TABLE 1-1. PERFORMANCE SPECIFICATIONS (Continued)

Covering: adequate for reentry heating

Size: thickness not to exceed 6 inches

Weight: not to exceed 25 pounds

Construction: MIC

Temperature cycling: -20° to $+85^{\circ}C$

Acceleration: 50 g in three orthogonal planes

Shock: half sinewave, 50 g for 11 ± 1 μs

Altitude: 9 months, $p = 10^{-7}$ mm Hg

Moisture resistance: relative humidity 95 percent with $15^{\circ}C < T < 70^{\circ}C$

Thermal vacuum: 50M 71810

Sinewave vibration: 10 to 2,000 Hz, 20 g peak in three orthogonal planes

Reliability: 50,000 hours MTBF; 30,000 hours continuous operation

Thermal shock: 20° to $85^{\circ}C$

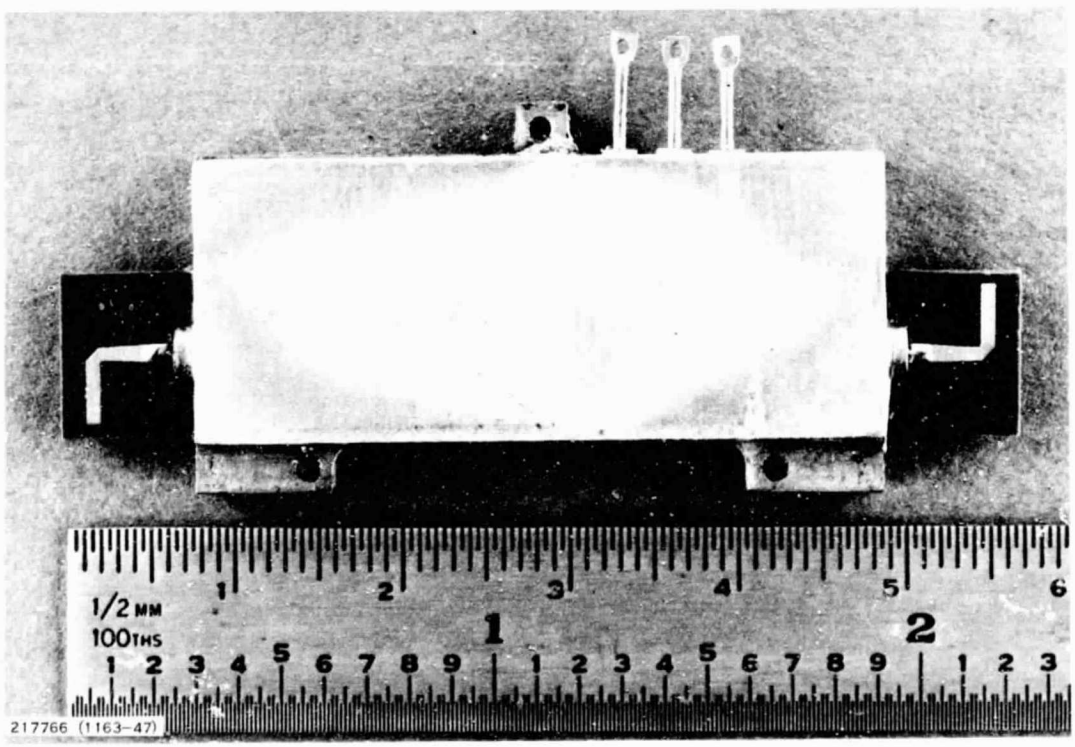

Figure 1-14. J-Band Transmissive Array Phase Shifter Module

SECTION II
STUDY CONSIDERATIONS

A. PROGRAM OBJECTIVES

Future space communication systems will require increased capabilities and more flexibility to attain projected performance. In order to expand the capability of the Airborne Electronically Steerable Phased Array, investigative studies have been performed to develop design concepts for the formation of simultaneous, independent, multiple steered beams from a single J-band aperture. This capability will permit independent continuous communication with several users such as orbiting satellites, docking vehicles, and earth stations.

B. ANTENNA REQUIREMENTS

The antenna system is to operate at a receive frequency of 13.4 to 14.0 GHz and a transmit frequency of 14.6 to 15.2 GHz. The transmit and receive antennas will be separate apertures and each shall be capable of scanning within a 120-degree cone about the normal to the plane of the array. Table 2-1 is a tabulation of the antenna requirements which were used as guidelines during the study program.

TABLE 2-1. ANTENNA REQUIREMENTS

Frequency (GHz)	
Receive	13.4 – 14.0
Transmit	14.6 – 15.2
Receive antenna bandwidth (percent)	4.4
Transmit antenna bandwidth (percent)	4.0
Number of simultaneous beams[1,2,3]	4 receive, 4 transmit
Independent variable gain control range (dB)	6 – 24
Scan volume	120-degree cone
Weight (kilograms)	27.2
Size, both apertures (meters)	1 × 1 × 0.15
Transmit-to-transmit isolation (dB)	30 minimum
Transmit-to-receive isolation (dB)	100 minimum
Polarization[4]	Right-hand circular
Gain (dB)	24
Sidelobe level (dB)	15
VSWR	1.5:1 maximum

[1] All 8 beams are to be at different frequencies
[2] Separate apertures for transmit and receive antennas
[3] No two transmit or receive beams are to be pointed in the same direction
[4] Linear polarized element with radome/polarizer

C. STUDY APPROACH

This study presents preliminary designs for arrays without amplifiers and arrays with amplifiers. The approaches without amplifiers are discussed in Section III and are as follows:

- Phased arrays
- Butler matrix fed arrays
- Luneberg lens.

The approaches with amplifiers are presented in Section IV and are as follows:

- Phased array with amplifiers
- Butler matrix fed array with amplifiers
- Phase-amplitude steered planar and reflective arrays with amplifiers.

In the section on arrays without amplifiers, each antenna system was configured and a comparison was completed so that a conclusion could be reached concerning these approaches. The comparison was based upon the mechanical packaging problems, size, weight, performance, component count, and complexity.

In the section on arrays with amplifiers, each antenna system was configured and a tradeoff was completed so that an approach could be selected as a recommended antenna system. The tradeoff was based upon expected electrical performance, growth potential, noise figure, system losses, component count, size, weight, and relative cost.

After the best approach was selected, a more detailed electrical and mechanical design was completed and is presented in Section V.

D. ARRAY ELEMENT SPACING AND GAIN

Common to all of the antenna configurations discussed in this report is the aperture design. It is well known that an equilateral triangular grid arrangement of elements minimizes the number of elements for a given aperture. This can be exceedingly important to the packaging of the antennas to meet AESPA size and weight constraints.

Figure 2-1 illustrates rectangular and triangular grid arrangements and the associated grating lobe diagrams. The spacing should be kept below:

$$d_R = \frac{\lambda (1 - 1/N)}{1 + \sin \theta_s} \quad \text{and} \quad d_T = \frac{d_R}{\sin 60^\circ}$$

where λ is the wavelength at the highest frequency of interest, N is the number of elements along one axis, and θ_s is the maximum scan angle.

The gain of the antenna is defined as follows:

$$G = 10 \log \frac{4\pi A}{\lambda^2}$$

where A is the aperture area.

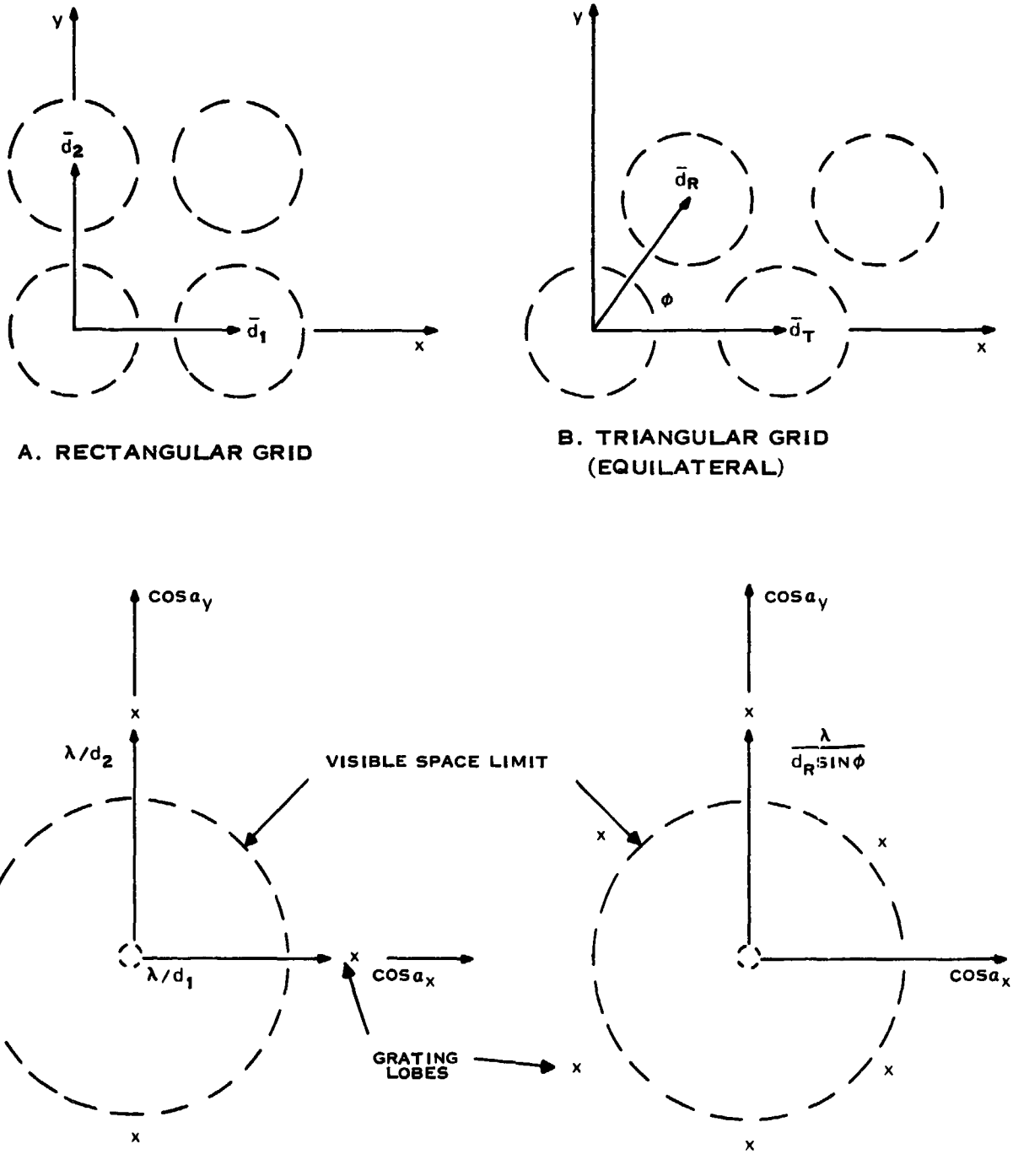

Figure 2-1. Rectangular and Triangular Grid Geometries and Grating Lobe Structures

217500

SECTION III
APPROACHES WITHOUT AMPLIFIERS

The purpose of this section is to address the candidate antenna systems, for the simultaneous, multiple beams, which do not use active elements. Three different antenna systems, namely a phased array, a Butler matrix fed array, and a Luneberg lens, were configured. Preliminary designs and tradeoffs, which included size, gain, loss budget, weight, and complexity, were completed on each configuration and then tradeoffs were made between the various designs that led to a conclusion on these approaches.

A. PHASED ARRAY

With the phased array antenna, four phase shifters are required for each element to achieve four independent beams with each having full aperture gain. Also to allow for gain and beamwidth control of each beam on/off switches are required with each phase shifter. A block diagram of the phased array antenna is presented in Figure 3-1. Four independent feed networks are necessary.

When the study began, it was understood that one of the requirements was to have variable gain and beamwidth control. In the phased array approach, switches were placed near the element with one switch per element per beam. The switches allowed for turning the element off, thus broadening the beam and reducing the gain. Since this added a considerable amount of complexity to the approach, the technical monitor for the program indicated that attenuators at the input to the four manifolds would suffice for the variable gain control. Because the phased array work had already been done, this approach has the switches in the system but the other concepts do not.

If the switches were removed, the loss budget would be reduced by 0.8 dB, thus reducing the array aperture size requirement by approximately 20 percent, the total number of switches, and the total weight. Even if the switches were removed, the conclusions reached in this section would not change.

The loss budget for the block diagram in Figure 3-1 is as follows:

Manifold	4.6
Switch	0.8
Phase shifter (3-bit)	4.0
4-way combiner	6.6
Interconnects	0.5
Phase quantization	0.4
Taper	0.2
Radome	0.3
Mismatch	0.2
Total Broadside Losses	17.6 dB

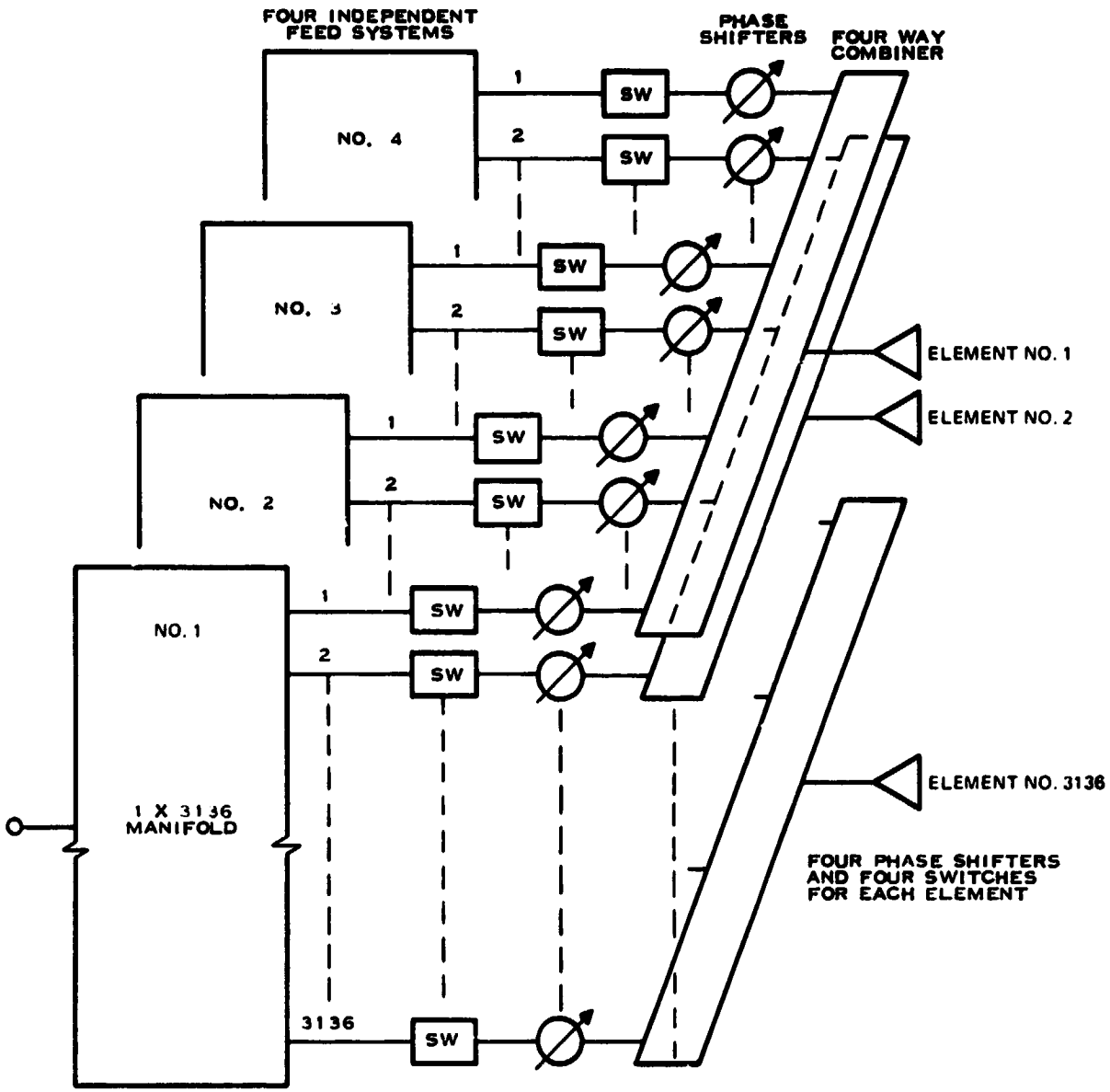

Figure 3-1. Block Diagram for Phased Array With Four Simultaneous, Independent Beams (56 × 56 Element Array)

217501

The manifold loss was estimated using a stripline design of nominal length of 42 cm and a loss factor of 0.11 dB/cm. The phase shifter loss was determined from the previous AESPA contract results. In addition to this there will be approximately 0.8 dB of loss due to mismatch caused by mutual coupling when the array is scanned off broadside. Since this will not affect the broadside gain, it is not used in determining the aperture size. The required broadside gain for the multiple beam antenna is 24 dB. With a feed loss of 17.6 dB, the required aperture gain is 41.6 dB. Table 3-1 shows the required area for the transmit and receive frequencies at the low end of the bands.

TABLE 3-1. PHASED ARRAY ANTENNA SIZE

Antenna	Frequency	Wavelength	Area
Transmit	14.6 GHz	2.055 cm (0.809 in.)	4857.5 cm^2 (752.8 in^2)
Receive	13.4 GHz	2.239 cm (0.881 in.)	5766.3 cm^2 (892.8 in^2)

The transmit antenna could be a 69.7 cm X 69.7 cm square aperture or a 78.6 cm diameter circular aperture while the receive antenna could be a 75.9 cm X 75.9 cm square aperture or a 85.7 cm diameter circular aperture. These aperture sizes would not fit in the 1 m X 1 m allowed space. To keep grating lobes from appearing in visible space, the maximum element spacing for the transmit and receive cases is determined by using a triangular grid spacing. The triangular grid spacing is used to maximize the element area for the required scan volume.

If we assume an element spacing of 0.6λ, and using a square aperture, the antenna would have 56 rows and 56 columns of elements for a total of 3136 elements. Therefore, 12,544 phase shifters and 12,544 switches are required.

From the above, the triangular element spacing and array size for the transmit and receive arrays at their highest frequency of operation, which is 15.2 GHz and 14.0 GHz respectively, is shown in Figure 3-2. The element area places a limitation on the allowable circuitry for the phased array approach.

Figure 3-3 is a conceptual drawing of the packaging for the phased array and Table 3-2 is a parameter list for the receive array.

TABLE 3-2. PHASED ARRAY (RECEIVE)

Number of elements	3,136
Azimuth element spacing (cm)	1.325
Elevation element spacing (cm)	1.148
Azimuth array dimension (cm)	74.86
Elevation array dimension (cm)	64.26
Array area (cm^2)	4,810.5
Array depth (cm)	130.0
Beamwidth, degrees (azimuth, elevation)	1.7, 1.9
Number of phase shifters	12,544
Number of switches	12,544
Number of four-way combiners	3,136
Gain control method	Switches
Aperture gain (dB)	41.6

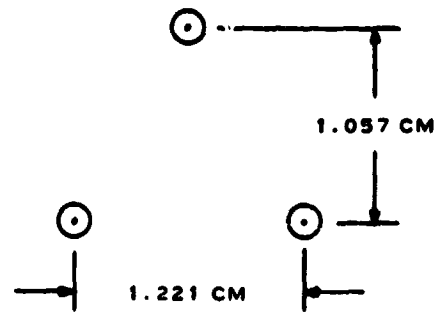

λ15.2 = 1.973 CM (0.777 IN.)

ARRAY SIZE

AZIMUTH PLANE = 68.959 CM (27.149 IN.)
ELEVATION PLANE = 59.192 CM (23.304 IN.)

A. TRANSMIT ARRAY

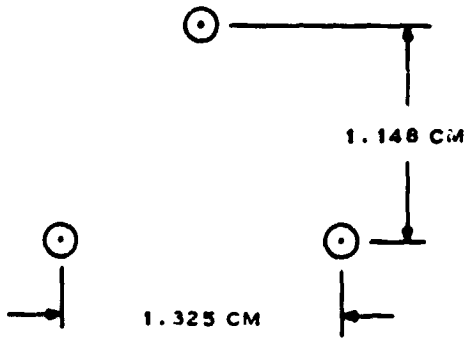

λ14.0 2.142 CM (0.844 IN.)

ARRAY SIZE

AZIMUTH PLANE 74.863 CM (29.475 IN.)
ELEVATION PLANE = 64.262 CM (25.300 IN.)

B. RECEIVE ARRAY

Figure 3-2. Phased Array Element Spacings and Array Dimensions for 56 x 56 Element Transmit and Receive Arrays

217502

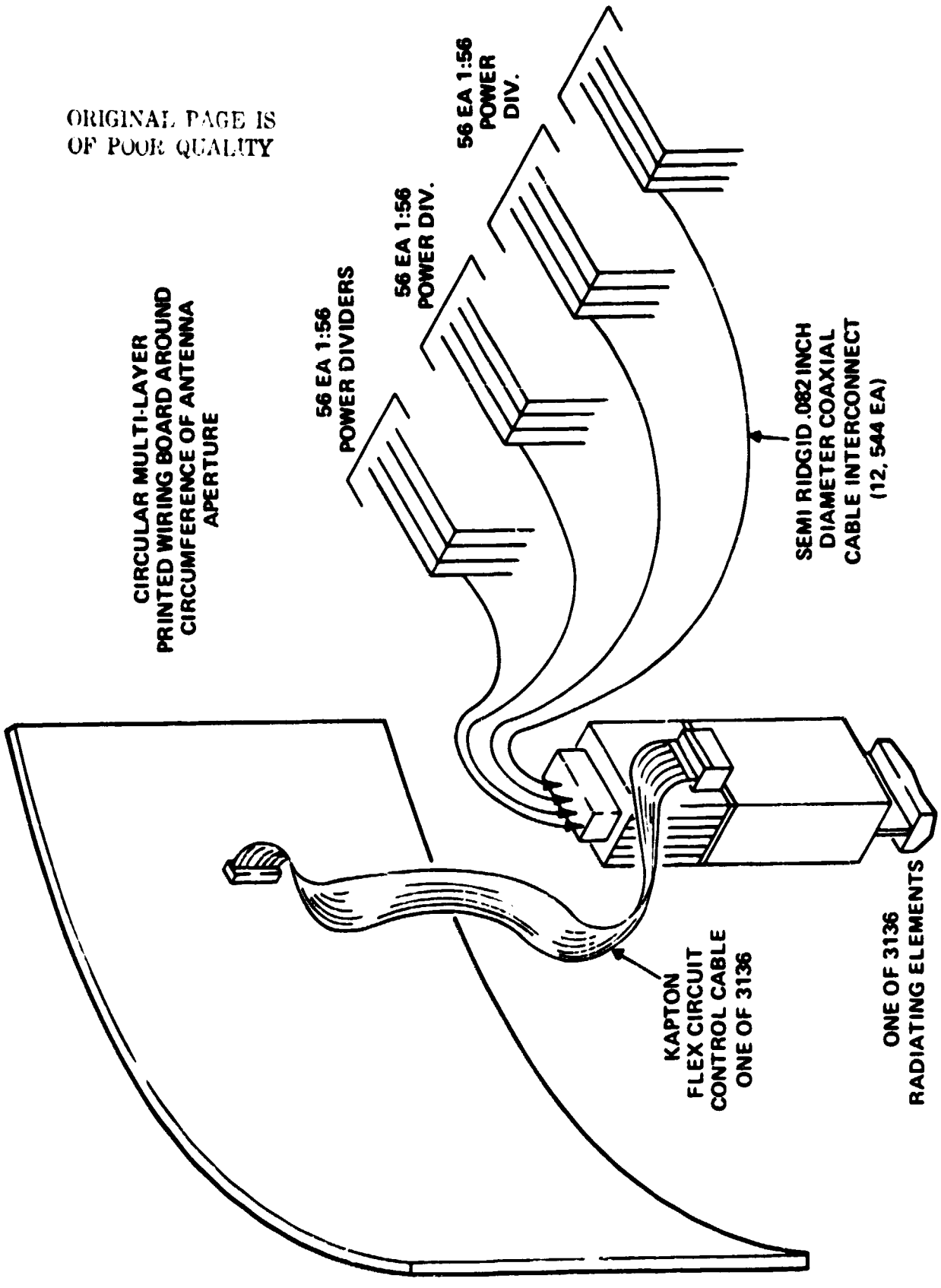

Figure 3-3. 4-Beam Phased Array

B. BUTLER MATRIX

One technique by which multiple beams can be formed involves feeding the array with a multiport beamforming network. One such network is the Butler matrix, which consists of hybrids and fixed phase shifters. When this network is used with an array of N elements, N beams are available at the N output ports of the matrix.

Each beam is characterized by a pointing direction, beamwidth and sidelobe level. Adjacent beams cross about 4 dB below the beam maxima.

The number of elements in a Butler matrix must be equal to a power of 2, namely 2, 4, 8, 16, 32, etc. A 16 X 16 matrix would have 256 elements which is an insufficient amount. The next square possibility would be a 32 X 32 matrix which would have 1024 elements.

The maximum rectangular element spacing for the transmit case using 1024 elements and based on the highest frequency of 15.2 GHz (λ = 1.973 cm) to keep grating lobes from being a problem would be 1.025 cm. The triangular element spacing and array size is shown in Figure 3-4.

The number of couplers required is $N/2 \log_2 N$, where N equals the number of elements in the array.

$$\text{Number of couplers for 1024 element array} = \frac{1024}{2} \quad \frac{\log_{10} 1024}{\log_{10} 2} = 5120$$

The loss of the Butler matrix can be qualitatively estimated by noting that the hybrid couplers are arranged so that there are $\log_2 N$ couplers in any path to an element in a linear array.

$$\text{Number of couplers in path} = \frac{\log_{10} 1024}{\log_{10} 2} = 10$$

At J-band frequencies, stripline couplers using Duroid typically achieve insertion losses of 0.5 dB. Thus, the insertion loss of a 32 X 32 matrix at J-band is at least 5 dB, plus connecting cable losses which would be approximately 2.0 dB.

The Butler matrix would require switching networks to connect the desired channel to the desired beam. A 4-channel antenna with 32 X 32 ports requires 4 single-pole, 1024-throw switches and 1024 single-pole, 4-throw switches. The loss of the switch is proportional to the number of stages. For a 1024-throw switch where M = 10 (the power of the Butler matrix) the number of stages required is

$$\text{No. of Stages} = M = 10$$

For a single-pole, 4-throw switch there would be 2 stages for a total of 12 stages. Using 0.8 dB loss per stage, the switch would have 9.6 dB loss.

Figure 3-5 is a schematic for a 32 element Butler matrix without any switches. This represents 1/64 of the matrix portion. The number in the fixed phase shifter symbol indicates the units of phase shift of $\pi/32$ radians.

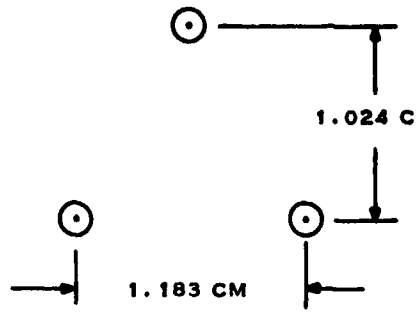

λ15.2 = 1.973 CM (0.777 IN.)

ARRAY SIZE

AZIMUTH PLANE = 38.448 CM (15.137 IN.)
ELEVATION PLANE = 32.000 CM (12.913 IN.)

A. TRANSMIT ARRAY

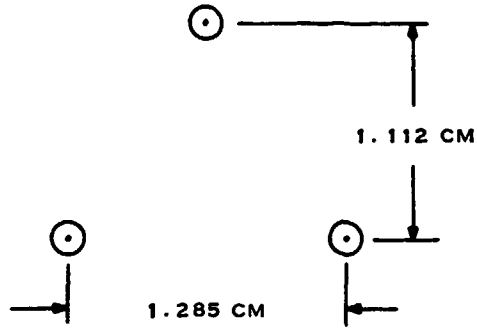

λ14.0 = 2.142 CM (0.844 IN.)

ARRAY SIZE

AZIMUTH PLANE = 41.763 CM (16.442 IN.)
ELEVATION PLANE = 35.584 CM (14.009 IN.)

B. RECEIVE ARRAY

217504

Figure 3-4. Butler Matrix Element Spacings and Array Dimensions for 32 X 32 Element Transmit and Receive Arrays

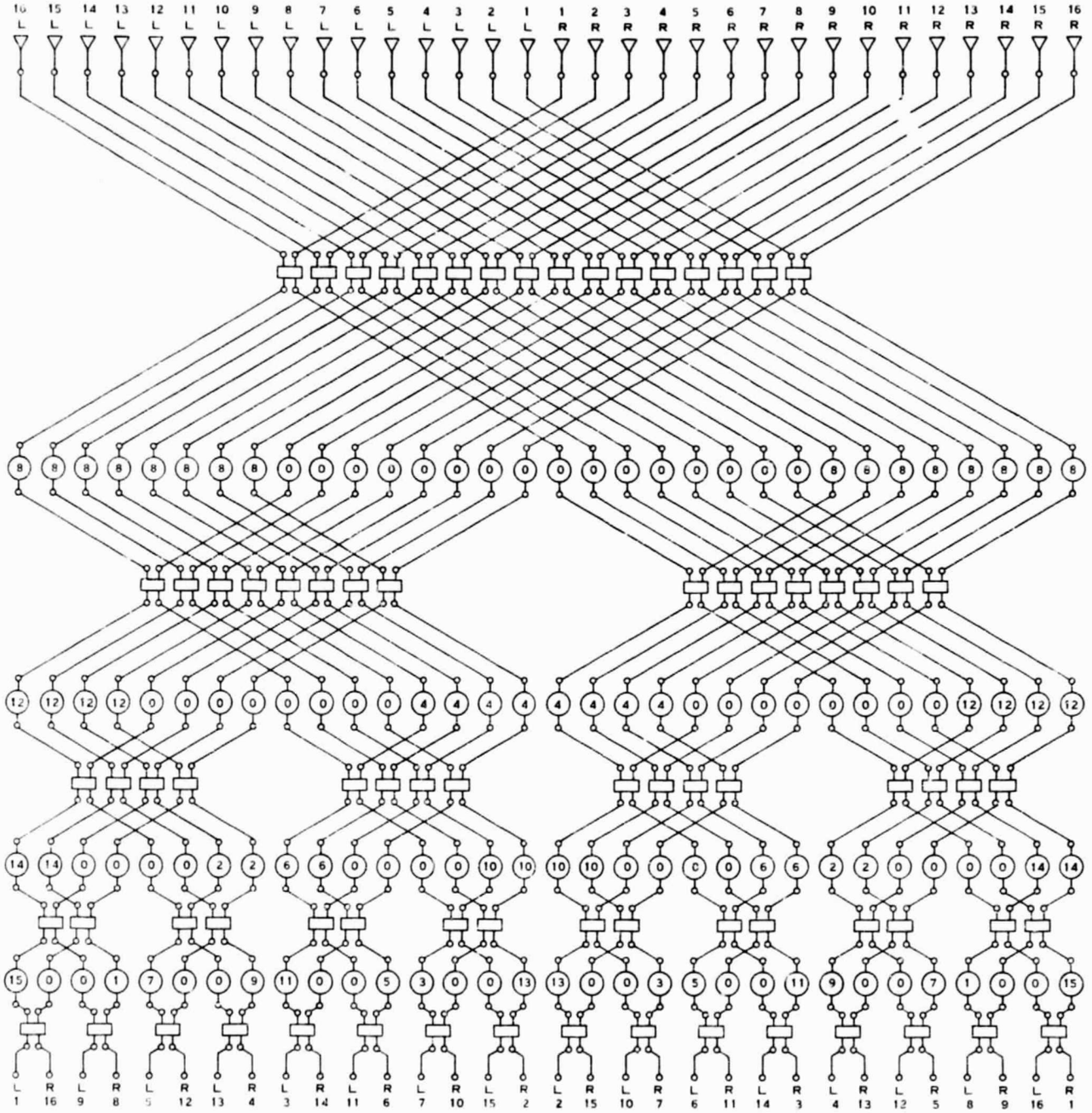

3 DB COUPLERS

FIXED PHASE SHIFTER

• NUMBER IN PHASE SHIFTER REPRESENTS UNITS OF PHASE SHIFT OF π 32 RADIANS

217505

Figure 3-5. 32-Element Butler Matrix

The loss of a stripline or microstrip switch at J-band would be approximately 2.0 dB and a waveguide switch would have about 0.8 dB. Therefore, from a loss standpoint it would be advantageous to use a waveguide switch if the weight and size would permit it to be used.

The loss breakdown for the 32 X 32 Butler matrix is as follows:

Radome	0.3
Butler matrix	5.0
Waveguide switches	9.6
Interconnects	2.0
Mismatch	0.2
Total Loss	17.1 dB

Based upon the size of the array, the aperture gain at 15.2 GHz would be 36.1 dB. The net gain would be 19.0 dB counting the fed losses. This is 5.0 dB less than the required gain of 24 dB.

Tables 3-3 and 3-4 are tradeoffs for the receive and transmit respectively when fed with a Butler matrix. The tradeoff is for four different sizes of matrices, namely a 16 X 32, 32 X 32, 32 X 64, and a 64 X 64. It is important to note that when the aperture is quadrupled in size from a 32 X 32 to a 64 X 64 to get six more dB of gain, the net gain increases by only 1.7 dB due to the increase in losses of the matrix, switches and interconnects. Figure 3-6 shows a layout of the switches and two layers of Butler matrices for azimuth and elevation scanning of an M X N array with four channels.

C. LUNEBERG LENS ANTENNA

This subsection briefly discusses the application of a Luneberg lens to the AESPA antenna problem. The study is to serve as an initial tradeoff and not as a design analysis. As a result, the major components of a single beam and four beam antenna configurations are identified. Parameter tradeoffs are given for the two configurations. From these tradeoffs baseline configurations are selected for the single- and four-beam antennas. Finally, some problem areas are identified.

The AESPA Luneberg lens antenna consists of six assemblies – a switch assembly, a beam steering unit, a feed assembly, an interconnect cable or waveguide assembly, a lens assembly, and a radome/polarizer assembly. Figures 3-7 and 3-8 respectively show single-beam and four-beam antenna configurations. Specific configurations for each assembly are possible. Variations in the design, such as having a circularly polarized feed instead of a polarizer, are possible. The polarizer has been selected here as a simple alternative to the CP feed. The four-beam antenna differs from the single-beam antenna by three additional single-pole, N-throw switches (N_b is the number of beams; see Appendix A for definition of terms), N_b single-pole, 4-throw switches, a different beam steering unit, and additional interconnect cables. Each of the four beams is independently positioned except that no two beams may be placed in the same direction. Computer control may be used to provide the logic for the beam positioning and the inputs to the beam steering unit.

Figure 3-9 shows the lens design for a four-beam antenna. The configuration is the same for the single-beam antenna except for a smaller radius and fewer feed elements. The feed elements are regularly distributed over a 60-degree spherical sector to provide the coverage. As a result, for

TABLE 3-3. BUTLER MATRIX TRADEOFF FOR RECEIVE ARRAY

F_{low} = 13.4 GHz λ_{low} = 2.239 cm

F_{high} = 14.0 GHz λ_{high} = 2.142 cm

	Butler Matrix Array			
	16 x 32	32 x 32	32 x 64	64 x 64
Number of elements	512	1,024	2,048	4,096
Azimuth element spacing	1.243	1.285	1.285	1.305
Elevation element spacing	1.112	1.112	1.130	1.130
Azimuth array dimension	20.510	41.763	41.763	84.173
Elevation array dimension	35.584	35.584	72.320	72.320
Number of 3-dB couplers	2,304	5,120	11,264	24,576
Number of couplers in path	9	10	11	12
Number of switches and type	4 SP512T 512 SP4T	4 SP1024T 1024 SP4T	4 SP2048T 2048 SP4T	4 SP4096T 4096 SP4T
Number of switches in path	11	12	13	14
Beamwidth, degrees (azimuth, elevation)	5.7,3.3	2.8,3.3	2.8,1.7	1.4,1.7
Aperture gain (dB)	33.0	36.1	39.2	42.2
Loss budget (dB)				
Radome	0.3	0.3	0.3	0.3
Butler matrix	4.5	5.0	5.5	6.0
Waveguide switches	8.8	9.6	10.4	11.2
Interconnects	1.2	2.0	2.8	3.6
Mismatch	0.1	0.2	0.3	0.4
Total loss	14.9	17.1	19.3	21.5
Net gain (dB)	18.1	19.0	19.9	20.7

1. Triangular element spacing is determined by using the highest frequency of operation.
2. Dimensions are in centimeters.
3. Aperture gain is calculated using the lowest frequency of operation (minimum gain).

TABLE 3-4. BUTLER MATRIX TRADEOFF FOR TRANSMIT ARRAY

F_{low} = 14.6 GHz λ_{low} = 2.055 cm

F_{high} = 15.2 GHz λ_{high} = 1.973 cm

	Butler Matrix Array			
	16 x 32	32 x 32	32 x 64	64 x 64
Number of elements	512	1,024	2,048	4,096
Azimuth element spacing	1.145	1.183	1.183	1.202
Elevation element spacing	1.024	1.024	1.041	1.041
Azimuth array dimension	18.893	38.448	38.448	77.529
Elevation array dimension	32.768	32.768	66.624	66.624
Number of 3-dB couplers	2,304	5,120	11,264	24,576
Number of couplers in path	9	10	11	12
Number of switches and type	4 SP512T 512 SP4T	4 SP1024T 1024 SP4T	4 SP2048T 2048 SP4T	4 SP4096T 4096 SP4T
Number of switches in path	11	12	13	14
Beamwidth, degrees (azimuth, elevation)	5.7,3.3	2.8,3.3	2.8,1.7	1.4,1.7
Aperture gain (dB)	33.0	36.1	39.2	42.2
Loss budget (dB)				
Radome	0.3	0.3	0.3	0.3
Butler matrix	4.5	5.0	5.5	6.0
Waveguide switches	8.8	9.6	10.4	11.2
Interconnects	1.2	2.0	2.8	3.6
Mismatch	0.1	0.2	0.3	0.4
Total loss	14.9	17.1	19.3	21.5
Net gain (dB)	18.1	19.0	19.9	20.7

1. Triangular element spacing is determined by using the highest frequency of operation.
2. Dimensions are in centimeters.
3. Aperture gain is calculated using the lowest frequency of operation (minimum gain).

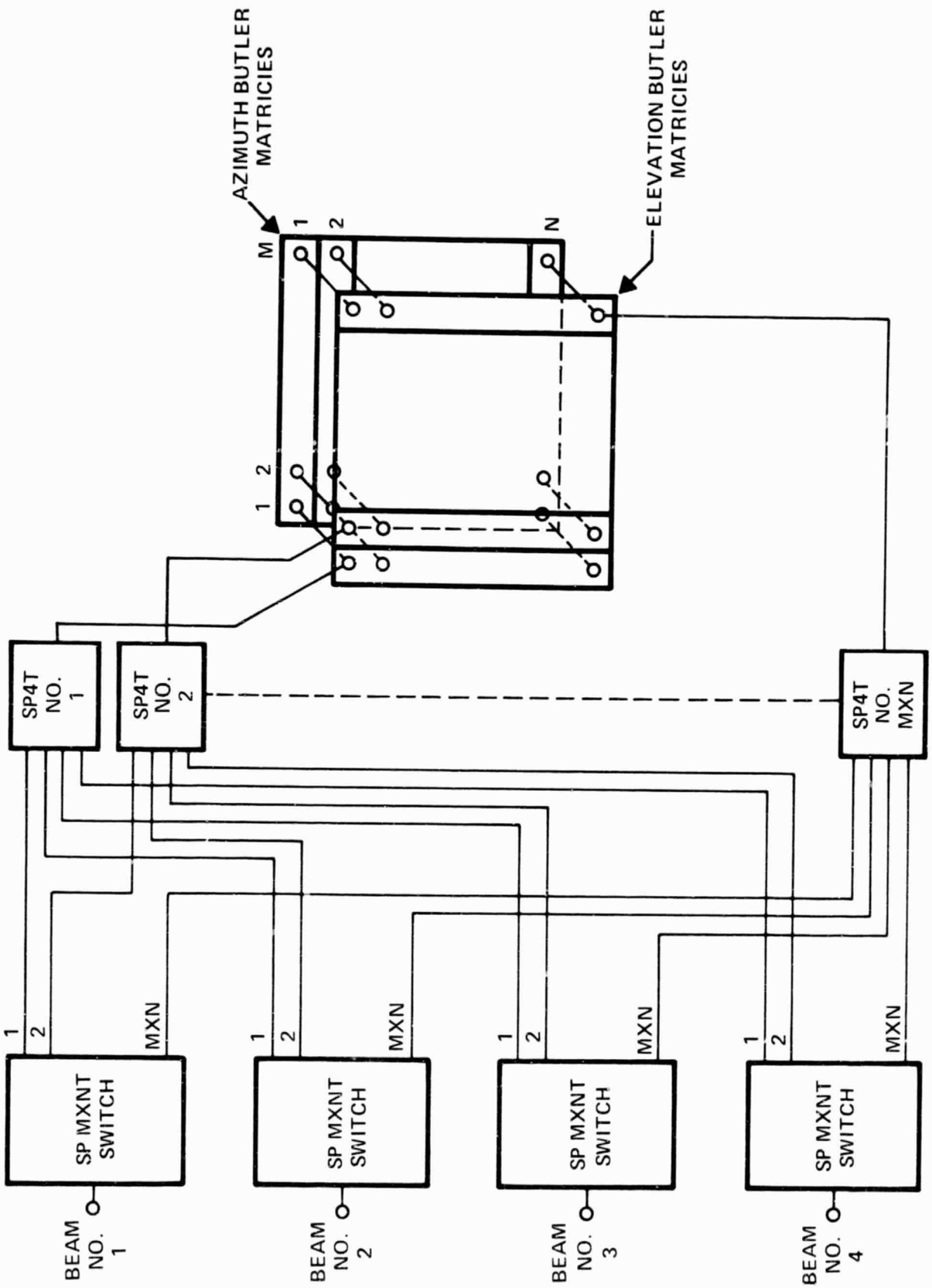

Figure 3-6. Switch and Matrix Layout for a MXN Butler Matrix Fed Array

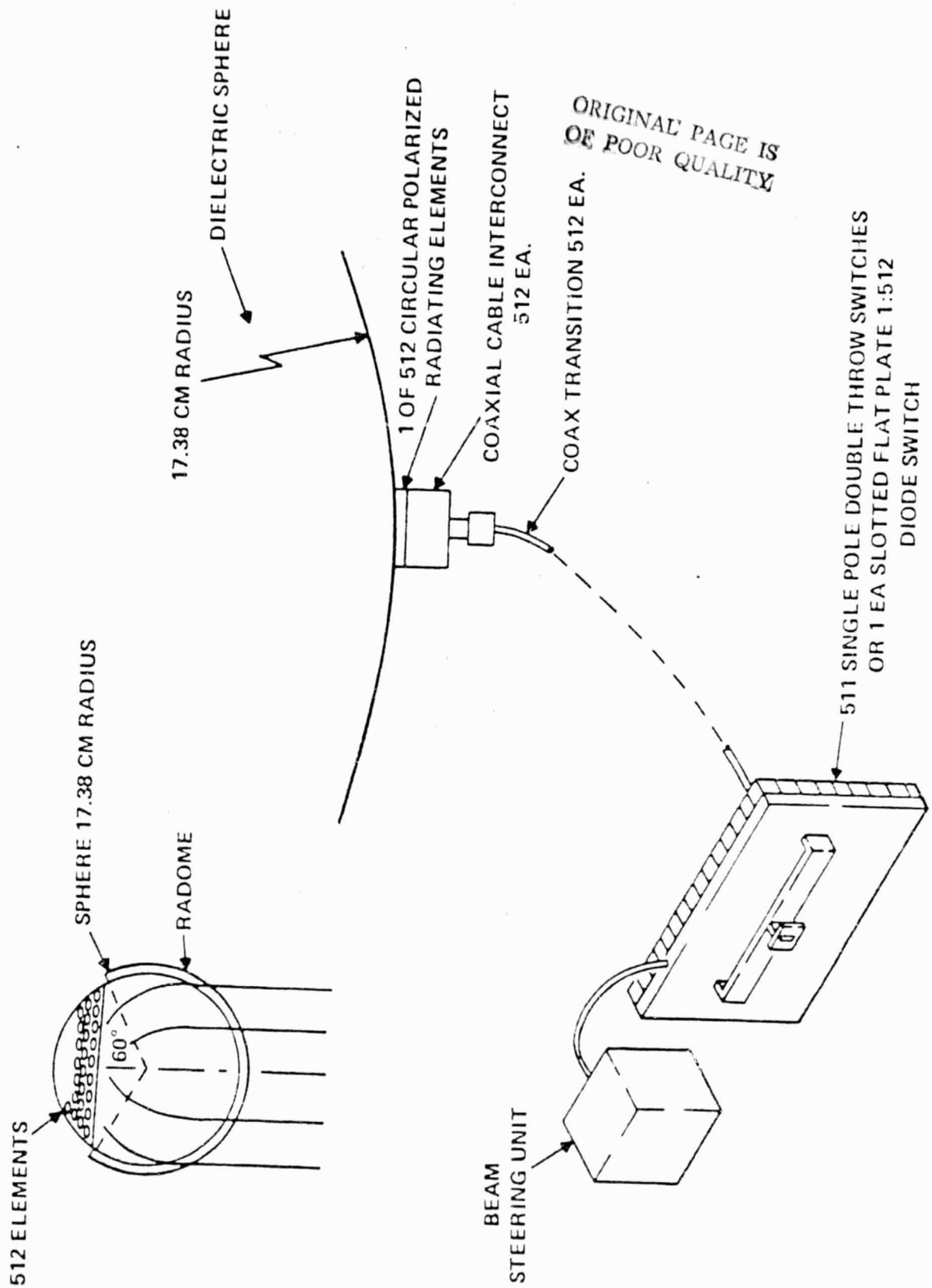

Figure 3-7. Single-Beam Luneberg Lens

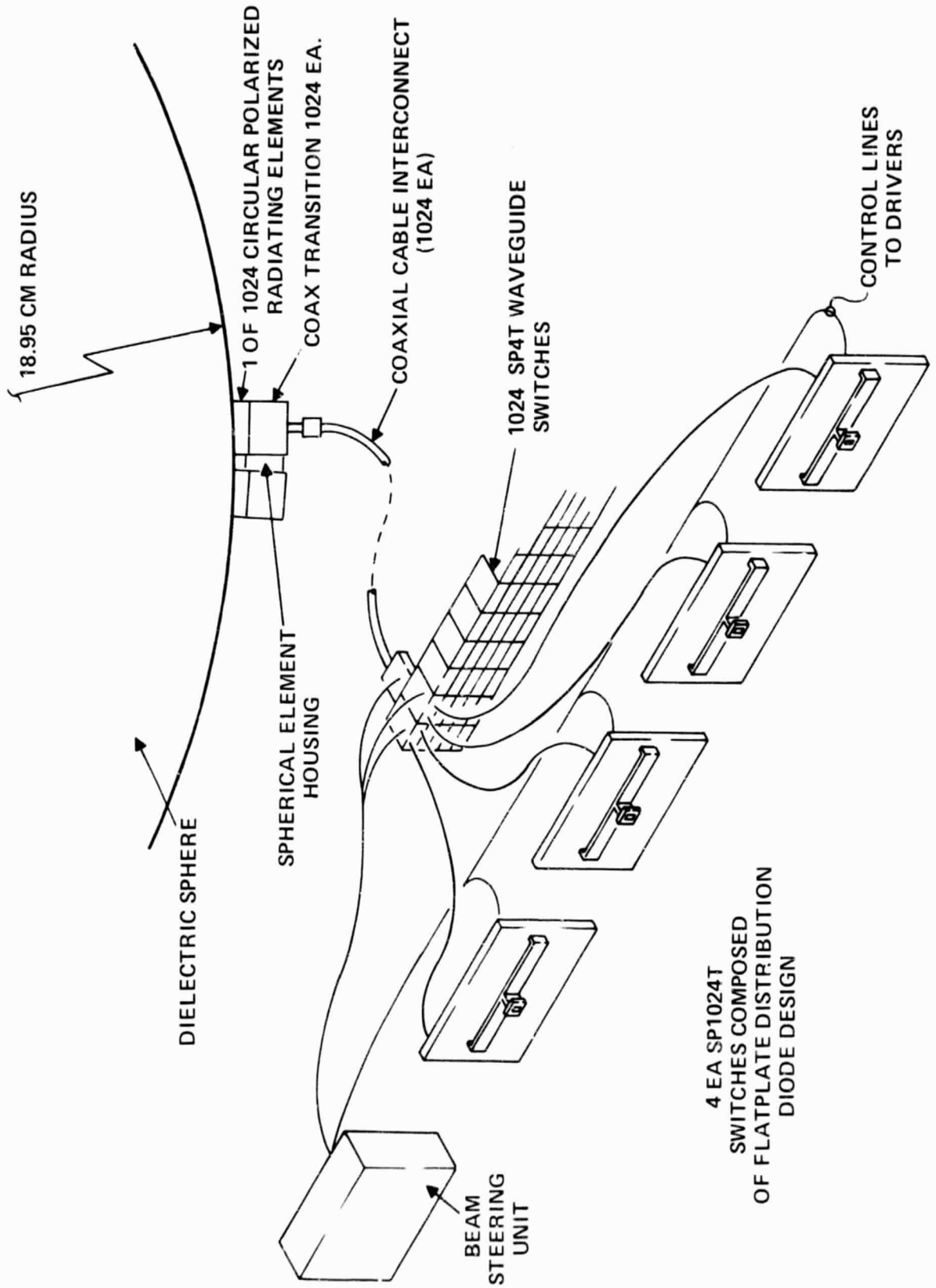

Figure 3-8. 4-Beam Luneberg Lens

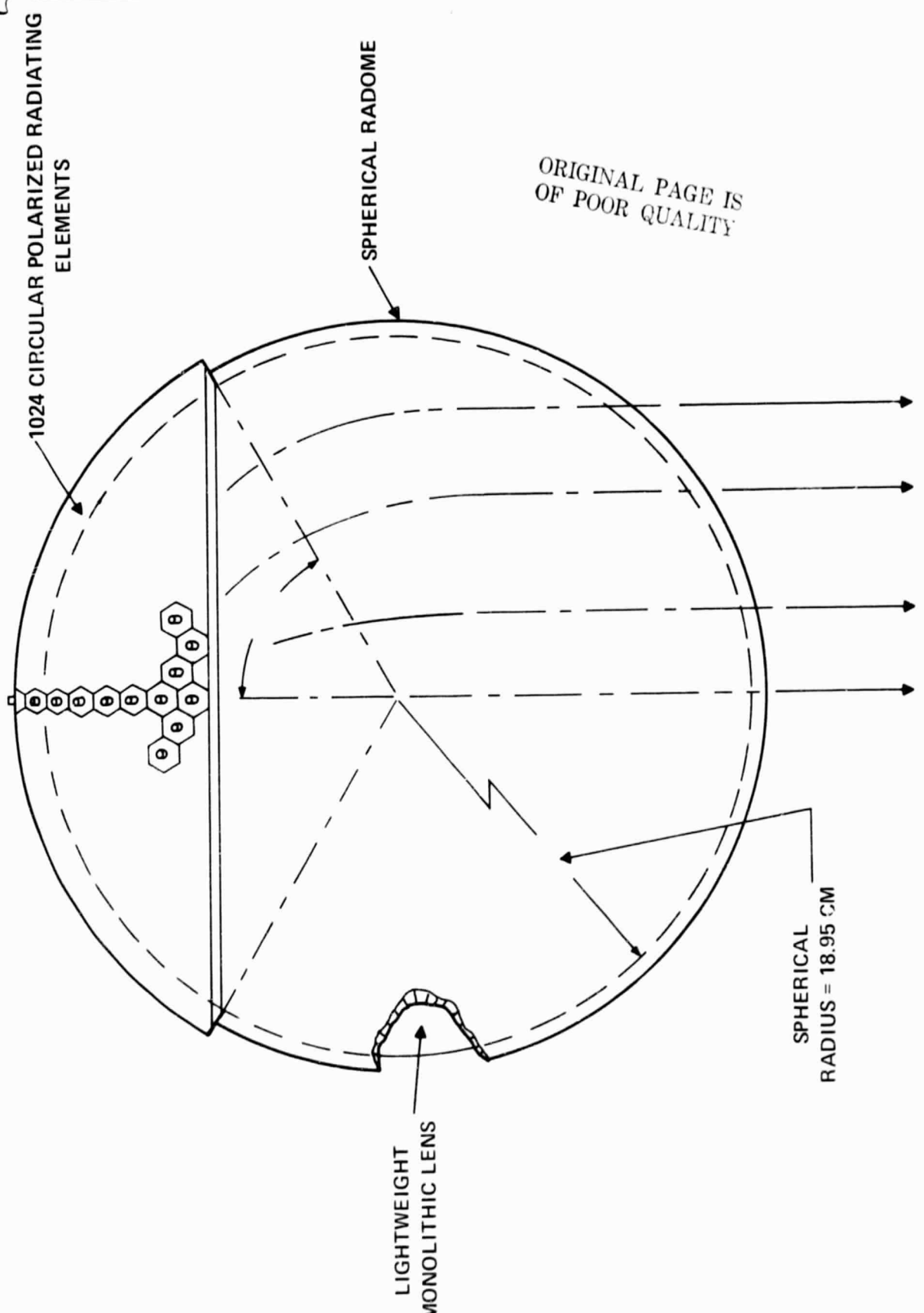

Figure 3-2. 4-Beam Luneberg Lens Antenna

scans between 30 to 60 degrees, there will be some aperture blockage due to the feed array. Hence, over this region the beam fidelity will degrade.

Appendix B describes a parameter tradeoff for the single and four beam configurations. The tradeoffs give antenna parameters as a function of lens diameter with an antenna gain of 24 dB. Loss budgets for the antenna configurations are given in the following table.

	Single Beam	Four Beam
Radome/polarizer	0.3	0.3
Lens	0.7	0.7
Element mismatch	0.2	0.2
Interconnects (0.6 dB/ft)	1.5	1.5
SP4T	–	1.6
L_0	2.7 (dB)	4.3 (dB)
SPNT	$0.8 \log_2 N_b$	$0.8 \log_2 N_b$

Tables 3-5 and 3-6 which summarize the tradeoff results show a variation in the beam crossover levels and the number of beams. Baseline configurations for the two cases were selected as explained in Appendix B and the resulting antenna parameters are shown in Table 3-7. The baseline configurations require switch matrices at least as complicated as a SP(512)T switch. Using present technologies, such a switch matrix does not appear reasonable because of weight, size, and packaging problems.

An approach to alleviate the switch problem is to place RF amplifiers, with significant gain and low noise figure, behind each feed element. This approach will simultaneously decrease the size of the lens and the number of beams so that the switch matrix becomes a more reasonable size.

TABLE 3-5. WEIGHT ESTIMATE 4-BEAM LUNEBERG LENS

	Weight (kg)
Spherical lens	2.5
Radiating elements	2.3
Waveguide coaxial adapters	2.6
Coaxial cable interconnect	20.5
1024 single-pole, four-throw switches (0.54 x 1024)	557.0
Single-pole, double-throw switches used in SP1024 throw switching matrix (0.18 x 1023 x 4)	742.0
Total system weight	1327.0

TABLE 3-6. LUNEBERG LENS ANTENNA PARAMETERS

Number of elements	1024
Element spacing (λ)	0.6
Diameter of sphere (cm)	37.9
Depth (cm)	137.0
Weight (kg)	1327.0
Beamwidth (degrees)	3.1
Number of attenuators	4
Gain control method	Attenuators
Aperture gain (dB)	36.3
Losses (dB)	12.3
Net Gain (dB)	24.0

TABLE 3-7. PHASED ARRAY ANTENNA SIZE (SINGLE-BEAM)

Antenna	Frequency	Wavelength	Area
Transmit	14.6 GHz	2.055 cm (0.809 in.)	718.4 cm^2 (111.3 in^2)
Receive	13.4 GHz	2.239 cm (0.881 in.)	852.9 cm^2 (132.1 in^2)

Finally, fabrication of a high quality lens is not without some risk. There are several techniques to fabricate a lens, including the method of concentric shells and the method of artificial dielectrics. Both types of lenses may be purchased from Emerson & Cuming. However, the best method may be to "grow" the lens by simultaneously spinning a dielectric core and spraying on a dielectric whose permitivity is appropriately changed with time to yield the lens [$\epsilon(r) = 2-(2r/D)^2$], which has a dielectric constant of 2.0 at the center and 1.0 at the edge of the sphere.

A weight estimate for the four-beam Luneberg lens is 1327 kilograms, broken down in Table 3-5, and a parameter list is shown in Table 3-6.

D. PHASED ARRAY (SINGLE BEAM PER APERTURE)

After investigating the possibility of using a phased array with four phase shifters per element, a Butler matrix fed array and lens antennas to obtain four beams per aperture, it appeared that it was not feasible to fit any of these approaches into the allowed specified volume of space. Some analysis was done to see if a phased array with one beam per aperture would fulfill the requirements. This meant that for both the transmit and receive antennas there would be eight separate antennas with their associated hardware.

The loss budget for the single beam aperture is as follows:

Single Beam Per Aperture	
Manifold (stripline)	3.7
Phase shifter (3-bit)	4.0
Interconnects	0.5
Phase quantization	0.4
Taper	0.2
Radome/polarizer	0.3
Mismatch	0.2
Total Loss	9.3 dB

The required broadside gain is 24 dB with a feed loss of 9.3 dB, the required aperture gain is 33.3 dB.

Table 3-7 shows the required area for the transmit and receive frequencies at the low end of the bands.

The transmit antenna could be a 26.8 cm X 26.8 cm (10.5 in. X 10.5 in.) square aperture or a 30.2 cm (11.9 in.) diameter circular aperture, while the receive antenna could be a 29.2 cm X 29.2 cm (11.5 in. X 11.5 in.) square aperture or a 32.9 cm (12.9 in.) diameter circular aperture. A block diagram of the phased array and a diagram of the element spacings are shown in Figures 3-10 and 3-11 respectively.

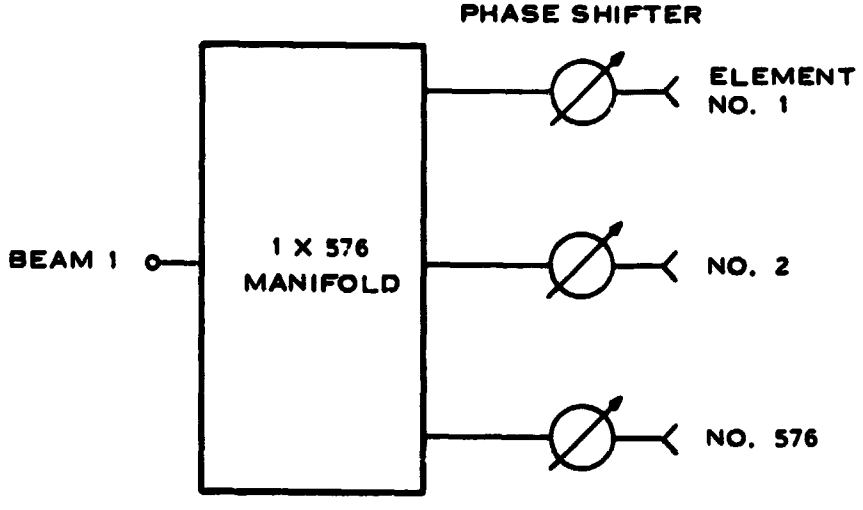

Figure 3-10. Block Diagram for Phased Array With One Beam Per Aperture (24 x 24 Element Array)

217510

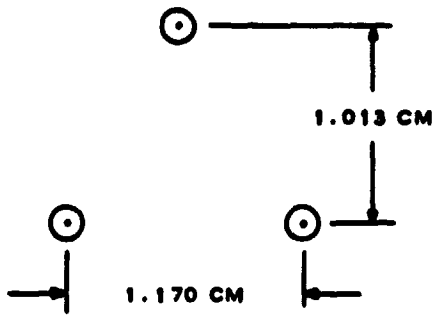

λ15.2 = 1.973 CM (0.777 IN.)

ARRAY SIZE

AZIMUTH PLANE = 2[illegible]65 CM (11.285 IN.)
ELEVATION PLANE = 24.312 CM (9.571 IN.)

A. TRANSMIT ARRAY

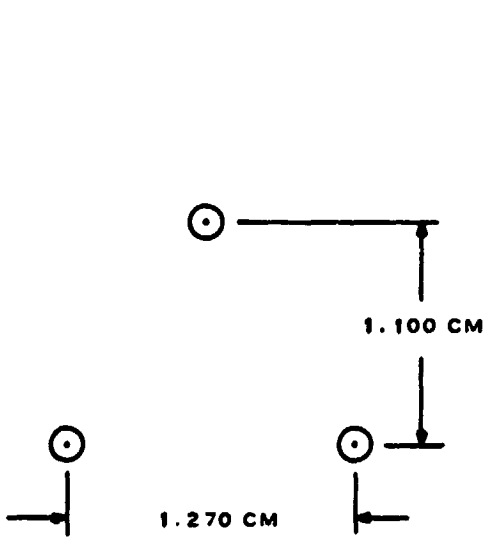

λ14.0 = 2.142 CM (0.844 IN.)

ARRAY SIZE

AZIMUTH PLANE = 31.115 CM (12.250 IN.)
ELEVATION PLANE = 26.400 CM (10.393 IN.)

B. RECEIVE ARRAY

217511

Figure 3-11. Phased Array Element Spacings and Array Dimensions for 24 x 24 Element Transmit and Receive Arrays

E. CONCLUSION ON APPROACHES WITHOUT AMPLIFIERS

After a considerable amount of effort had been spent looking at phased arrays, Butler matrix fed arrays and lens antennas, it appeared that there was no way to meet the size, weight, and gain requirements with these approaches. All the above became large in size and the number of components increased accordingly. Therefore, due to the resultant complexity of these antennas, it was concluded that antennas with amplifiers should be evaluated.

Some of the advantages and disadvantages which led to this decision are listed in Table 3-8

TABLE 3-8. ADVANTAGES AND DISADVANTAGES OF MULTIPLE BEAM ANTENNAS WITHOUT AMPLIFIERS

Advantages	Disadvantages
56 x 56 phased array	
a. -15.0-dB sidelobes	a. Four manifolds
	b. Phase shifter count (4/element)
	c. Phase shifter redesign
	d. Total package too large and heavy
	e. BSU complexity
Butler matrix	
a. Symmetry of matrices	a. Coupler count
	b. Complex and large switching matrix
	c. Switch loss
	d. Total package too large and heavy
	e. BSU complexity
	f. -13.5-dB sidelobes
	g. Crossover losses
Luneberg lens	
a. -15.0-dB sidelobes	a. Lens diameter (aperture protrudes out)
	b. Complex and large switching matrix
	c. Switch loss
	d. Pattern degrades beyond 30 degrees due to blockage
	e. Crossover losses

SECTION IV
APPROACHES WITH AMPLIFIERS

This section addresses some candidate antenna systems that use active elements to produce the simultaneous, multiple beams. The antenna systems presented are a phase-amplitude steered multibeam planar and reflective array, a phased array, and a Butler matrix fed array. As in the previous section, preliminary designs and tradeoffs which included size, gain, system loss, noise figure, and complexity were completed on each configuration and then tradeoffs were made between the various designs that led to a conclusion on these approaches.

A. PHASE-AMPLITUDE STEERED MULTIBEAM PLANAR ARRAY WITH AMPLIFIERS

The phase-amplitude steered multibeam array uses phase shifters and attenuators to form the desired multiple-beam radiation pattern by placing a predetermined phase and amplitude distribution across the array. Scanning of the beam is controlled with a beam steering computer.

Figure 4-1 is a block diagram for a four-beam receive array. Any desired frequency in the band is formed by mixing an intermediate frequency with the frequency of a tunable local oscillator. The tuned yttrium iron garnet (YIG) filter frequency tracks with the local oscillator and enhances the image rejection. Each of the four beams could be formed over the entire frequency band.

A circular aperture of 96 elements would have a diameter of 14.8 cm and an aperture gain of 26.4 dB. A block diagram showing the system losses to determine the noise figure of the array is shown in Figure 4-2. Figure 4-3 is the equivalent block diagram showing the noise figure calculation which is 9.08 dB. Figure 4-4 is a block diagram of the transmit array and Figure 4-5 represents the loss budget.

In order to compare the relative TWT size needed for two different approaches, a 1 mW signal for the four beams was the input to the power amplifier. This would require a –6 dBm signal for each beam at this point. This required a TWT with a 3.16-watt output (+35 dBm) to be fed into the four-way divider, or 12.6 watts total for the four channels.

An alternate approach is shown in Figure 4-6 with a single TWT after the four-way combiner. By using the TWT after the combiner, this would require only 2.8 watts of TWT power and lower power sources at the input to the four-way combiner.

The components on the front of the aperture, which include the element, filter, amplifier, attenuator, and phase shifter, could be integrated into a single plug-in module. Figure 4-7 is a conceptual configuration of the module attributing approximate volumes for the front-end components. It has a depth of 20.3 cm from the front of the element to a point at which it plugs into the 96-way divider. Figure 4-8 is a conceptual configuration showing RF and digital distributions to the modules.

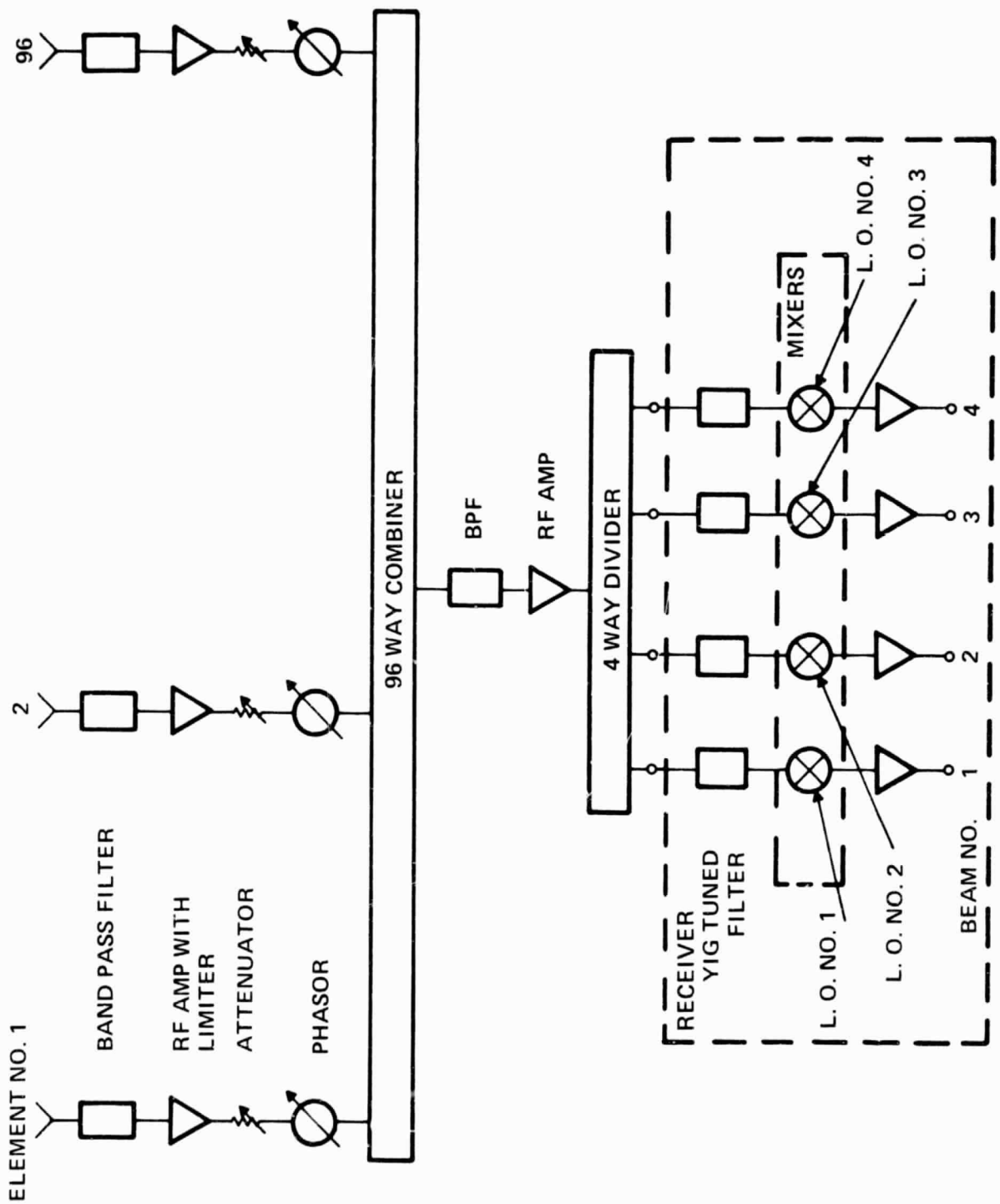

Figure 4-1. Phase-Amplitude Steered Multibeam Receive Array

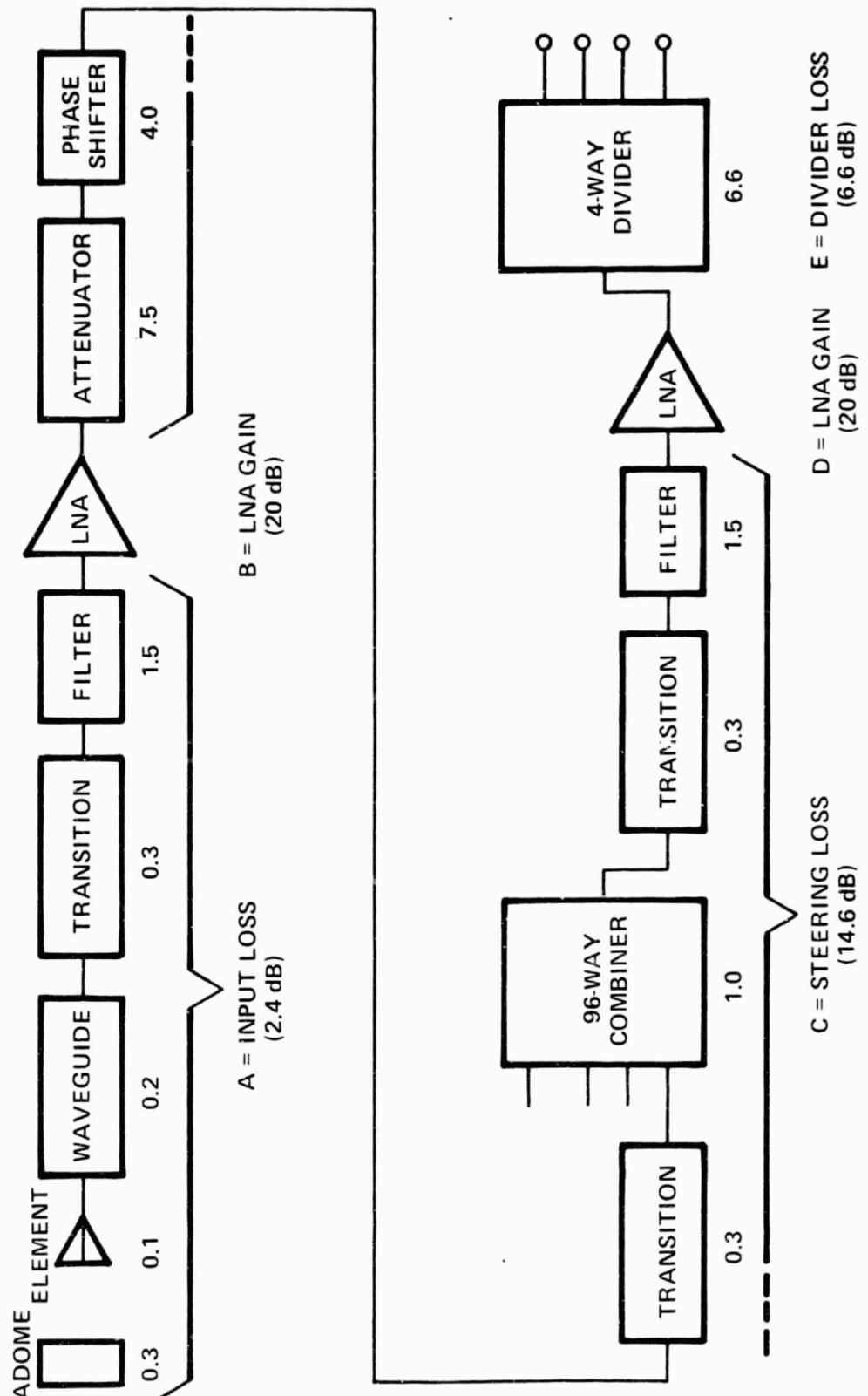

Figure 4-2. Block Diagram to Determine Noise Figure of Phase-Amplitude Steered Multibeam Receive Array

217513

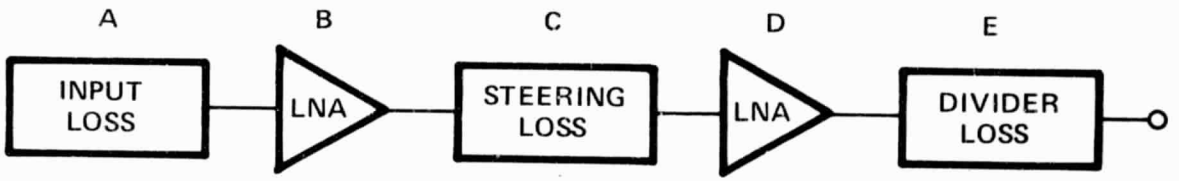

L = 2.4 dB
$P_r = 1.74$
$G_A(P_r) = 1/1.74 = .58$

NF = 5.5 dB
$P_r = 3.55$
$G_B = 20$ dB
$G_B(P_r) = 100$

L = 14.6 dB
$P_r = 28.84$
$G_C = 1/28.84 = .03$

NF = 5.5 dB
$P_r = 3.55$
$G_D = 20$ dB
$G_D = (P_r) = 100$

L = 6.6 dB
$P_r = 4.57$
$G_E = 1/4.57 = .22$

$$NF = NF_A + \frac{NF_B - 1}{G_A} + \frac{NF_C - 1}{G_A G_B} + \frac{NF_D - 1}{G_A G_B G_C} + \frac{NF_E - 1}{G_A G_B G_C G_D}$$

$$= 1.74 + \frac{3.55 - 1}{.58} + \frac{28.84 - 1}{(.58)(100)} + \frac{3.55 - 1}{(.58)(100)(.03)} + \frac{4.57 - 1}{(.58)(100)(.03)(100)}$$

$$= 1.74 + 4.40 + 0.48 + 1.46 + .02$$

$$= 8.1$$

NF (dB) = 10 log P_r = 10 log 8.1 = 9.08 dB

NF = 9.08 dB

Figure 4-3. Noise Figure Calculation for Phase-Amplitude Steered Multibeam Receive Array

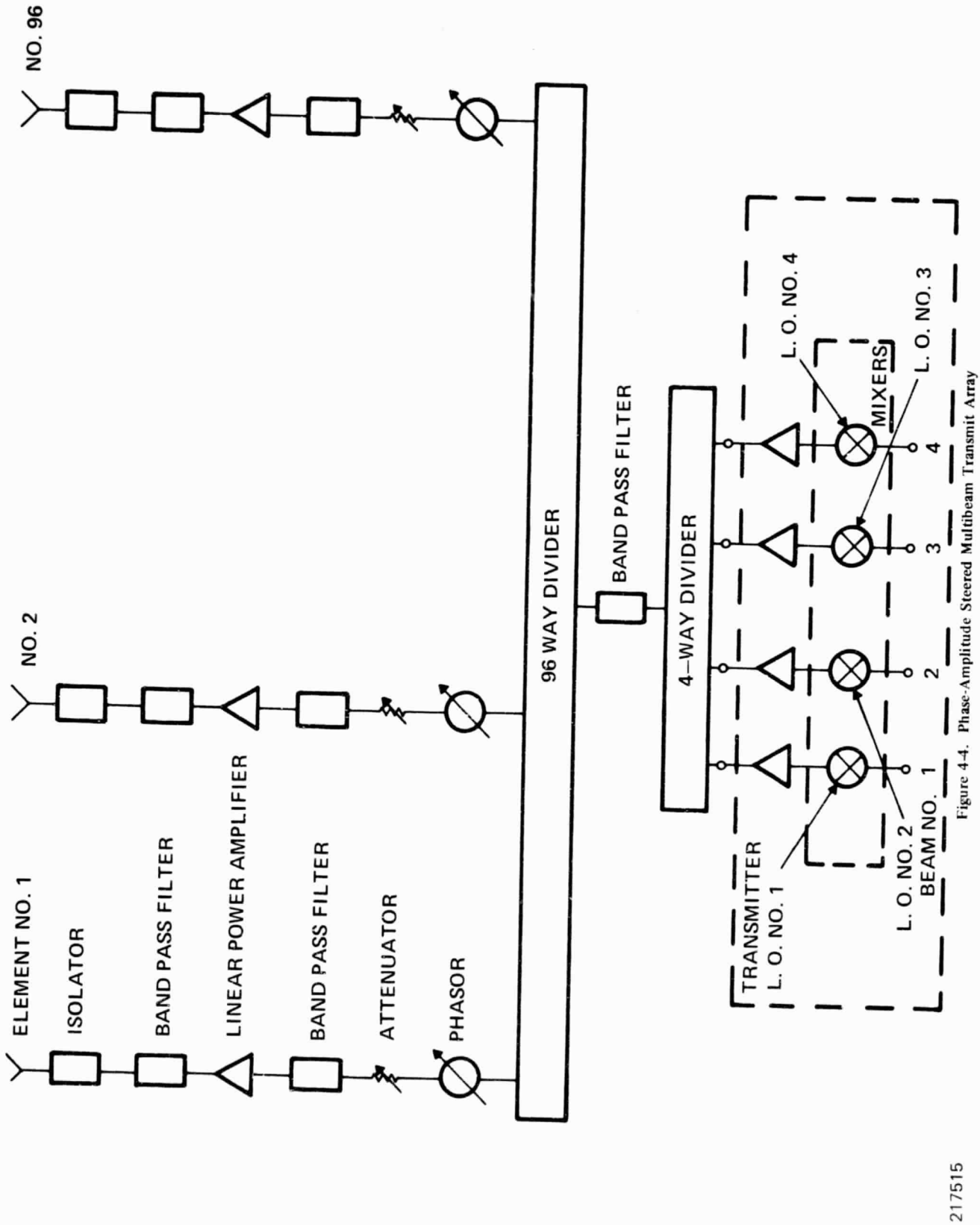

Figure 4-4. Phase-Amplitude Steered Multibeam Transmit Array

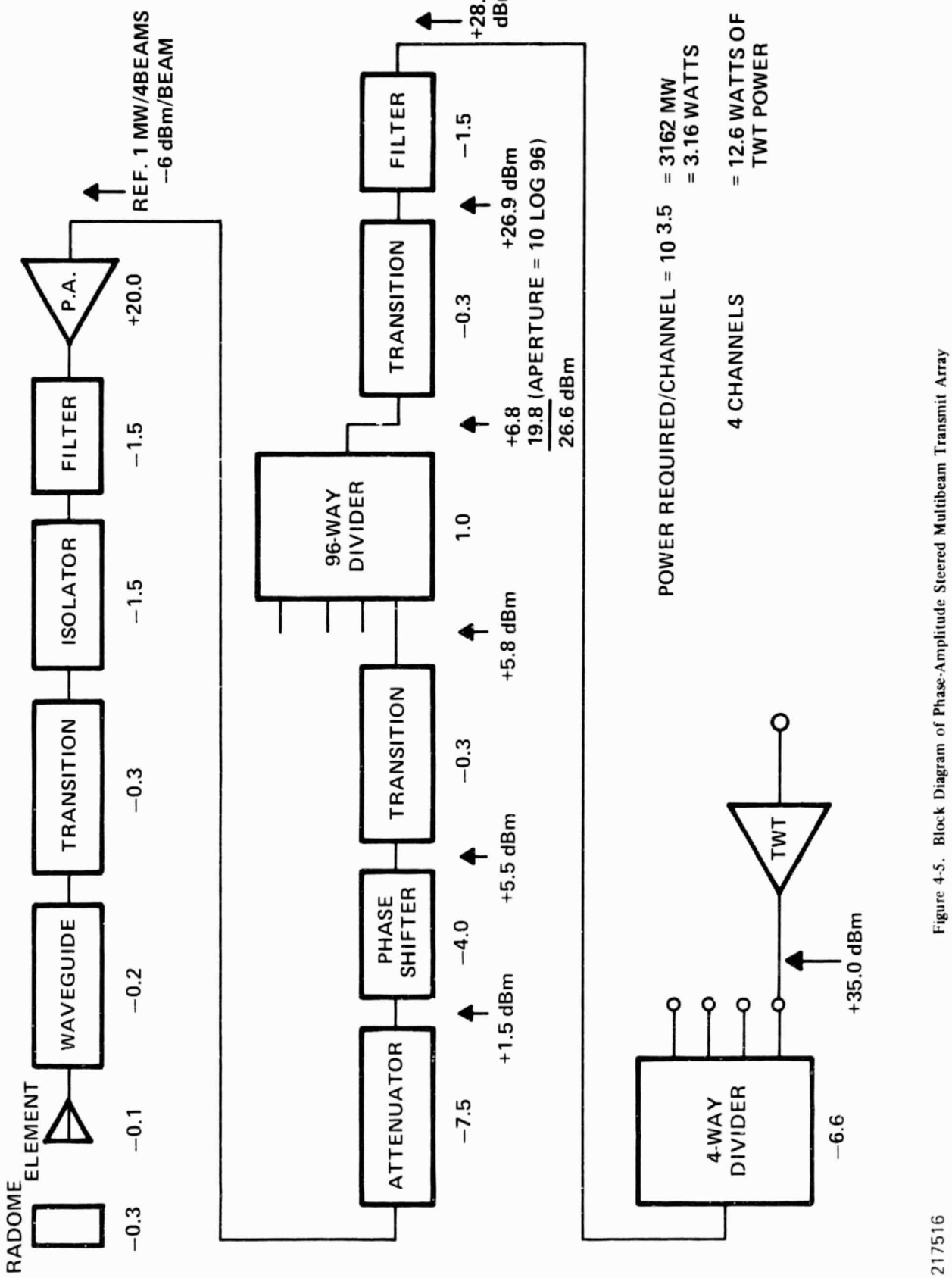

Figure 4-5. Block Diagram of Phase-Amplitude Steered Multibeam Transmit Array

217516

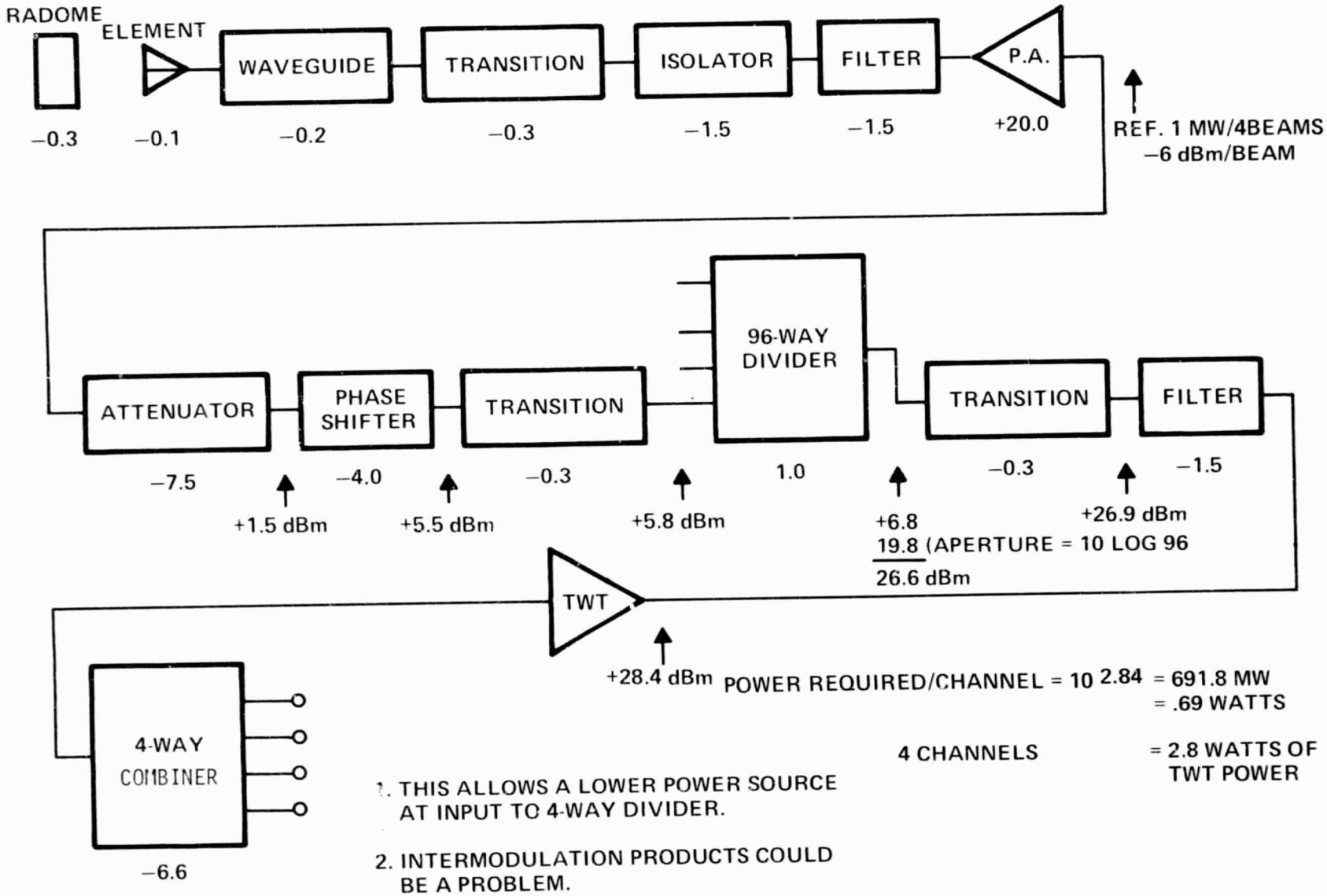

217517

Figure 4-6. Alternate Approach Block Diagram of Phase-Amplitude Steered Multibeam Transmit Array

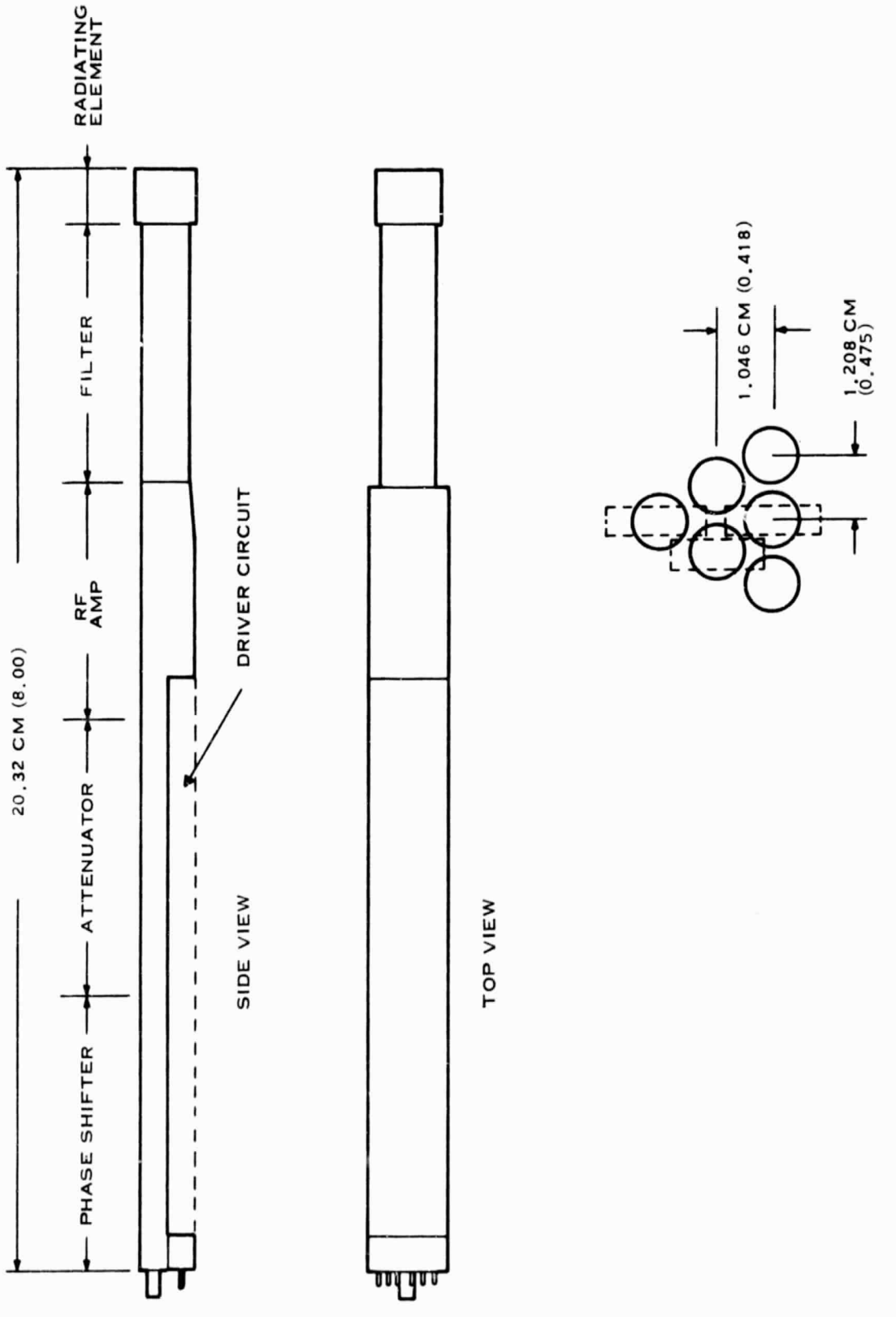

Figure 4-7. Phase-Amplitude Steered Multibeam Receive Array Module

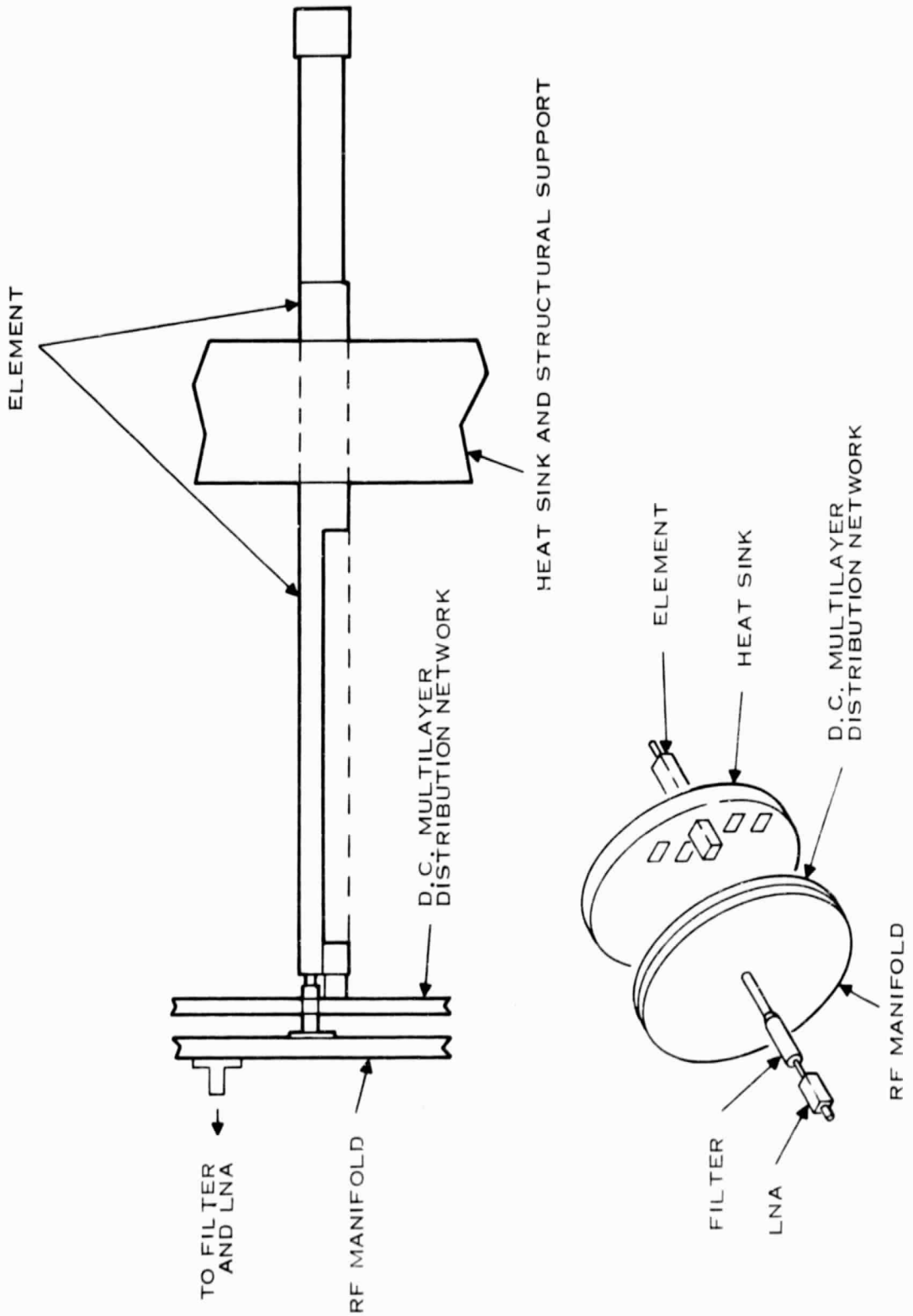

Figure 4-8. Phase-Amplitude Steered Multibeam Receive Array Distribution

TABLE 4-1. PHASE-AMPLITUDE STEERED MULTIBEAM ARRAY (RECEIVE)

Number of elements	96
Azimuth element spacing (cm)	1.208
Elevation element spacing (cm)	1.046
Azimuth array dimension (cm)	14.8
Elevation array dimension (cm)	14.8
Array area (cm^2)	173.89
Array depth (cm)	30.0
Beamwidth, degrees (azimuth, elevation)	9, 9
Number of phase shifters	96
Number of attenuators	96
Number of filters	101
Number of amplifiers	97
Gain control method	Steering hardware
Aperture gain (dB)	26.4
Noise figure (dB)	9.1
Weight (kg)	27.0

Table 4-1 is a list of the characteristics for the planar array.

B. PHASE-AMPLITUDE STEERED MULTIBEAM REFLECTIVE ARRAY WITH AMPLIFIERS

The reflective array is shown in Figure 4-9. A 4-horn assembly is the portion of the RF manifold that provides the four-beam capability. For the transmit case the linear polarization propagated by the horn is reflected by the reflector/polarizer to a quad-ridged waveguide at the array surface. The phase shifters and attenuators control the array pointing direction. The signal from the phase shifters and attenuators excite the orthogonal linear polarization in the waveguide and is transmitted to the polarizer where it is converted to circular polarization.

A block diagram to determine the noise figure of the reflective array is shown in Figure 4-10, and Figure 4-11 is the combined losses along with the noise figure calculation. Figure 4-12 is a block diagram of the reflective transmit array with the losses indicated for the components of the system. As in the planar array case, a 1 mW signal for the four beams is the reference input to the power amplifier. The required TWT power for the four channels is 8.6 watts.

Table 4-2 is a list of the characteristics for the reflective array.

C. COMPARISON OF PHASE-AMPLITUDE STEERED PLANAR AND REFLECTIVE ARRAYS

A comparison between the phase-amplitude steered multibeam planar array and reflective array was made to determine which of the two approaches would be the better. Table 4-3 lists the comparisons in what was felt to be the most important to the least important item. As far as

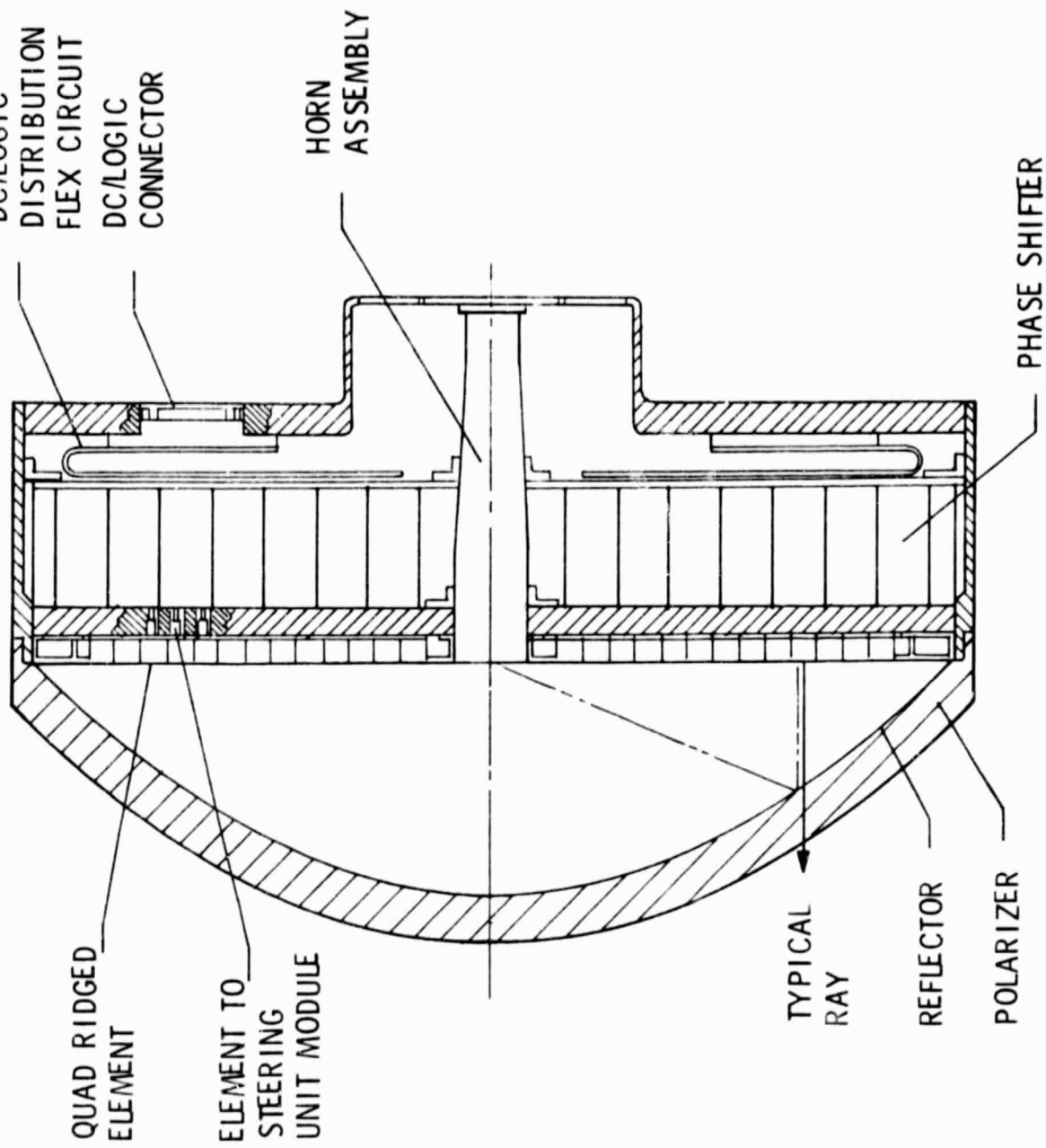

Figure 4-9. Amplitude Steered Multibeam Reflective Array

217520

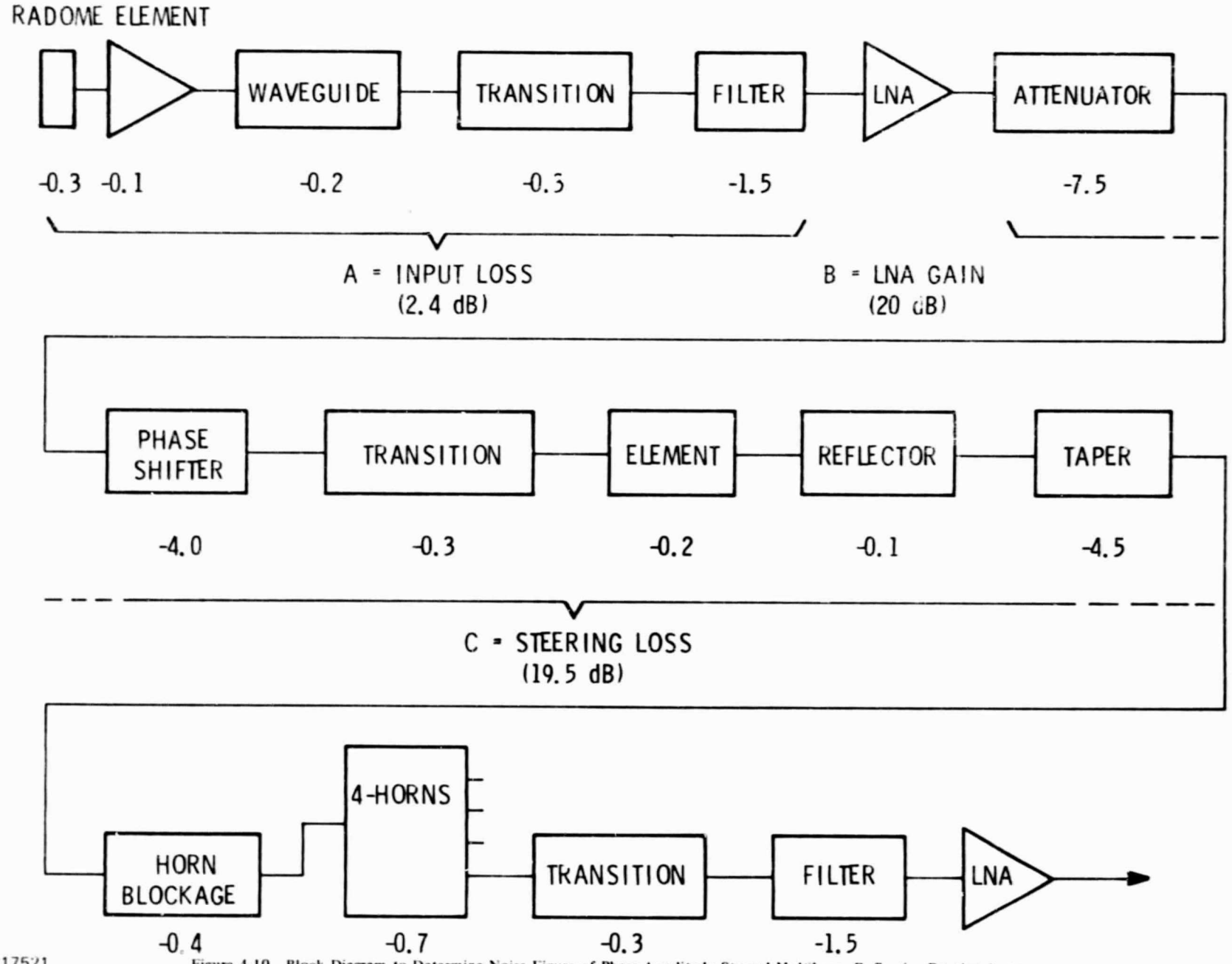

217521

Figure 4-10. Block Diagram to Determine Noise Figure of Phase-Amplitude Steered Multibeam Reflective Receive Array

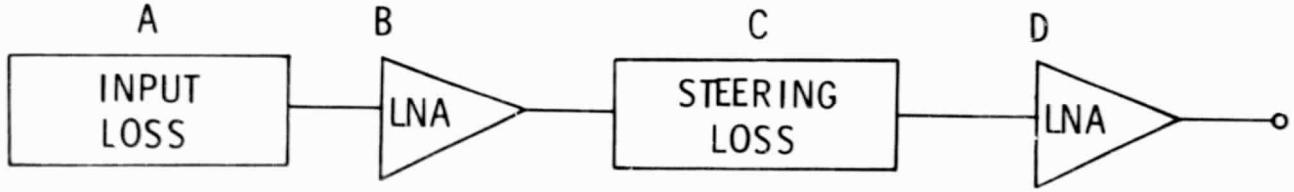

L = 2.4dB
Pr = 1.74
$G_A(Pr) = 1/1.74 = .58$

NF = 5.5dB
Pr = 3.55
$G_B = 20dB$
$G_B(Pr) = 100$

L = 19.5dB
Pr = 89.12
$G_C = 1/89.12 = .01$

NF = 5.5dB
Pr = 3.55
$G_D = 20dB$
$G_D(Pr) = 100$

$$NF = NF_A + \frac{NF_B - 1}{G_A} + \frac{NF_C - 1}{G_A G_B} + \frac{NF_D - 1}{G_A G_B G_C}$$

$$= 1.74 + \frac{3.55 - 1}{.58} + \frac{89.12 - 1}{(.58)(100)} + \frac{3.55 - 1}{(.58)(100)(.01)}$$

$$= 1.74 + 4.40 + 1.52 + 4.39$$

$$= 12.05$$

$$NF(dB) = 10 \text{ LOG } Pr = 10 \text{ LOG } 12.05 = 10.81$$

NF = 10.81 dB

217522

Figure 4-11. Noise Figure Calculation for Phase-Amplitude Steered Multibeam Reflective Receive Array

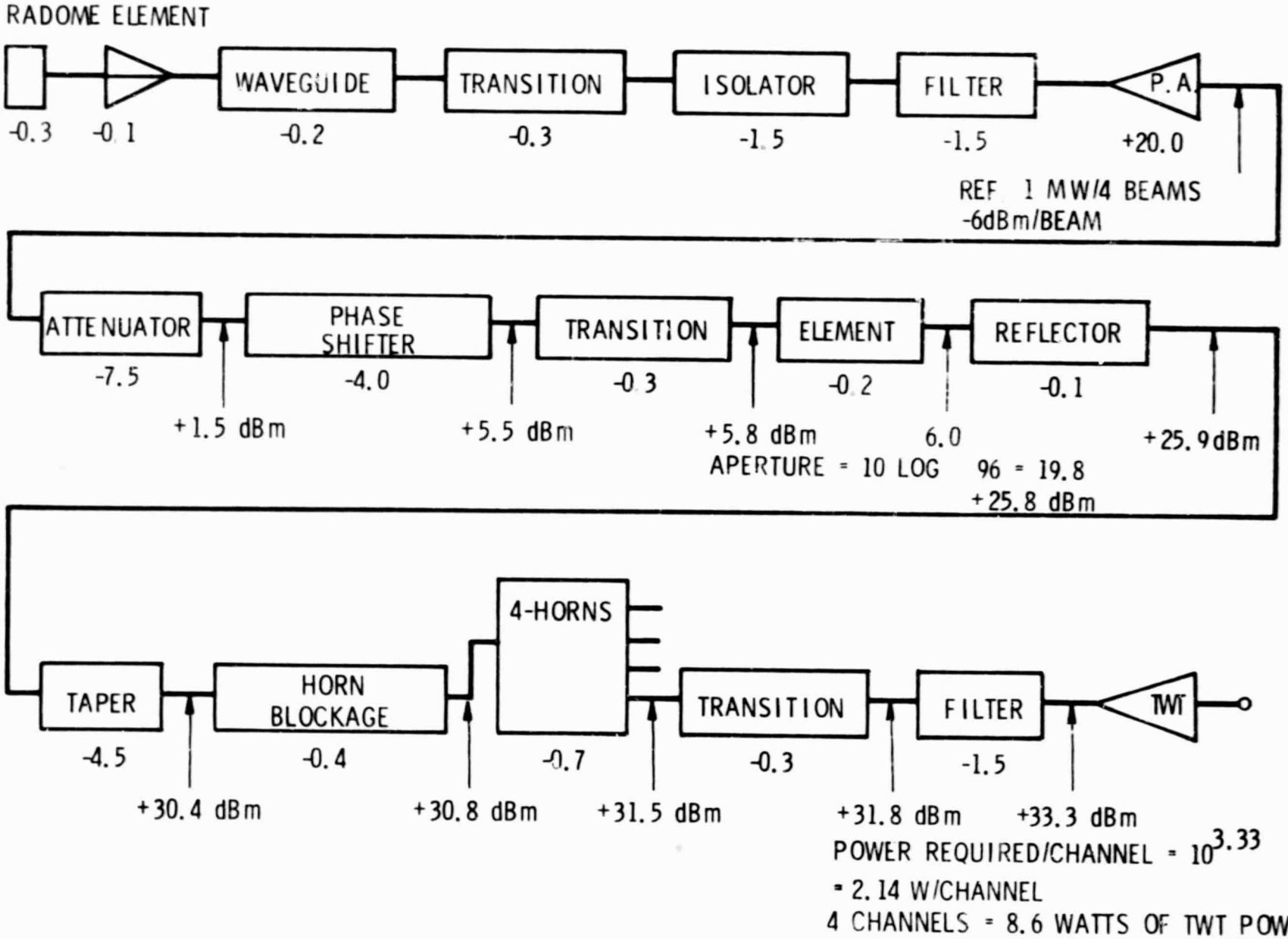

217523

Figure 4-12. Block Diagram of Phase-Amplitude Steered Multibeam Reflective Transmit Array

TABLE 4-2. PHASE-AMPLITUDE STEERED MULTIBEAM REFLECTIVE ARRAY (RECEIVE)

Reflector	1
Number of horns	4
Number of elements	96
Azimuth element spacing (cm)	1.312
Elevation element spacing (cm)	1.136
Azimuth array dimension (cm)	14.8
Elevation array dimension (cm)	14.8
Array area (cm^2)	173.89
Array depth (cm)	30.0
Beamwidth, degrees (azimuth, elevation)	9, 9
Number of phase shifters	96
Number of attenuators	96
Number of filters	101
Number of amplifiers	100
Gain control method	Steering hardware
Aperture gain (dB)	26.4
Noise figure (dB)	10.8
Weight (kg)	27.0

TABLE 4-3. COMPARISON OF PHASE-AMPLITUDE STEERED MULTIBEAM ARRAYS

Planar Array	Reflective Array
Best growth potential	More horns will degrade performance
Less risk	More complex
Transmit power requirement is 12.6 watts (2.8 watts if one TWT can be used)	Transmit power required is 8.6 watts
Noise figure = 9.1 dB	Noise figure = 10.8 dB
Flat polarizer	Three-dimensional polarizer
Requires less depth	Reflector increases depth
Meets area requirements except for depth	Requires slightly larger area

growth potential, the reflective array is limited in the sense that as more beams are required, more horns would need to be added at the center of the array. When this is done the performance of the illumination is degraded due to offsetting the feed from the focal point of the reflector.

This comparison led to the conclusion that the planar array was the better of the two approaches.

D. PHASED ARRAY WITH AMPLIFIERS

To keep a common comparison between the array configurations in the trade analysis, the phased array with amplifiers has 96 elements also. Figure 4-13 is a block diagram of the array. The aperture gain is 26.4 dB. Losses before the low noise amplifier account for 2.4 dB, leaving a

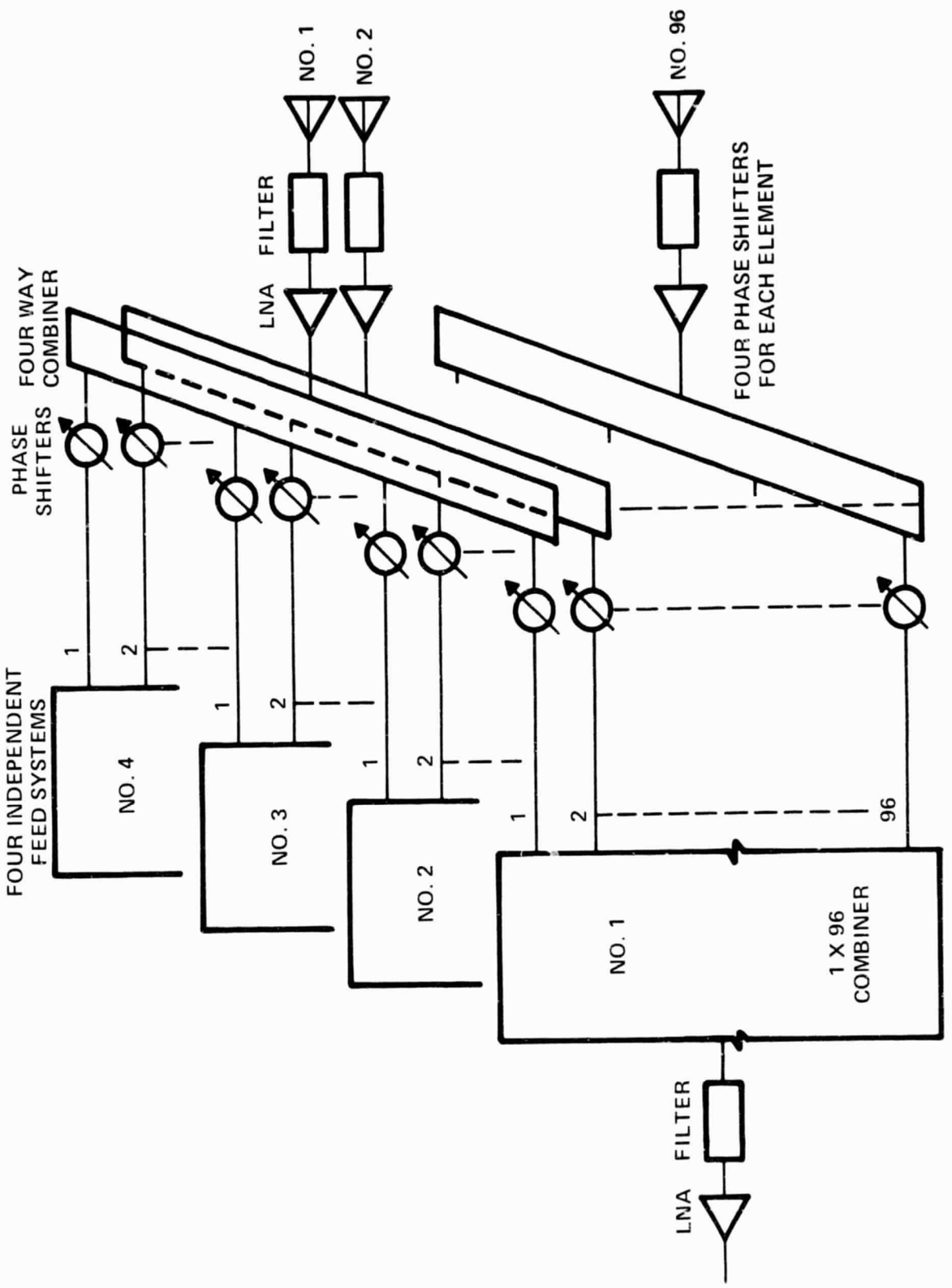

Figure 4-13. Block Diagram for Phased Array With Amplifiers (96 Element Circular Aperture)

net gain of 24 dB for the receive case. Figure 4-14 is a block diagram of the array showing the system losses which were used in the noise figure calculation. Figure 4-15 is the equivalent block diagram showing the noise figure calculation which is 9.12 dB. A block diagram of the transmit phased array is shown in Figure 4-16. The input to the power amplifier is 1 mW for the four beams. This would require a TWT with 3.25 watts of power for the four channels.

Figures 4-17 and 4-18 are conceptual drawings of the integrated element module and system configuration respectively. A list of the characteristics for this array is shown in Table 4-4.

TABLE 4-4. PHASED ARRAY WITH AMPLIFIERS (RECEIVE)

Number of elements	96
Azimuth element spacing (cm)	1.312
Elevation element spacing (cm)	1.136
Azimuth array dimensions (cm)	14.88
Elevation array dimensions (cm)	14.88
Array area (cm^2)	173.89
Array depth ( )	45.0
Beamwidth, degrees (azimuth, elevation)	9, 9
Number of phase shifters	384
Number of attenuators	4
Number of filters	100
Number of amplifiers	100
Gain control method	Attenuator
Aperture gain (dB)	26.4
Noise figure (dB)	9.1
Weight (kg)	28.0

E. BUTLER MATRIX FED ARRAY WITH AMPLIFIERS

The Butler matrix is a rectangular aperture with 8 elements in the azimuth plane and 16 elements in the elevation plane for a total of 128 elements. A block diagram of the switch and matrix layout is shown in Figure 4-19. Beam pointing is accomplished with a solid state waveguide switch. Figure 4-20 is the block diagram used in determining the noise figure of the array and Figure 4-21 shows the calculation of the noise figure which is 8.86 dB.

Figure 4-22 is a block diagram of the transmit array. Since this array has 32 more elements than the other arrays, only 0.75 mW of power is required at the input to the power amplifier to get the same output power. This requires a total of 2.2 watts of TWT power at the input for the four channels.

Conceptual drawings of the Butler matrix with amplifiers can be viewed in Figures 4-23 and 4-24. Table 4-5 is a list of the parameters for this case.

One major disadvantage of the Butler matrix is the crossovers in the matrix itself.

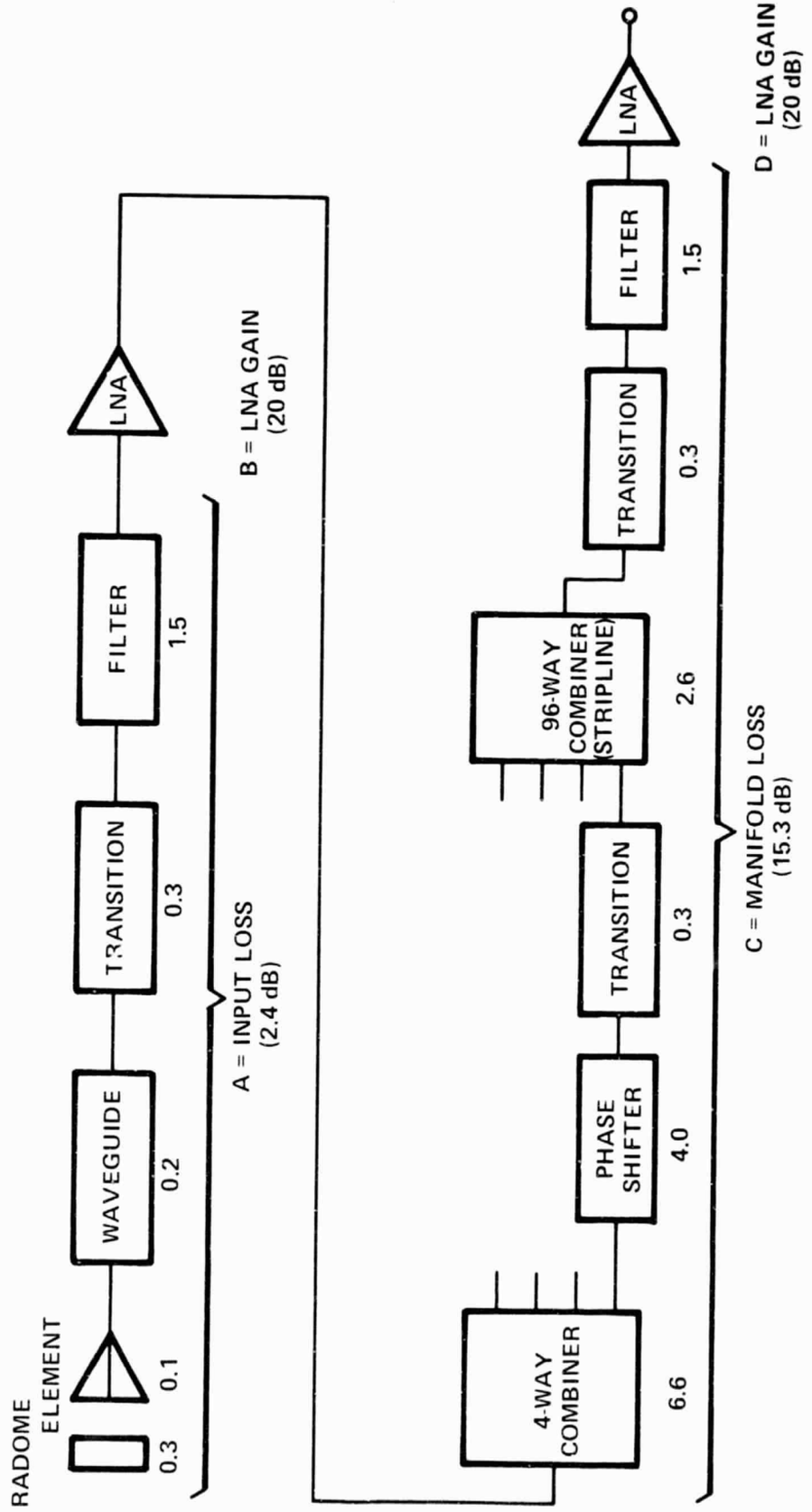

Figure 4-14. Block Diagram to Determine Noise Figure of Receive Phased Array

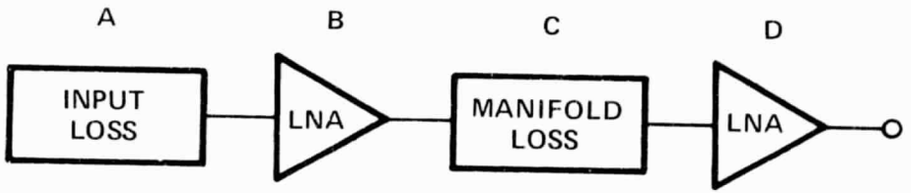

L = 2.4 dB
P_r = 1.74
$G_A(P_r)$ = 1/1.74 = .58

NF = 5.5 dB
P_r = 3.55
G_B = 20 dB
$G_B(P_r)$ = 100

L = 15.3 dB
P_r = 33.88
G_c = 1/33.88 = .03

NF = 5.5 dB
P_r = 3.55
G_D = 20 dB
$G_D(P_r)$ = 100

$$NF = NF_A + \frac{NF_B - 1}{G_A} + \frac{NF_C - 1}{G_A G_B} + \frac{NF_D - 1}{G_A G_B G_C}$$

$$= 1.74 + \frac{3.55 - 1}{.58} + \frac{33.88 - 1}{(.58)(100)} + \frac{3.55 - 1}{(.58)(100)(.03)}$$

$$= 1.74 + 4.40 + .57 + 1.46$$

$$= 8.67$$

NF (dB) = 10 log P_r = 10 log 8.17 = 9.12 dB

NF (dB) = 9.12 dB

Figure 4-15. Noise Figure Calculation for Phased Array

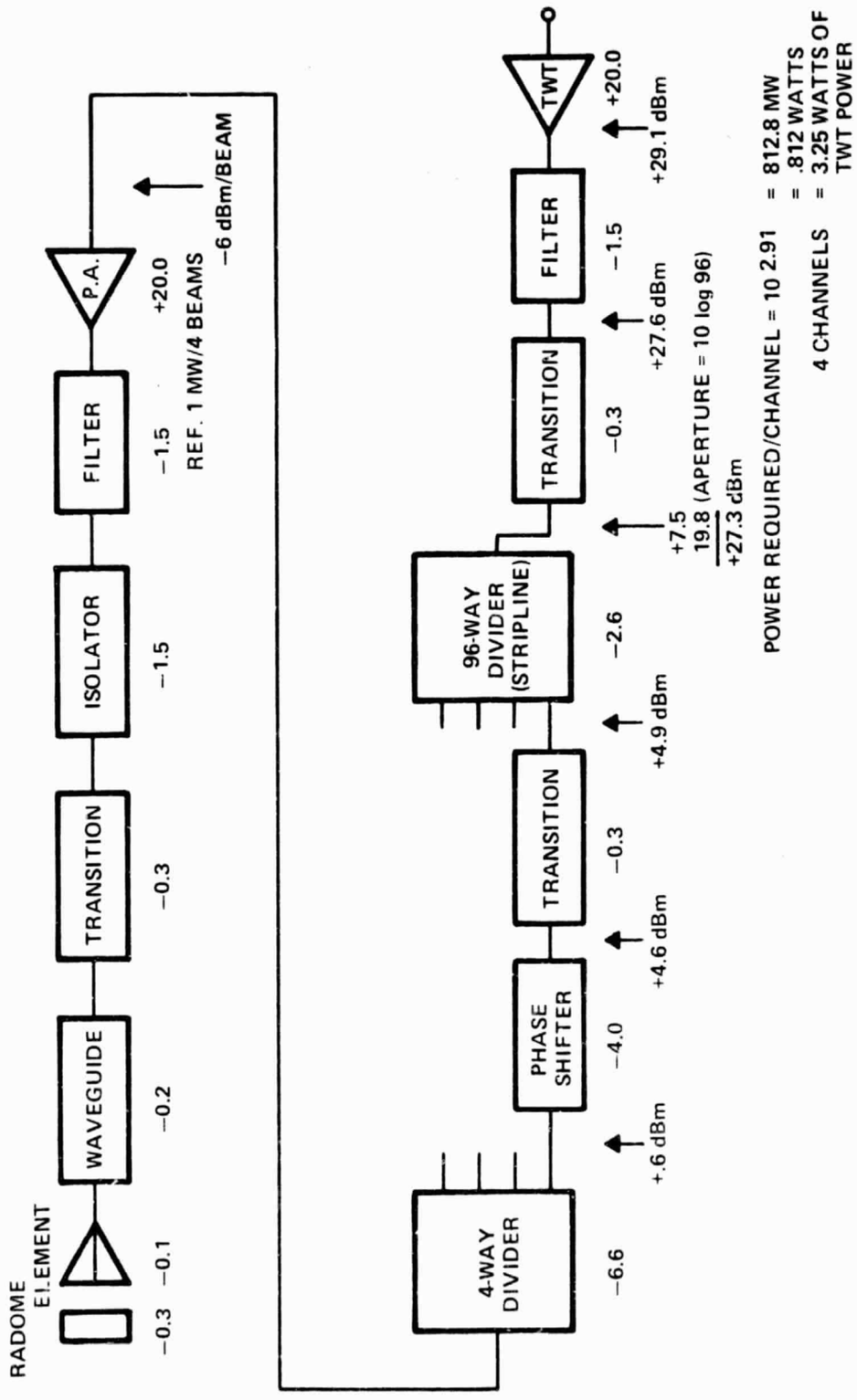

Figure 4-16. Block Diagram for Transmit Phased Array

217527

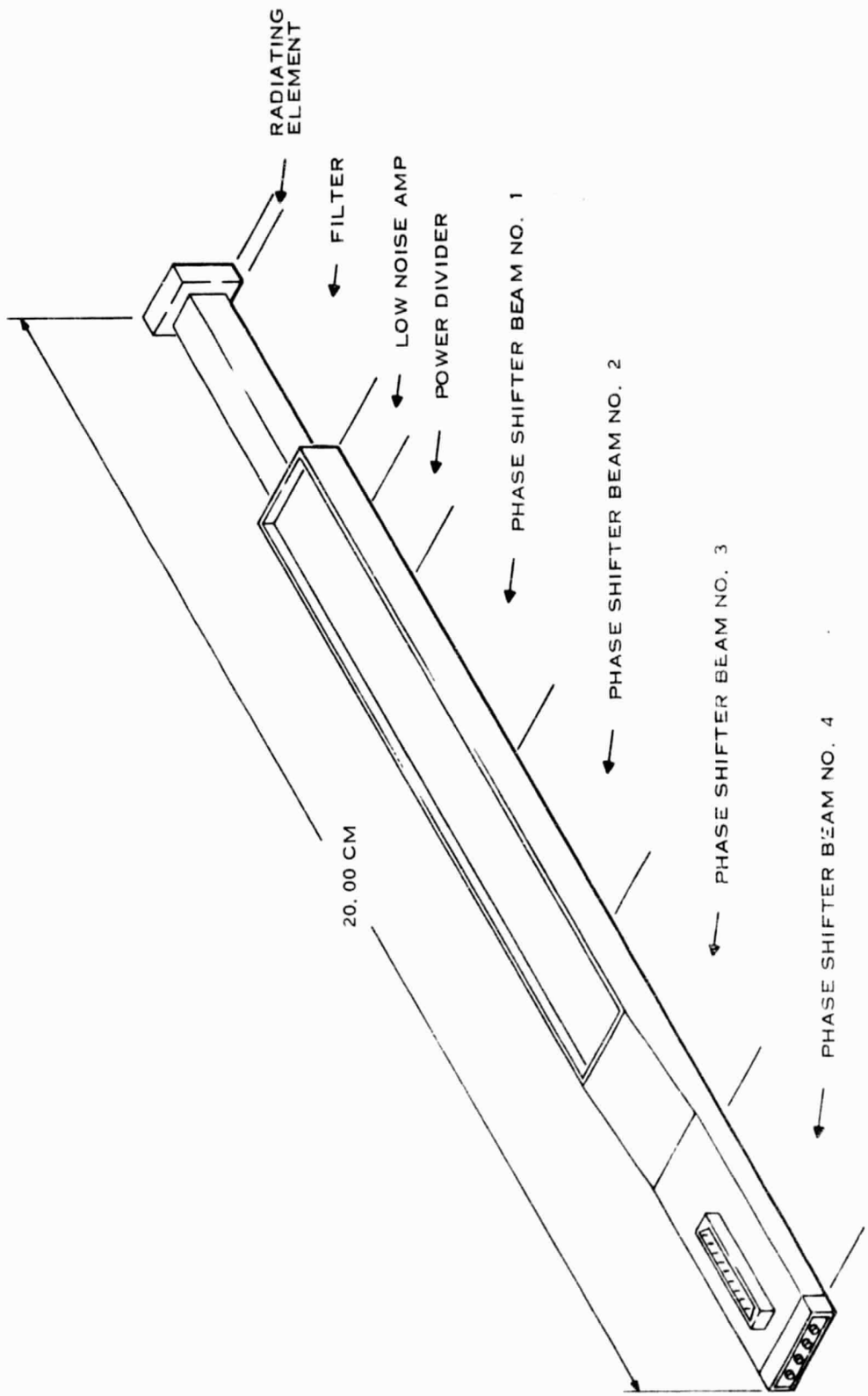

Figure 4-17. Phased Array 96 Element Circular Aperture

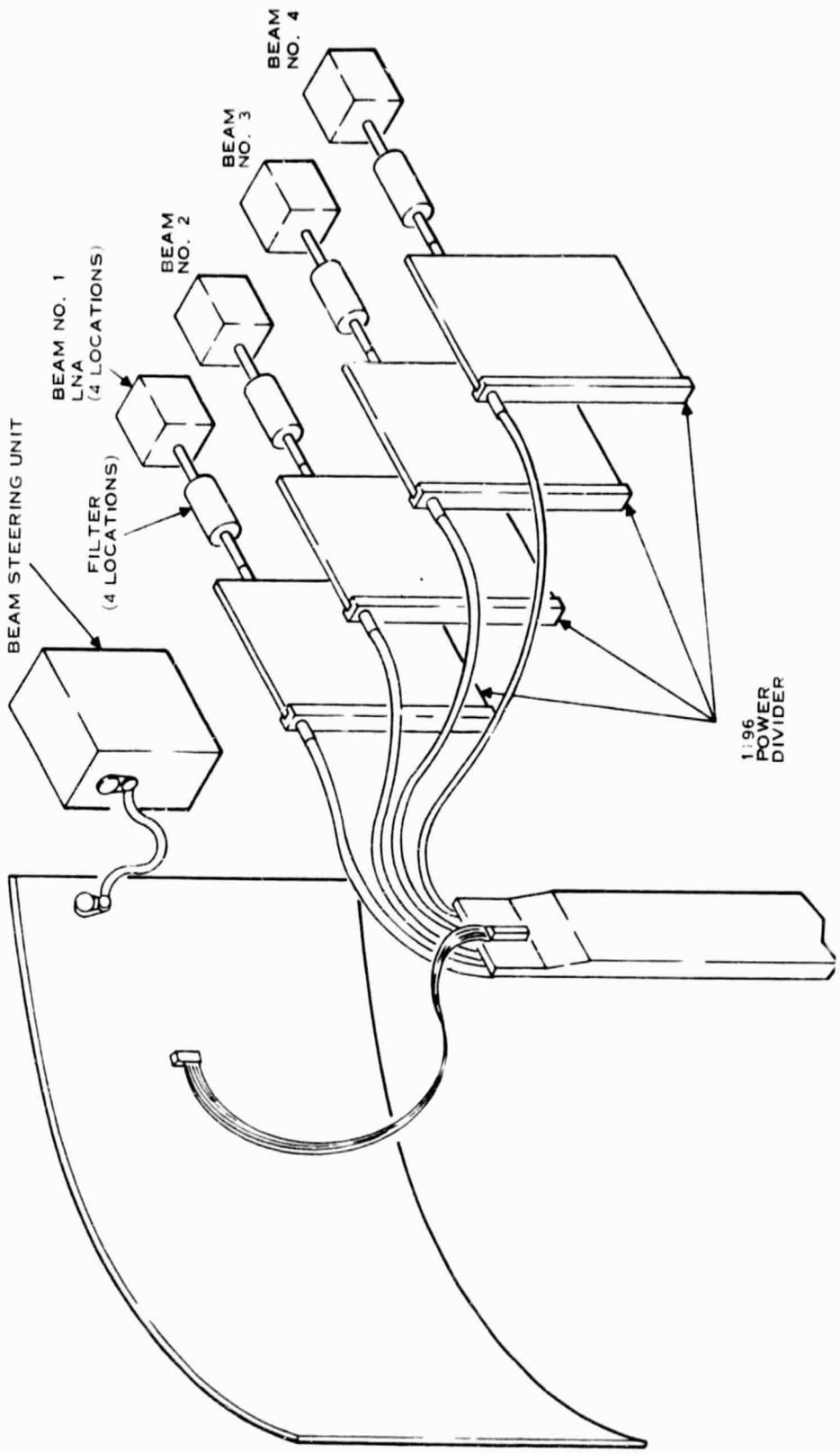

Figure 4-18. Phased Array 96 Element Circular Aperture

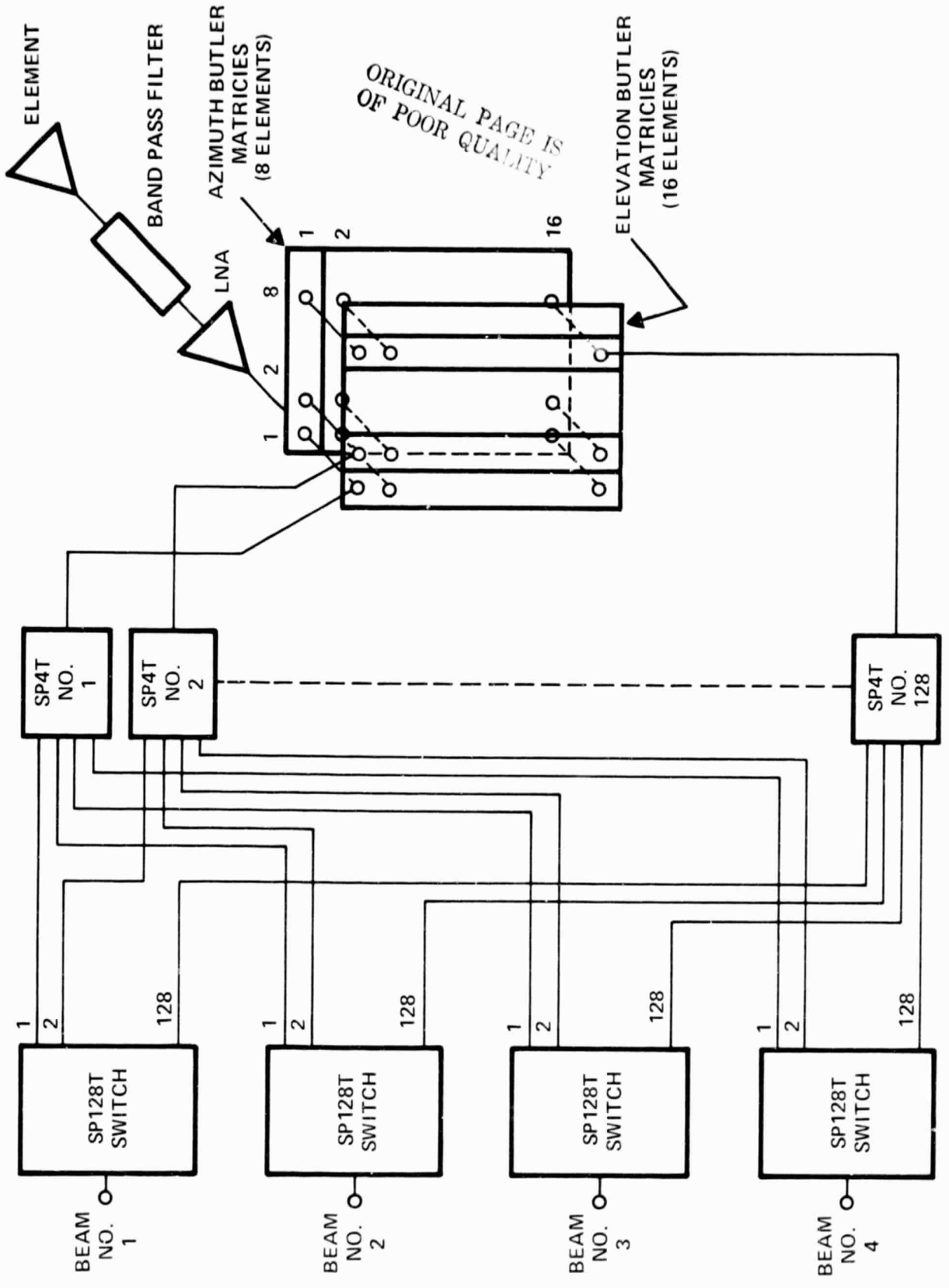

Figure 4-19. Switch and Matrix Layout for 8 × 16 Butler Matrix Fed Array

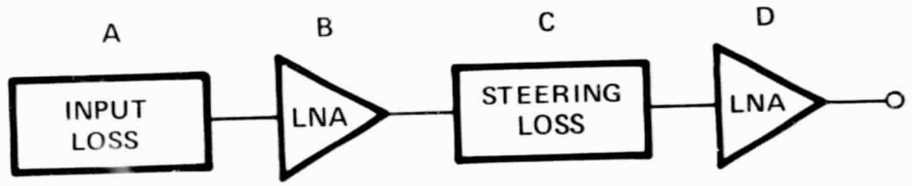

A	B	C	D
L = 2.4 dB	NF = 5.5 dB	L = 13.5	NF = 5.5 dB
P_r = 1.74	P_r = 3.55	P_r = 22.38	P_r = 3.55
$G_A(P_r)$ = 1/1.74 = .58	G_B = 20 dB	G_c = 1/22.38 = .04	G_A = 20 dB
	$G_B(P_r)$ = 100		$G_B(P_r)$ = 100

$$NF = NF_A + \frac{NF_B - 1}{G_A} + \frac{NF_C - 1}{G_A G_B} + \frac{NF_D - 1}{G_A G_B G_c}$$

$$= 1.74 + \frac{3.55 - 1}{.58} + \frac{25.11 - 1}{(.58)(100)} + \frac{3.55 - 1}{(.58)(100)(.04)}$$

$$= 1.74 + 4.40 + .45 + 1.10$$

$$= 7.69$$

$$NF\ (dB) = 10 \log P_r = 10 \log 7.69 = 8.86\ dB$$

NF = 8.86 dB

Figure 4-21. Noise Figure Calculations for 8 × 16 Butler Matrix Fed Array

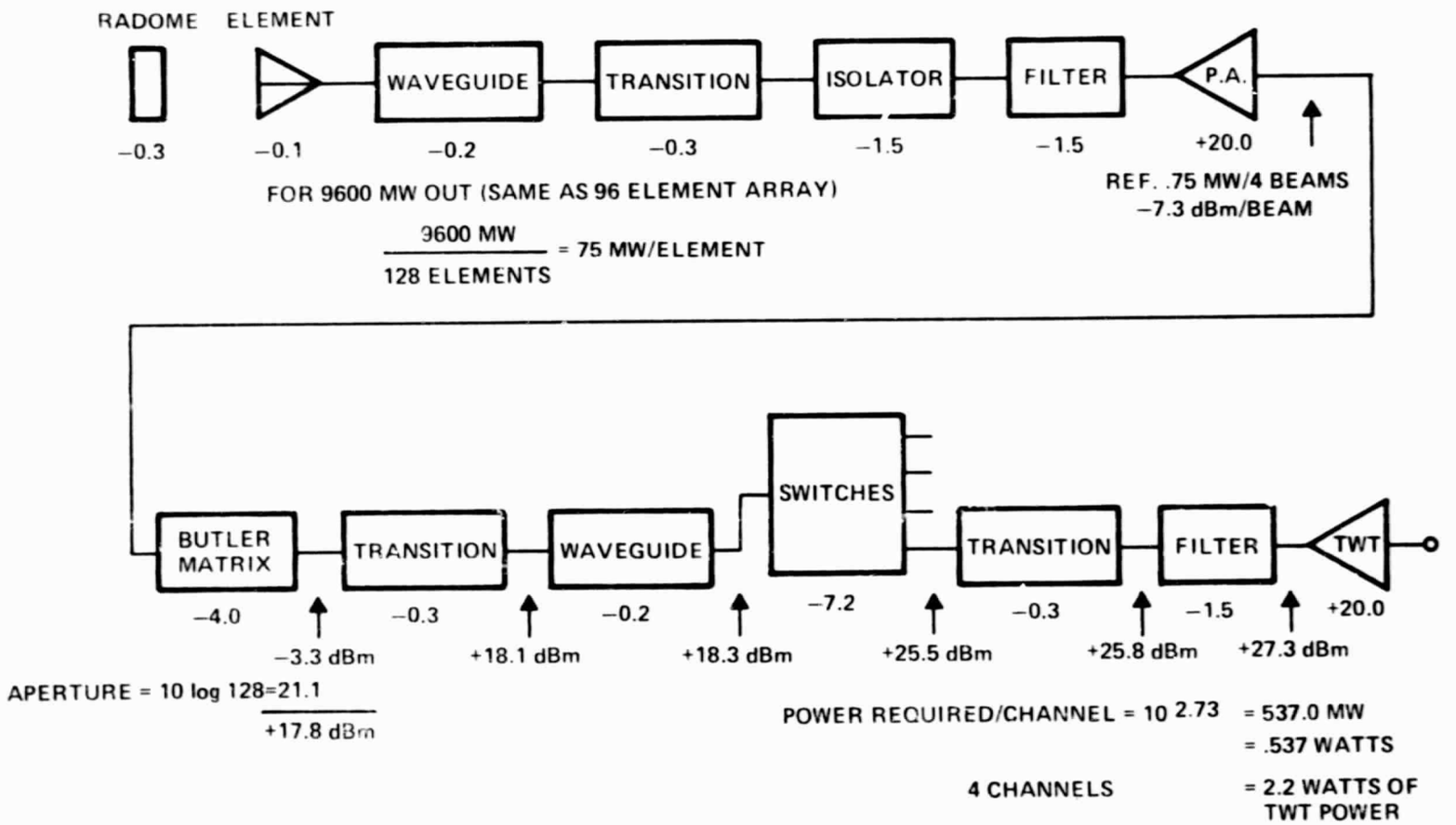

Figure 4-22. Block Diagram of Butler Matrix Transmit Array

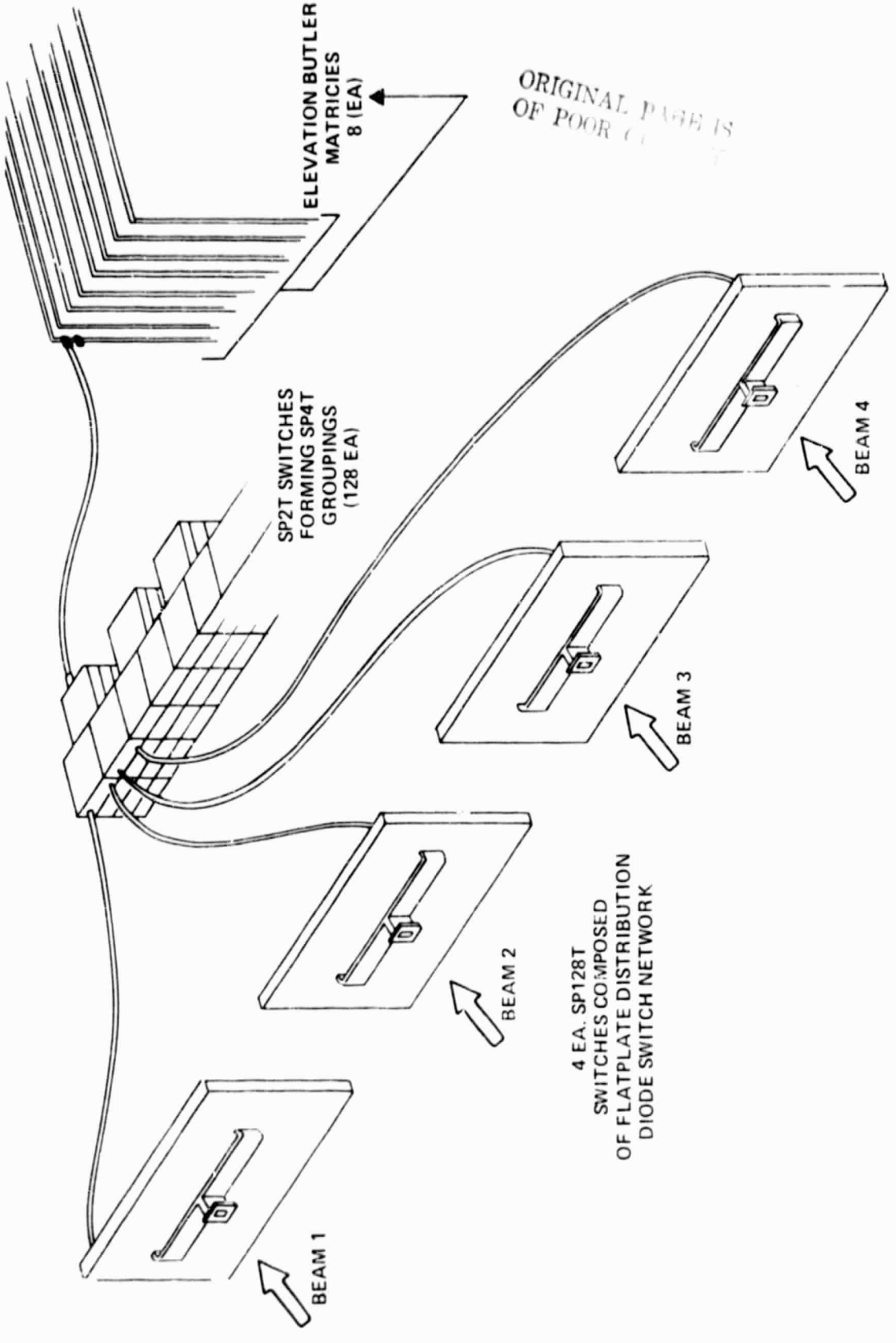

Figure 4-23. 8 × 16 Butler Matrix RF Circuit

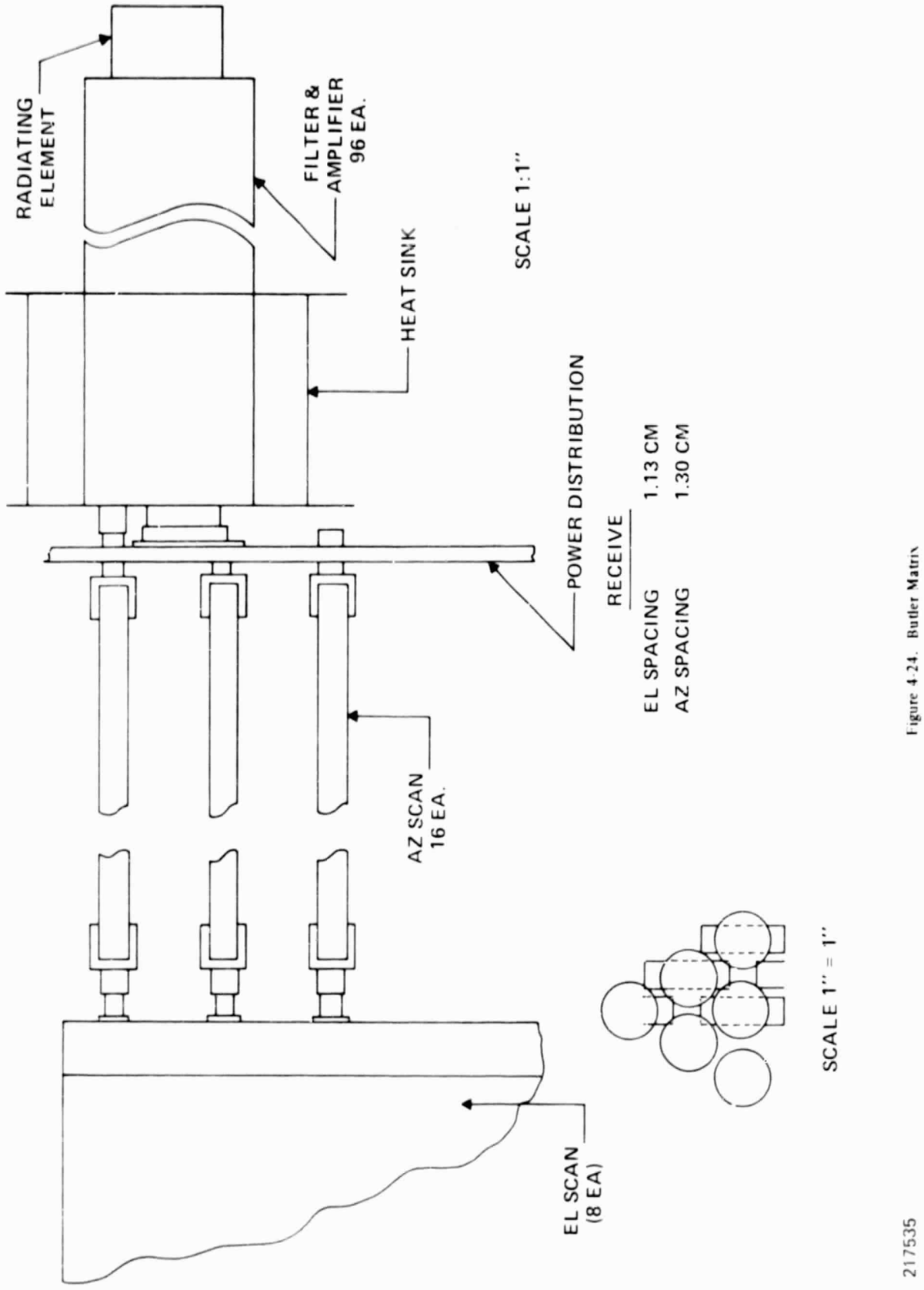

Figure 4-24. Butler Matrix

TABLE 4-5. 8 x 16 BUTLER MATRIX WITH AMPLIFIERS (RECEIVE)

Number of elements	128
Azimuth element spacing (cm)	1.212
Elevation spacing (cm)	1.125
Azimuth array dimension (cm)	10.3
Elevation array dimension (cm)	18.0
Array area (cm^2)	185.4
Array depth (cm)	137.0
Beamwidth, degrees (azimuth, elevation)	11.0, 6.3
Number of switches	892
Number of attenuators	4
Number of filters	132
Number of amplifiers	132
Gain control method	Attenuator
Aperture gain (dB)	26.6
Noise figure (dB)	8.9
Weight (kg)	226.0

F. ADVANTAGES AND DISADVANTAGES OF MULTIBEAM ANTENNAS WITH AMPLIFIERS AND TRADEOFF OF APPROACHES

A tradeoff was completed to determine the best approach between the phase-amplitude steered multibeam array, a phased array with amplifiers, and a Butler matrix fed array with amplifiers.

Table 4-6 is a list of the advantages and disadvantages of the phased array, Butler matrix fed array, and phase-amplitude steered array with amplifiers, and Table 4-7 is a tradeoff of the three approaches. in Table 4-7, the normalized cost and quantities of the main components are listed for each of the three arrays. The amplifier cost was normalized to 1.0 since it is probably the most expensive single component. Since the phase-amplitude steered multibeam array had the lowest total relative cost, it was normalized to 1.0, with the phased array being the next with 1.282 and the Butler matrix fed array as the most expensive (1.669) approach.

The tradeoff analysis shows the planar phase-amplitude steered multibeam array to be the desired approach because of the following:

Less complex – lowest component count

Power consumption is small

Smallest size – meets aperture area requirements but not the depth

Lowest weight – meets requirements

Most versatile – most adaptable for more beams

Lowest cost

Innovative

TABLE 4-6. ADVANTAGES AND DISADVANTAGES OF MULTIPLE BEAM ANTENNAS WITH AMPLIFIERS

Advantages	Disadvantages
Phased array (96-element circular aperture)	
−15.0-dB sidelobes	Four manifolds
Meets area requirements except for depth	Phase shifter redesign
Beam steering unit is not complex	Phase shifter count (4/element)
Butler matrix (128-element rectangular aperture)	
Meets area requirements except for depth	Complex and large switching matrix
Symmetry of matrices	13.5-dB sidelobes
Lowest noise figure (8.6 dB)	Largest component count
Lowest transmit power requirement (2.2 watts)	Most complex beam steering unit
Phase – amplitude steered multibeam array (96-element circular aperture)	
Best growth potential	0.0-dB sidelobes
Meets area requirements except for depth	Phase shifter and attenuator bit size
Lowest component count	Frequency isolation
Lowest weight	Stable LO required
Beam steering unit is not complex	Transmit power requirement 12.6 watts or 2.8 watts with alternate approach

TABLE 4-7. TRADEOFF OF APPROACHES WITH AMPLIFIERS

	Normalized Cost per Unit	Phased Array		Butler Matrix		Phase-Amplitude	
		Quantity	Cost	Quantity	Cost	Quantity	Cost
Elements	0.066	96	6.336	128	8.448	96	6.336
Phase shifters	0.266	348	92.568	0	0.0	96	25.536
Attenuators	0.266	4	1.064	4	1.064	96	25.536
Filters	0.066	100	6.6	132	8.712	101	6.666
Amplifiers	1.000	100	100.0	132	132.0	97	97.0
Switches	0.133	0	0.0	892	118.636	0	0.0
Array area (cm^2)	–	173.89	–	185.4	–	173.89	–
Weight (kg)	–	28.0	–	226.0	–	27.0	–
Noise figure (dB)	–	9.1	–	8.9	–	9.1	–
Transmit power (watts)	–	3.25	–	2.2	–	2.8	–
Relative cost			206.568		268.860		161.074
Normalized cost			1.282		1.669		1.0

SECTION V
PHASE-AMPLITUDE STEERED MULTIBEAM ARRAY SYSTEM DEFINITION

A. PHASE-AMPLITUDE STEERED MULTIBEAM ARRAY PATTERNS

The phase-amplitude steered multibeam array is a technique by which multiple simultaneous beams can be electronically steered from a single aperture. This capability will permit independent continuous communication with several users such as orbiting satellites, docking vehicles, and earth stations.

The technique described in this report has the capability to scan multiple beams ±60 degrees and the antenna system does not become bulky and heavy, as some of the other antenna systems do when the antenna is required to scan too large scan angles.

This approach offers the flexibility of 1 to 4 beams with an increase in gain of 6 dB if only one beam is selected.

For a planar array configuration, as shown in Figure 5-1, the array radiation pattern $E(\theta,\phi)$ is given by

$$E(\theta, \phi) = \sum_{m} \sum_{n} f_{m,n}(\theta, \phi)\, I_{m,n}\, e^{j\,(md_x \sin\theta \cos\phi + nd_y \sin\theta \sin\phi)}$$

where $F_{m,n}(\theta,\phi)$ is the element pattern

$$d_x = \frac{2\pi}{\lambda}\Delta_x \qquad d_y = \frac{2\pi}{\lambda}\Delta_y$$

$I_{m,n}$ = element excitation

If it is assumed that all elements in the array are identical and mutual coupling is neglected, then the element pattern is the same for all elements and

$$E(\theta, \phi) = f(\theta, \phi) \sum_{m} \sum_{n} I_{m,n}\, e^{j(md_x \sin\theta \cos\phi + nd_y \sin\theta \sin\phi)}$$

To scan the array pattern to some angle θ_1, ϕ_1, the element excitation $I_{m,n}$ becomes

$$I_{m,n} = i_{m,n}\, e^{-j(md_x \sin\theta_1 \cos\phi_1 + nd_y \sin\theta_1 \sin\phi_1)}$$

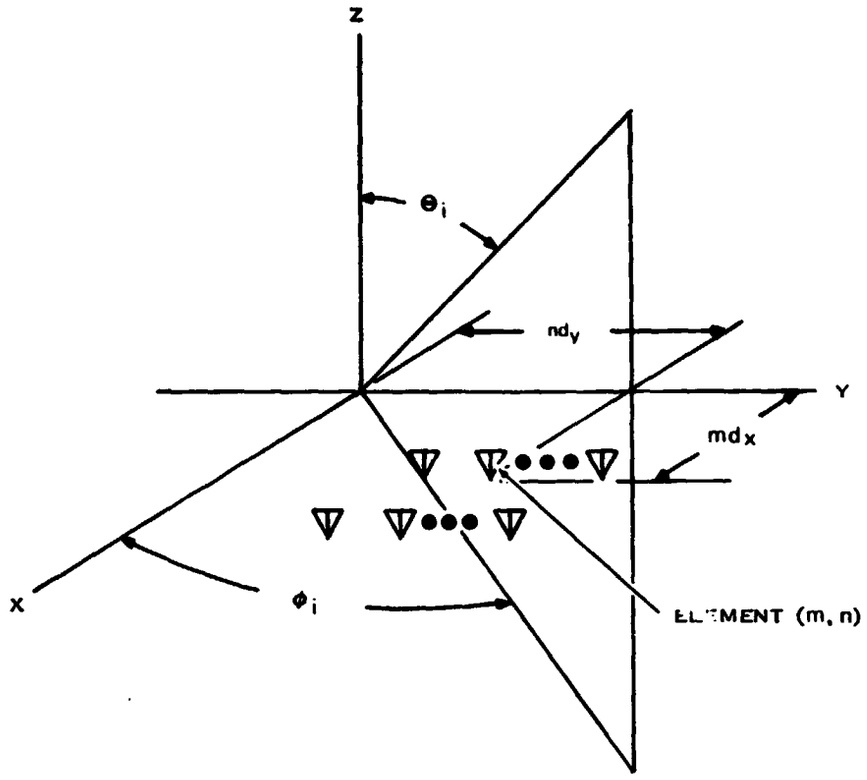

217536

Figure 5-1. Planar Array Geometry

For a single beam antenna this array excitation would be calculated in the beam steering computer and then transferred to the phase shifters and attenuators.

For the four beam antenna, four similar type calculations will be combined in a single algorithm to compute the array excitation.

$$I_{m,n} = \sum_{j=1}^{4} i_{j(m,n)} \, e^{-j(md_x \sin\theta_j \cos\phi_j + nd_y \sin\theta_j \sin\phi_j)}$$

Each of the above terms will be at a separate frequency.

Since comprehensive system parameters are not available, the exact excitation algorithm was not developed. Initial analysis has shown that for larger scan angles the beam tends to overscan by a few degrees. Thus, the final algorithm would contain a scan correction to eliminate this situation. Also, the phase shifter and attenuator responses will vary with frequency and this must be taken into account in the final algorithm. The array pattern calculations presented in this section used the linear array form of the above algorithm to compute the array excitation, and for simplicity all beams were assumed to be at the same frequency. In addition to this, a uniform amplitude distribution was used to form the excitation across the array although a taper could have been used to improve the sidelobe levels.

A 96-element circular aperture would have approximately 11 elements in one plane across the array. Figure 5-2 is a simplified block diagram of the approach for an 11-element case.

The beam steering computer sends the angular direction information to the beam steering controller, which in turn sets the phase shifters and attenuators to the correct phase and amplitude distribution across the array to form the multibeam pattern. The steering hardware has the capability of changing the amplitude of any or all of the beams. A one-dimensional linear array program was used to generate the radiation patterns from the array. The linear array analysis is probably a worst case since the beams are all in the same plane and overlap each other. In a more realistic case, the beams would not be in the same plane and would not overlap each other. The program has the capability of forming any or all of the four beams at any of the scan angles from −60 to +60 degrees. The input parameters for the program include the number of bits for the attenuator and phase shifter and the range of the attenuator in dB.

Figure 5-3 is a Calcomp plot of a four-beam pattern from an 11-element array with the peaks located at −60, −30, +10, and +50 degrees. The element spacing is 0.56 λ (0.475 inches) at 14.0 GHz. All the beams are at the same relative amplitude. The range of the attenuator on each element is 30 dB. A 4-bit attenuator with an attenuation range of 30 dB has a step size which is given by:

$$\text{Step Size (dB)} = \frac{\text{Attenuator Range}}{2^{\text{No. of Bits}} - 1} = 2 \text{ dB}$$

The resultant amplitude and phase distribution for this case is tabulated in Table 5-1.

TABLE 5-1. PHASE AND AMPLITUDE DISTRIBUTION FOR A FOUR-BEAM, 11 ELEMENT ARRAY

Element No.	Amplitude (Volts)	Phase (Degrees)
1	0.501	−179.8
2	0.251	−46.7
3	0.631	110.8
4	0.316	34.5
5	0.316	−177.2
6	1.0	0.0
7	0.316	177.2
8	0.316	−34.5
9	0.631	−110.8
10	0.251	46.7
11	0.501	179.8

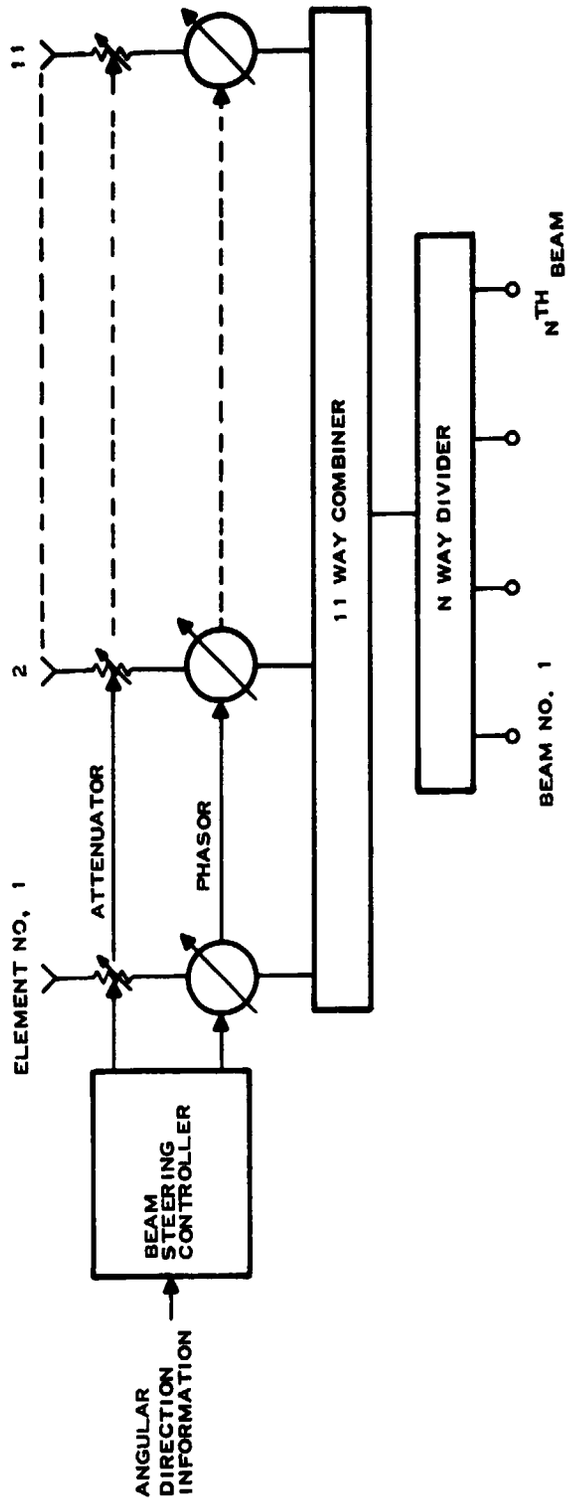

Figure 5-2. Simplified Block Diagram of an 11 Element Phase-Amplitude Steered Multibeam Receiver Array

217537

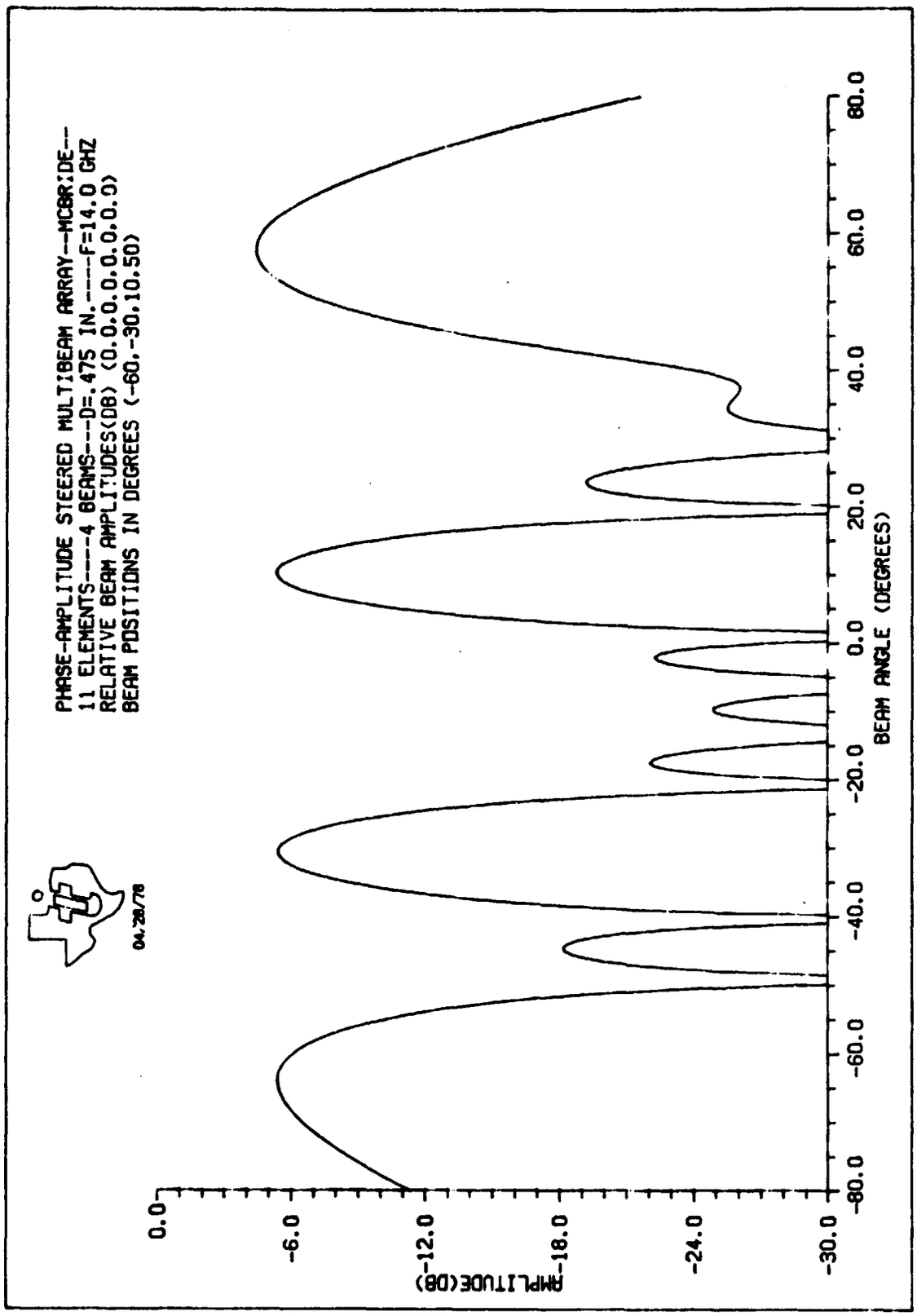

Figure 5-3. Phase-Amplitude Steered Multibeam Array Pattern Case 1

217538

Patterns were calculated for two- and four-beam cases. In both cases, an 8-bit attenuator with a range of 30 dB (step size = 0.117 dB) and an 8-bit phase shifter were used. The 8-bit phase shifter with a range of 360 degrees has a phase step which is given by:

$$\text{Phase Step (degrees)} = \frac{360}{2^8} = 1.4 \text{ degrees}$$

1. Two-Beam Case

In the two-beam case one of the beams was positioned at –45 degrees while the other beam was scanned to +60, +40, +20, 0, –20, and –40 degrees. The patterns for these cases are shown in Figures 5-4 through 5-9. In Figure 5-9 where there is a beam at –45 degrees and –40 degrees, the two beams merge. This is not a problem since the beams would have frequency separation and are on two different channels.

2. Four-Beam Case

In the four-beam case, beam 1 was positioned at –45 degrees, while the other three beams were scanned to the positions indicated in the following table.

Figure No.	Beam 1	Beam 2	Beam 3	Beam 4
5-10	–45°	10°	30°	50°
5-11	–45°	0°	20°	40°
5-12	–45°	–10°	10°	30°
5-13	–45°	–20°	0°	20°
5-14	–45°	–30°	–10°	10°
5-15	–45°	–40°	–20°	0°

Where there is a difference in the calculated pointing direction and amplitude of the beam than what was specified, it is due to the addition of the single component beams across the array.

3. Variable Gain Control

Figure 5-16 is a four-beam pattern with the beams pointing in the same direction as in Figure 5-13, but in this pattern beams 2 and 4 have been attenuated by 6 dB with respect to the other two beams.

4. Beam Normalization

Figure 5-17 is a four-beam pattern with the beams pointing in the same direction as in Figure 5-10, but in this pattern beams 1, 2, and 3 have been normalized to the same amplitude as beam 4.

This normalization feature allows for adjusting the amplitude of the beams when communication links require a more uniform signal at the various angles in space.

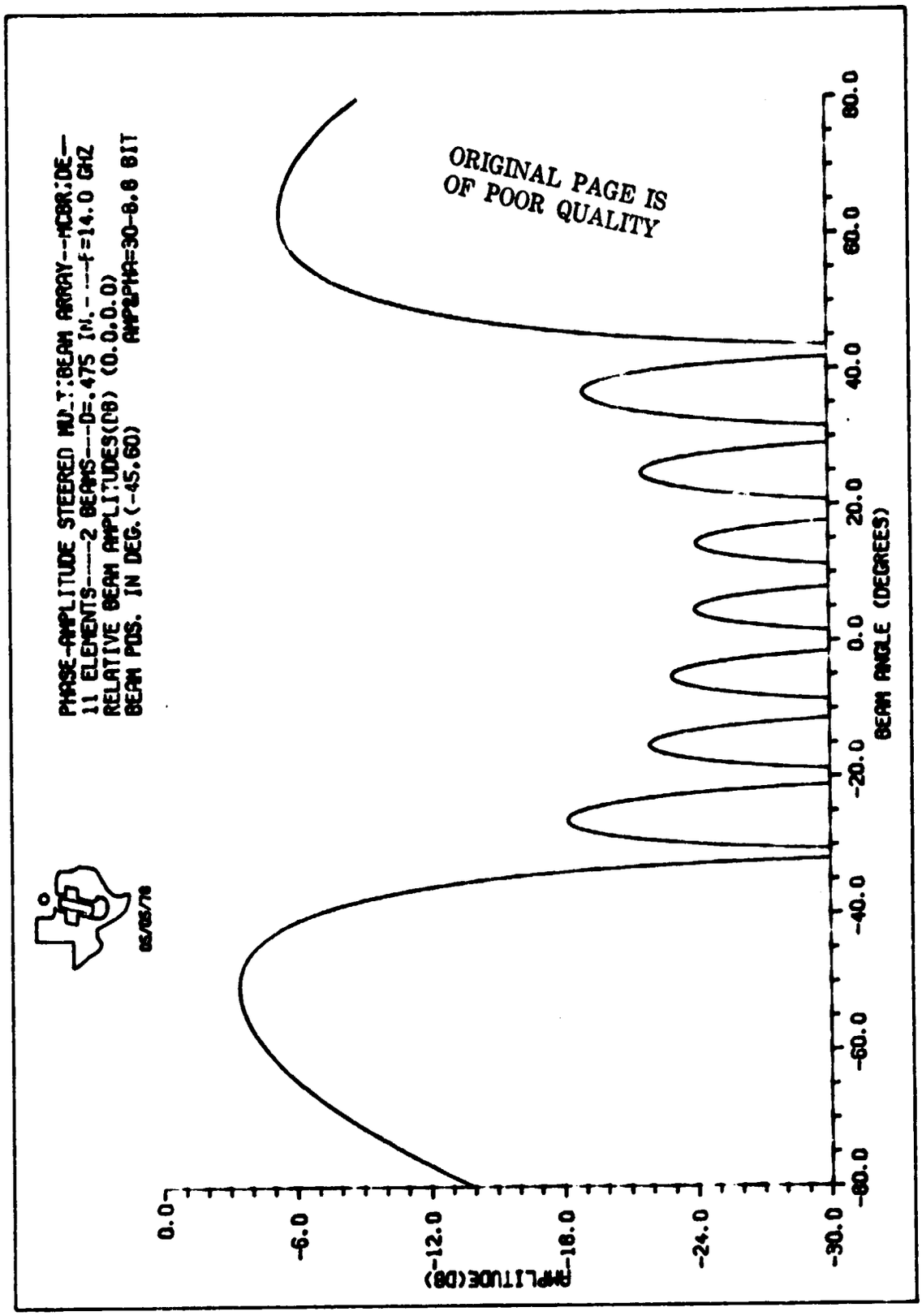

Figure 5-4. Phase-Amplitude Steered Multibeam Array Pattern Case 2

217539

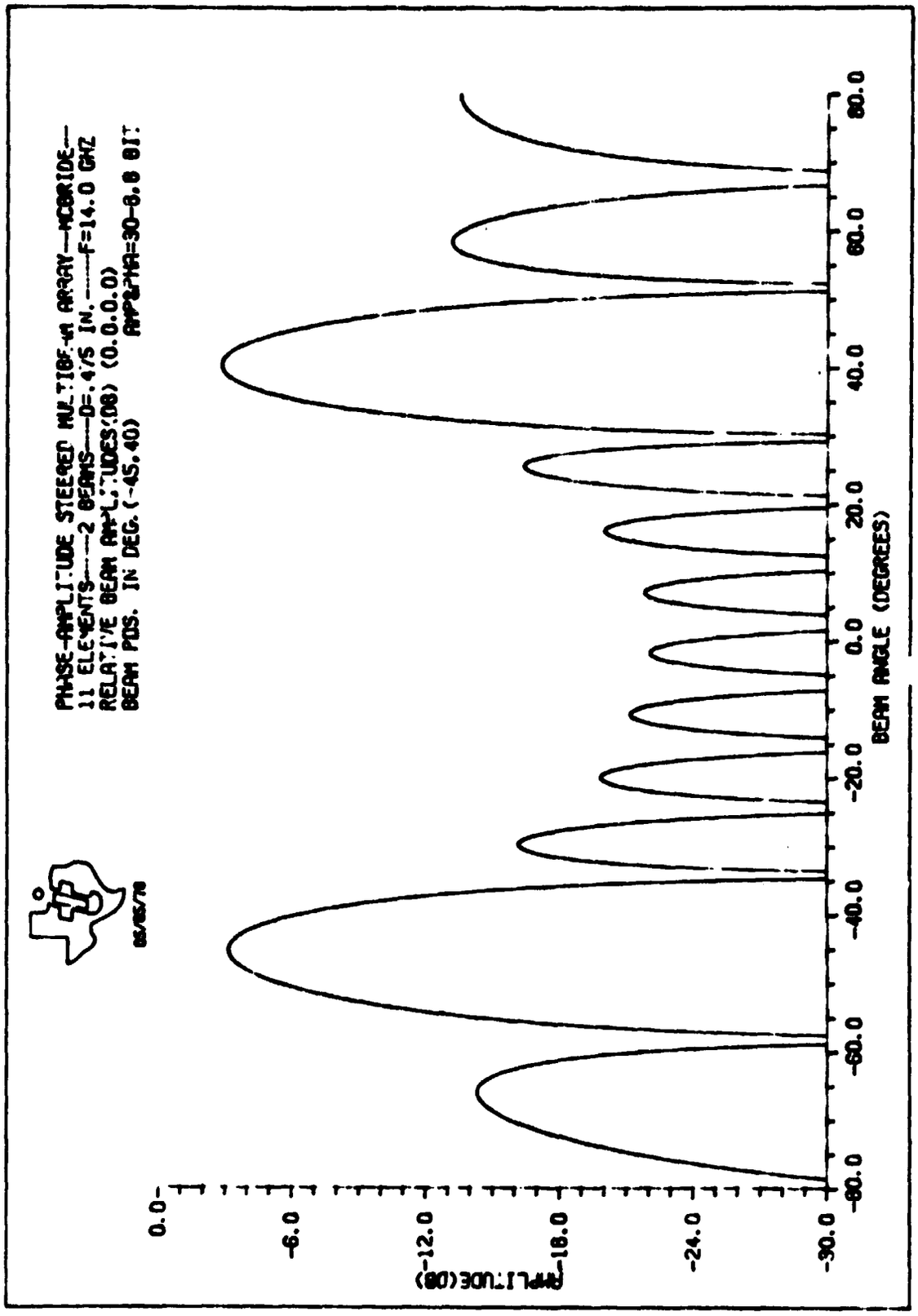

Figure 5-5. Phase-Amplitude Steered Multibeam Array Pattern Case 3

217540

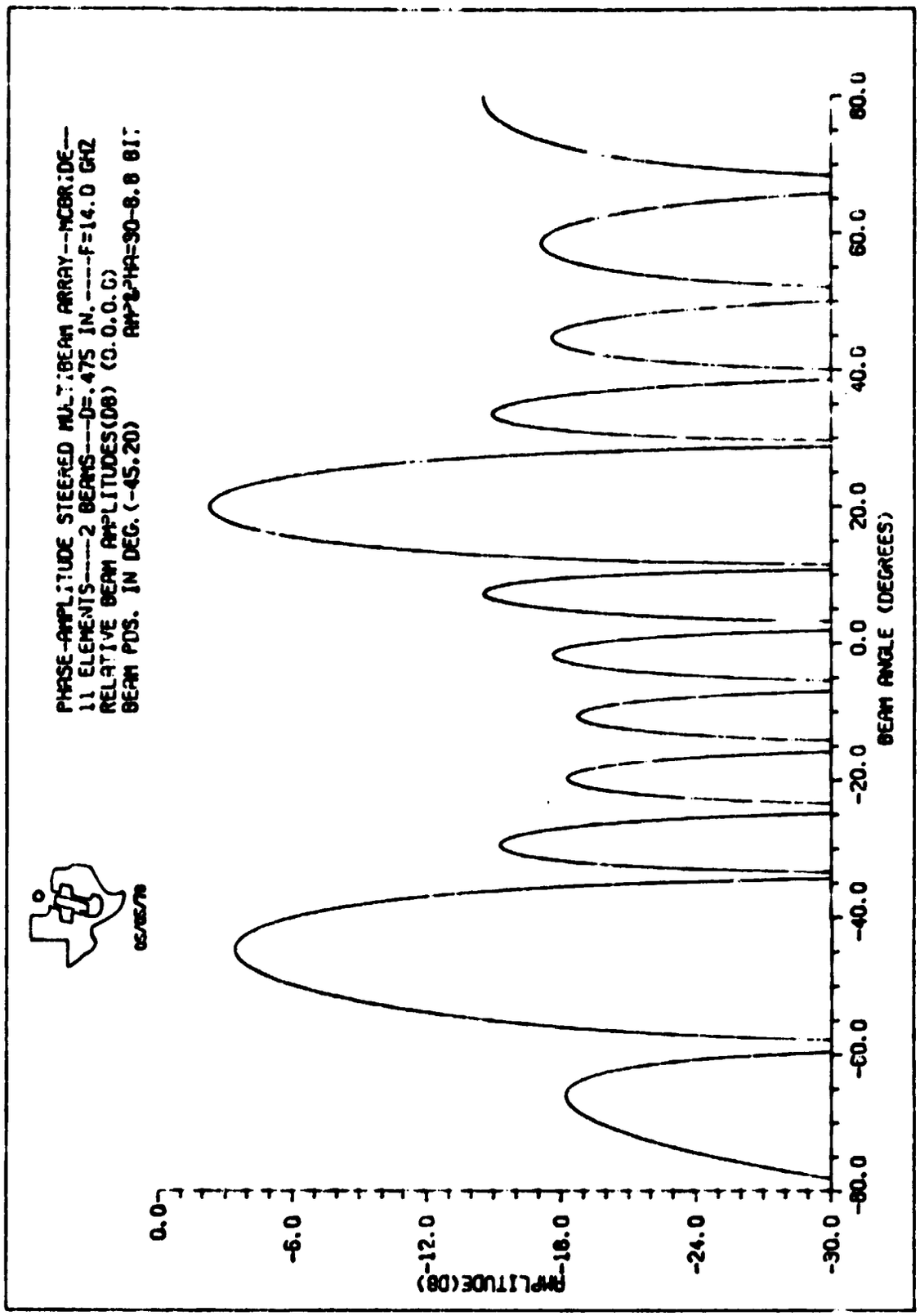

Figure 5-6. Phase-Amplitude Steered Multibeam Array Pattern Case 4

217541

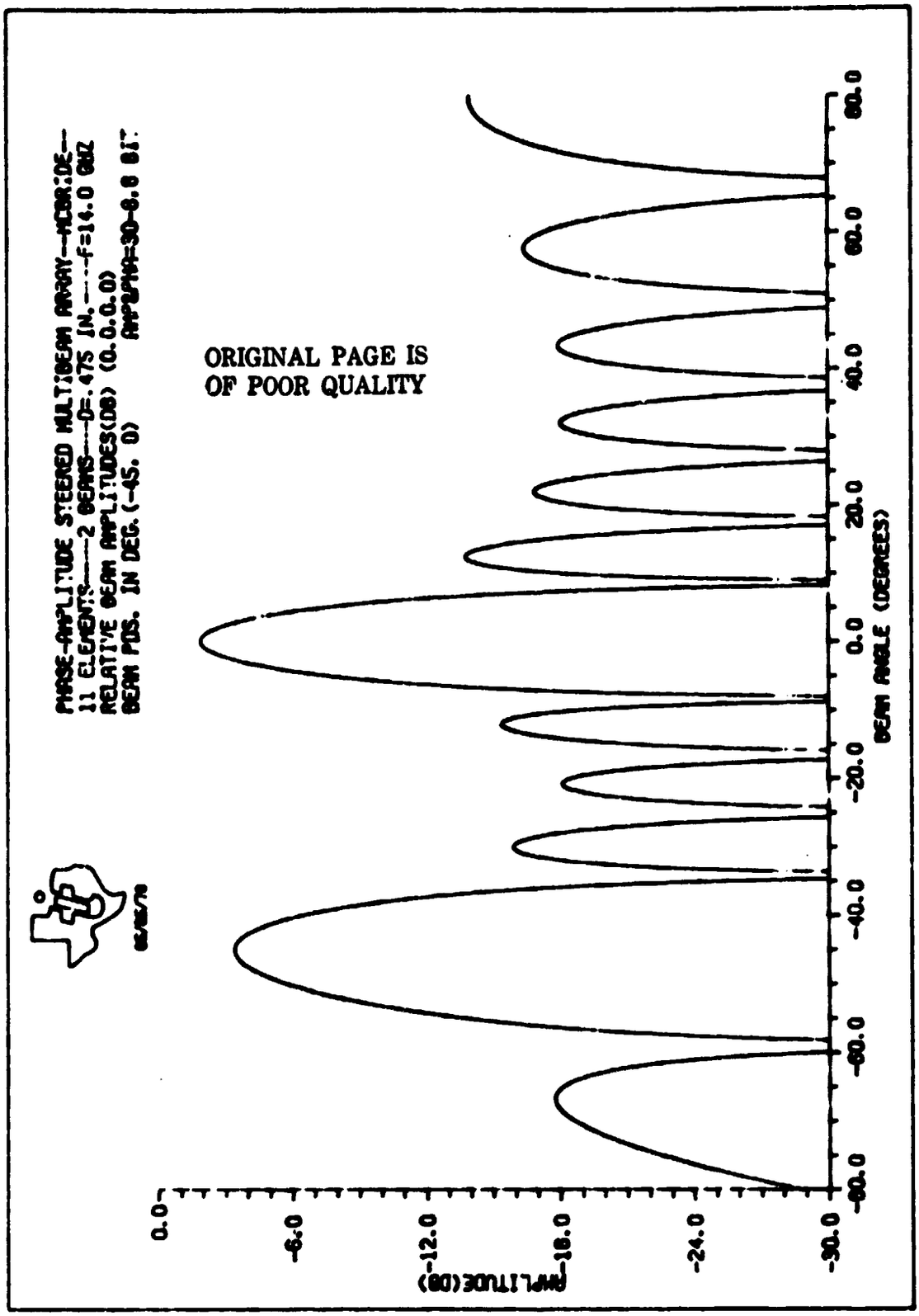

Figure 5-7. Phase-Amplitude Steered Multibeam Array Pattern Case 5

217542

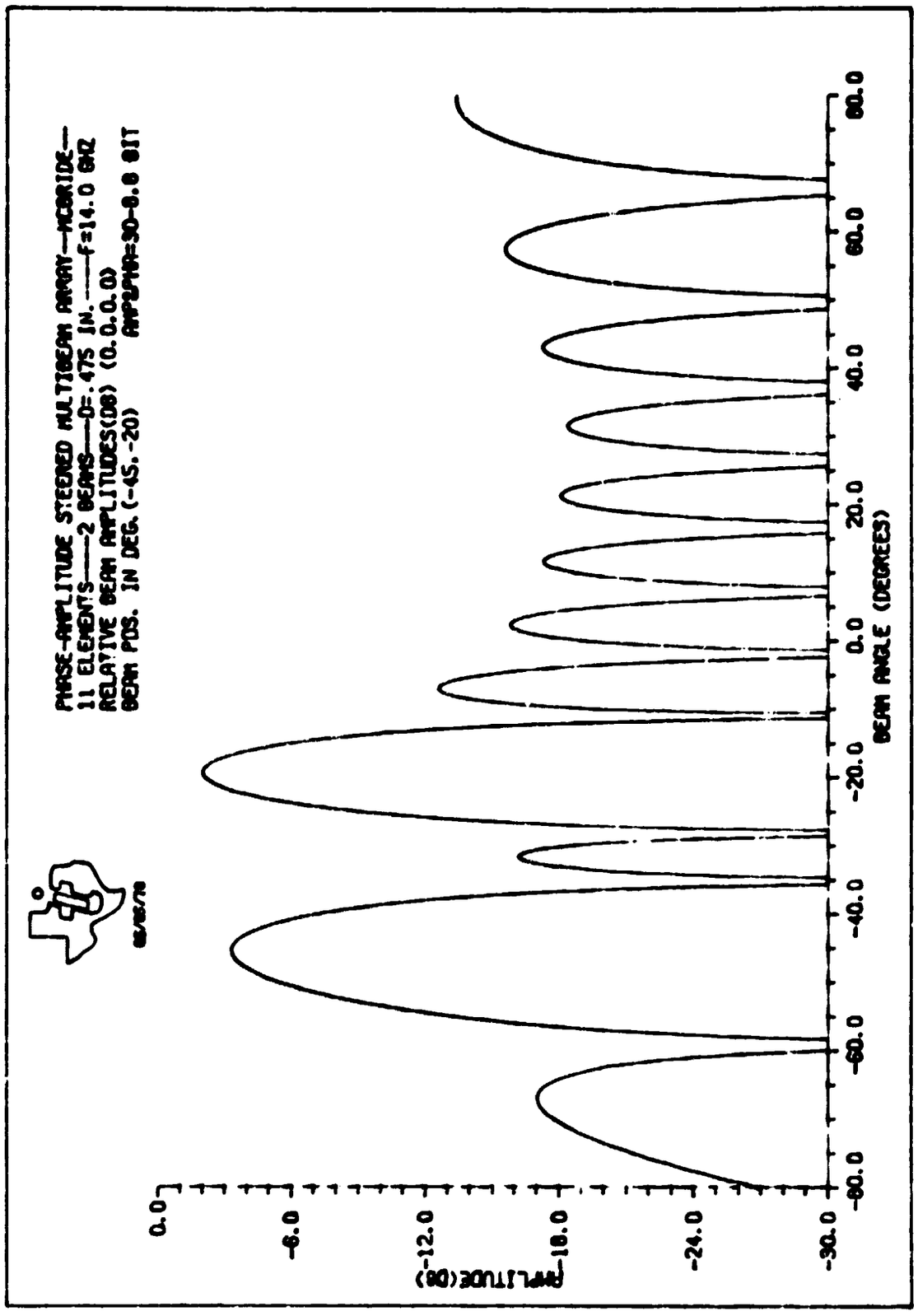

Figure 5-8. Phase-Amplitude Steered Multibeam Array Pattern Case 6

217543

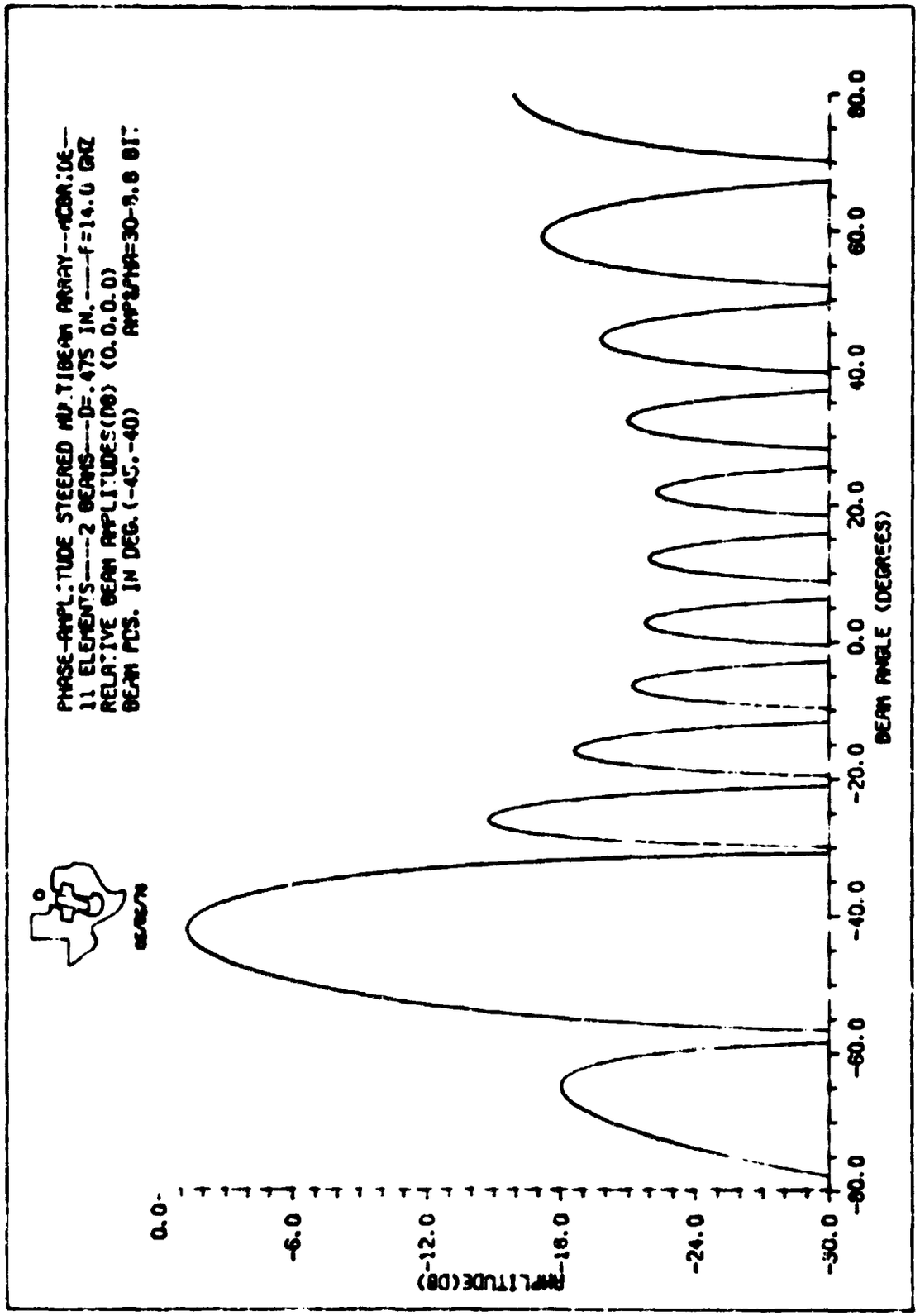

Figure 5-9. Phase-Amplitude Steered Multibeam Array Pattern Case 7

217544

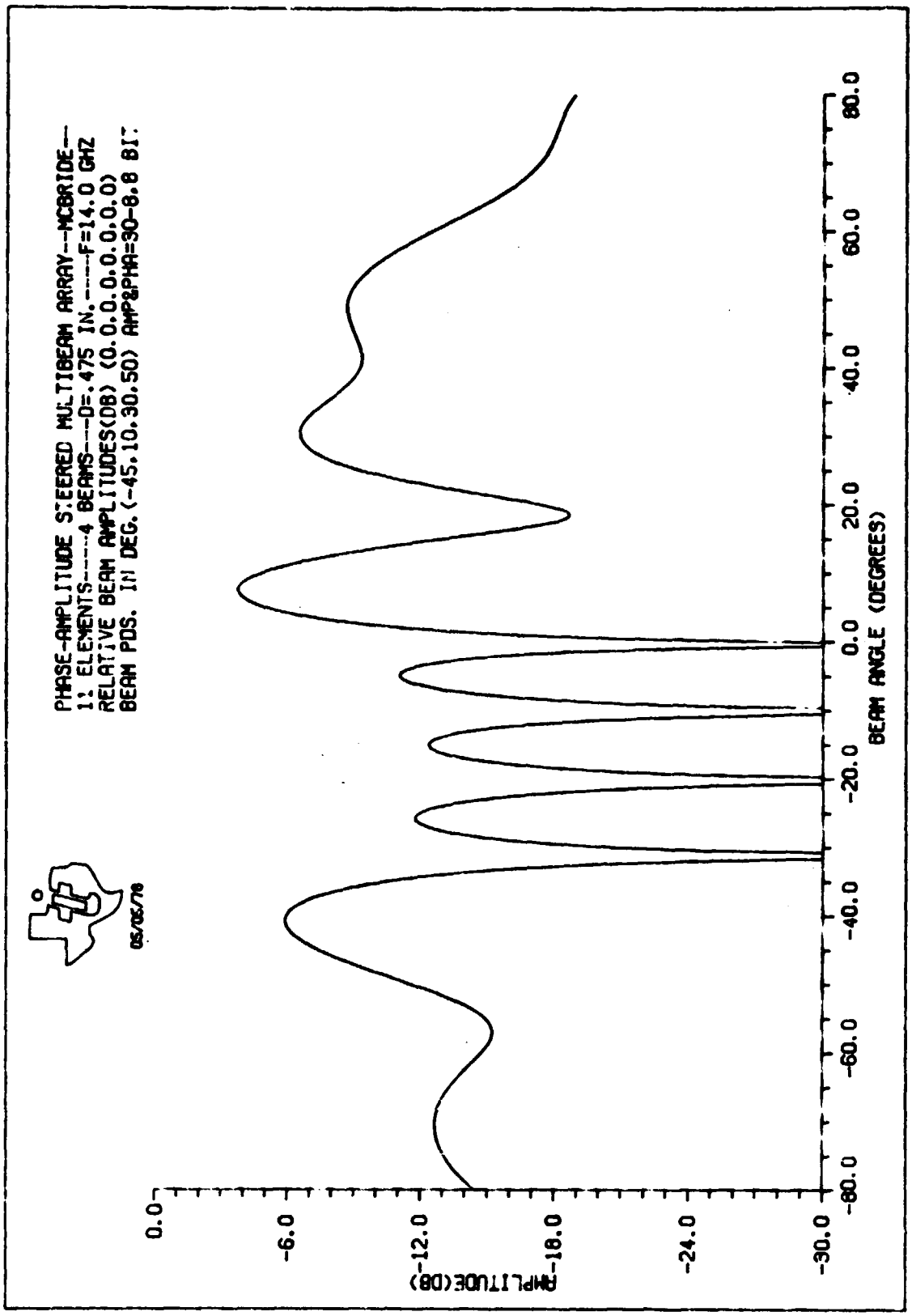

Figure 5-10. Phase-Amplitude Steered Multibeam Array Pattern Case 8

217545

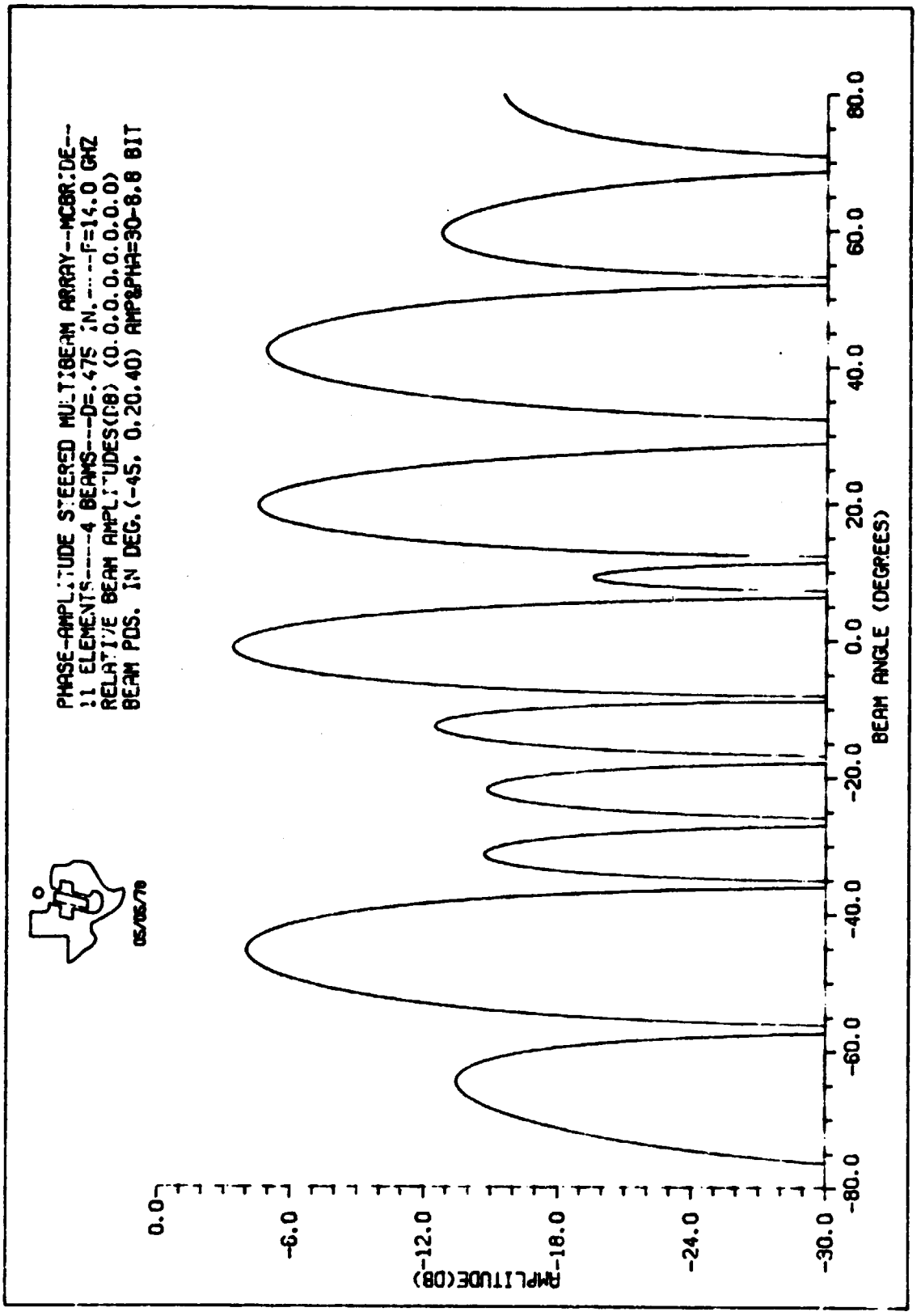

Figure 5-11. Phase-Amplitude Steered Multibeam Array Pattern Case 9

217546

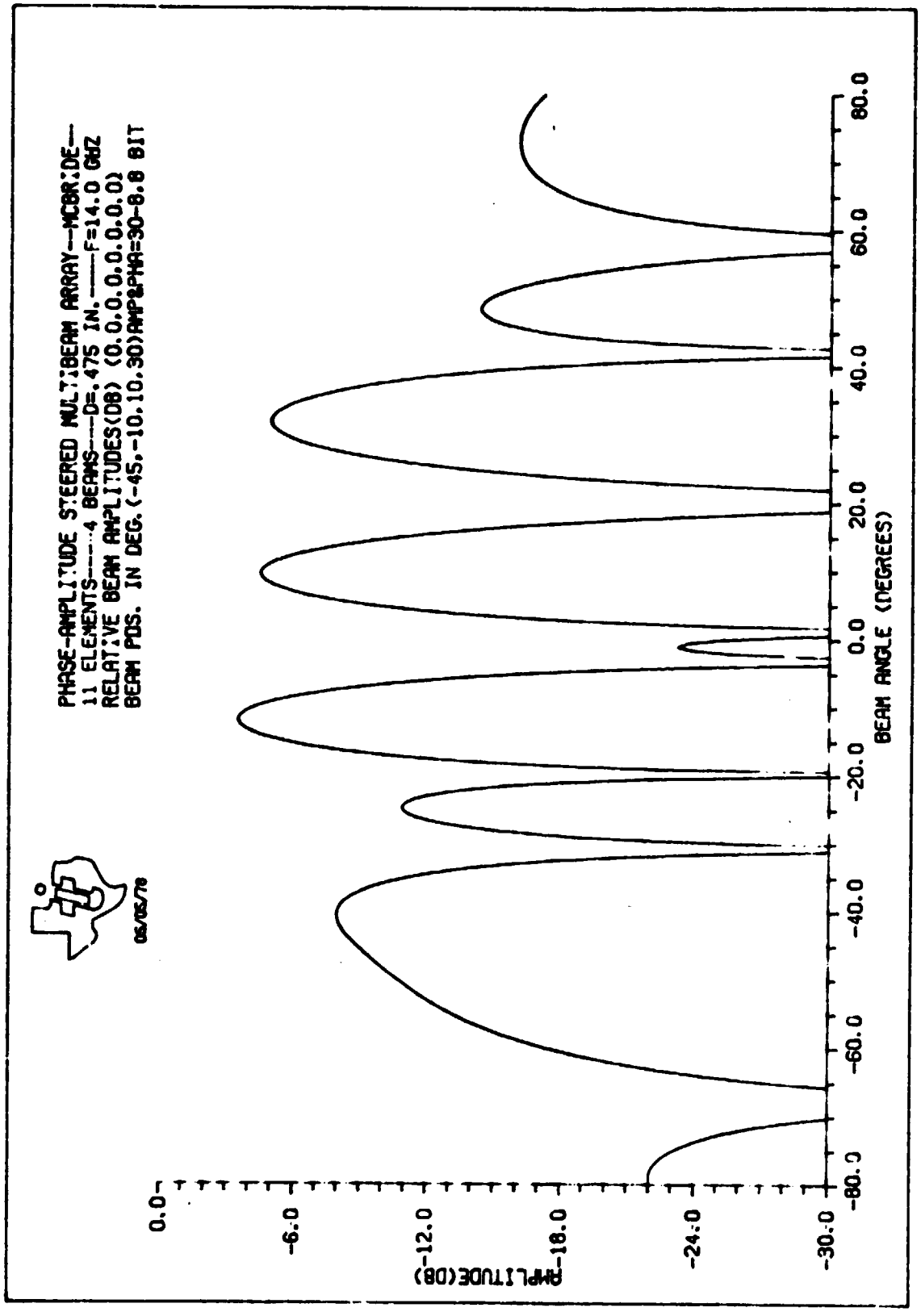

Figure 5-12. Phase-Amplitude Steered Multibeam Array Pattern Case 10

217547

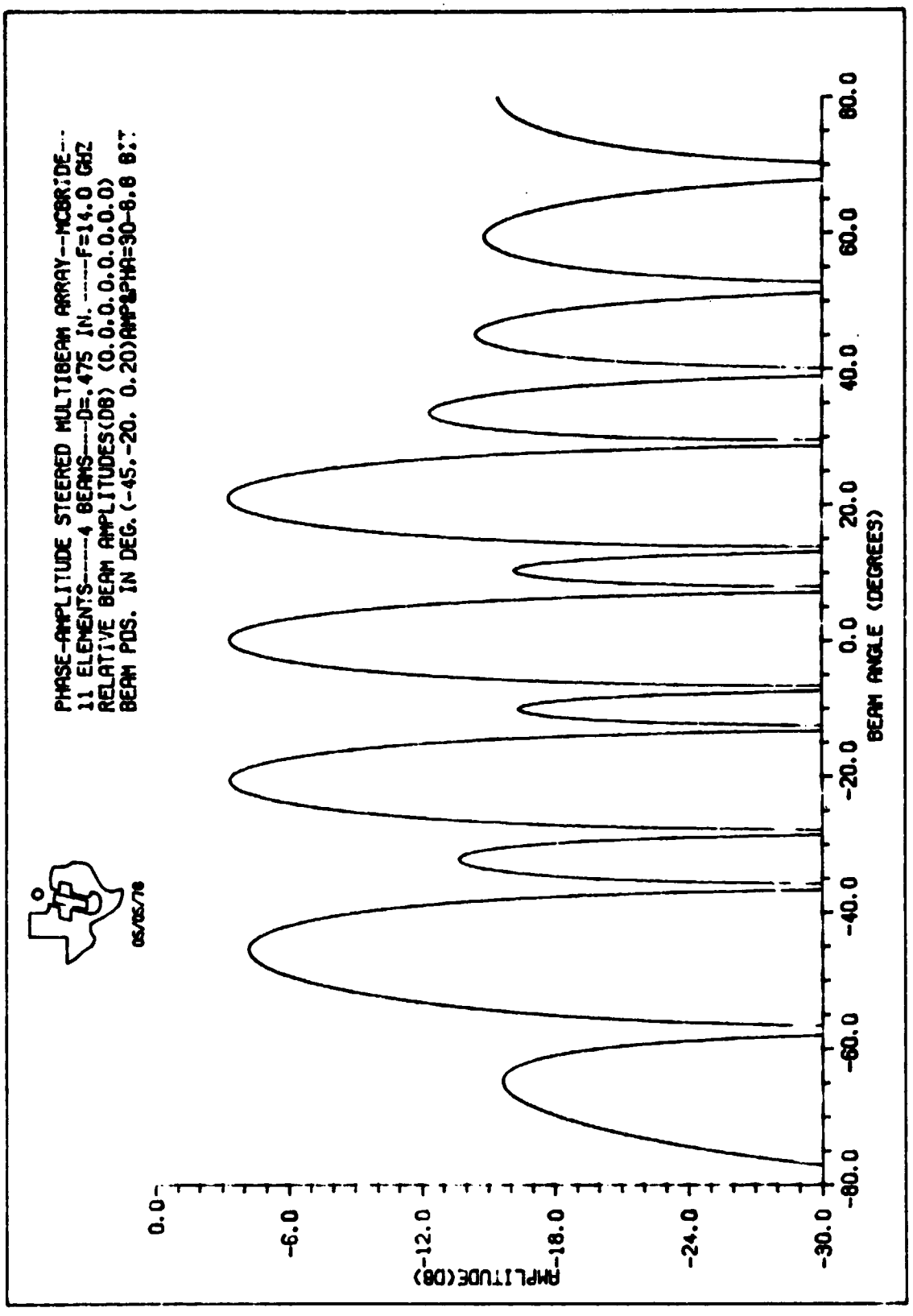

Figure 5-13. Phase-Amplitude Steered Multibeam Array Pattern Case 11

217548

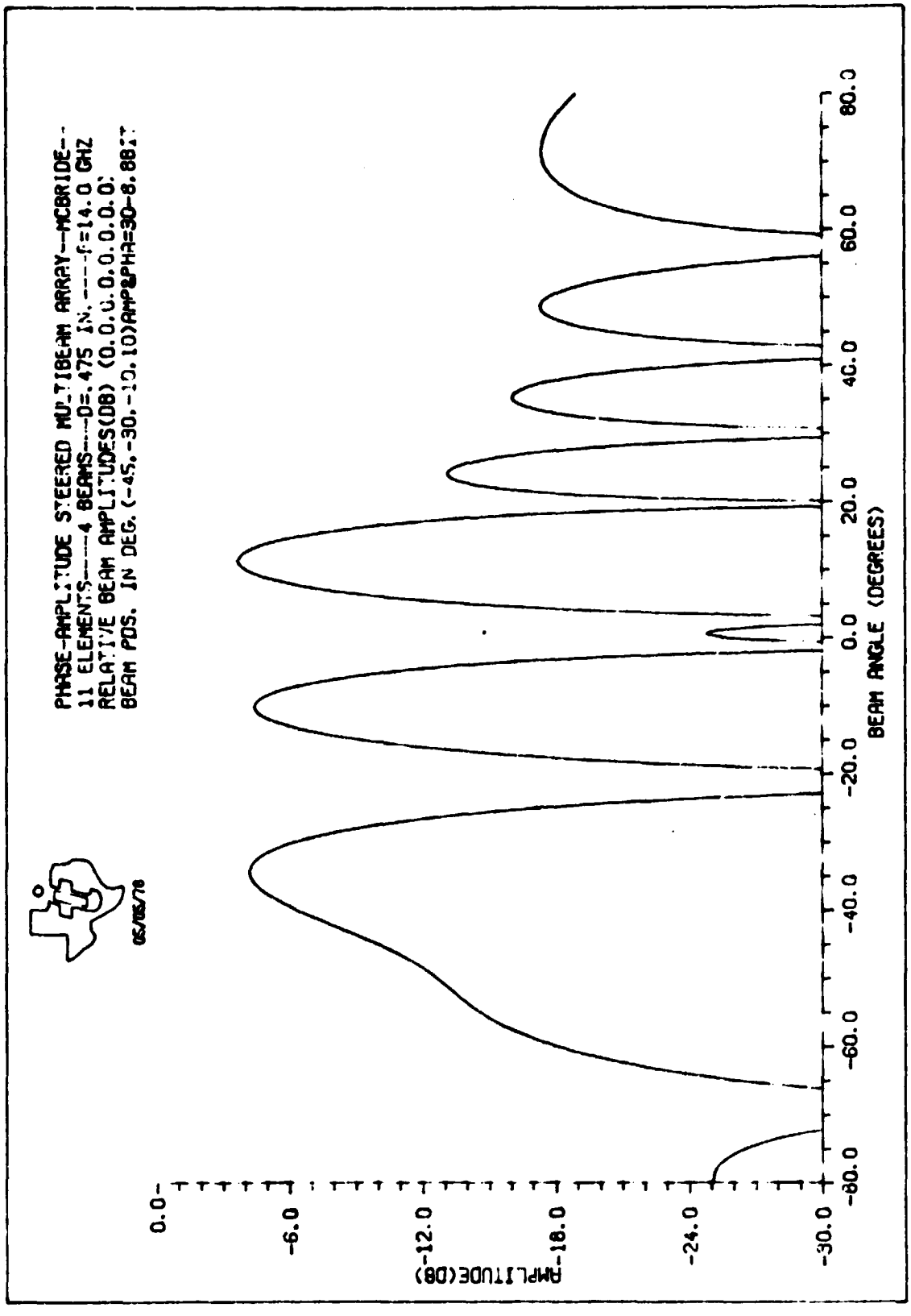

Figure 5-14. Phase-Amplitude Steered Multibeam Array Pattern Case 12

217549

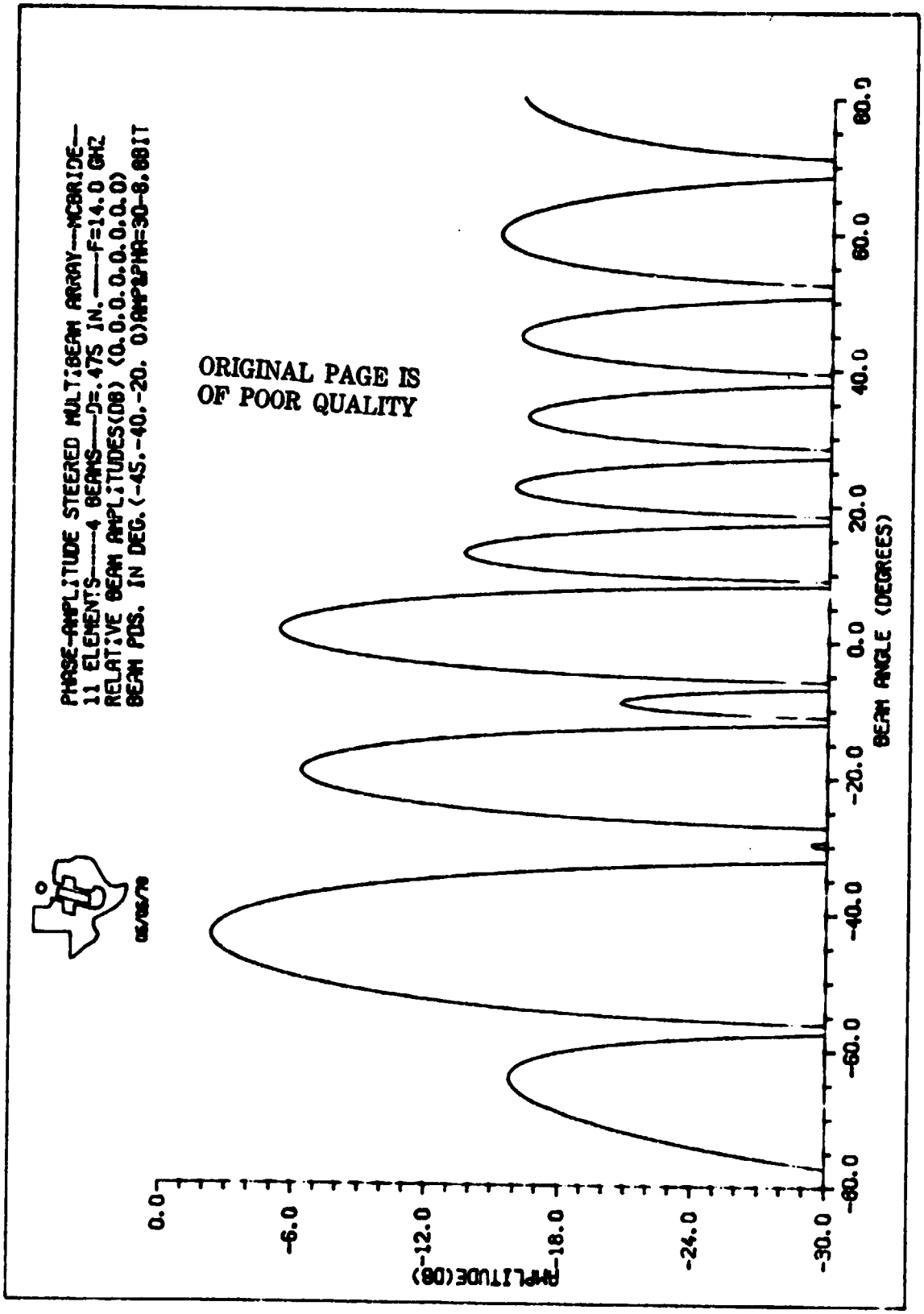

Figure 5-15. Phase-Amplitude Steered Multibeam Array Pattern Case 13

217550

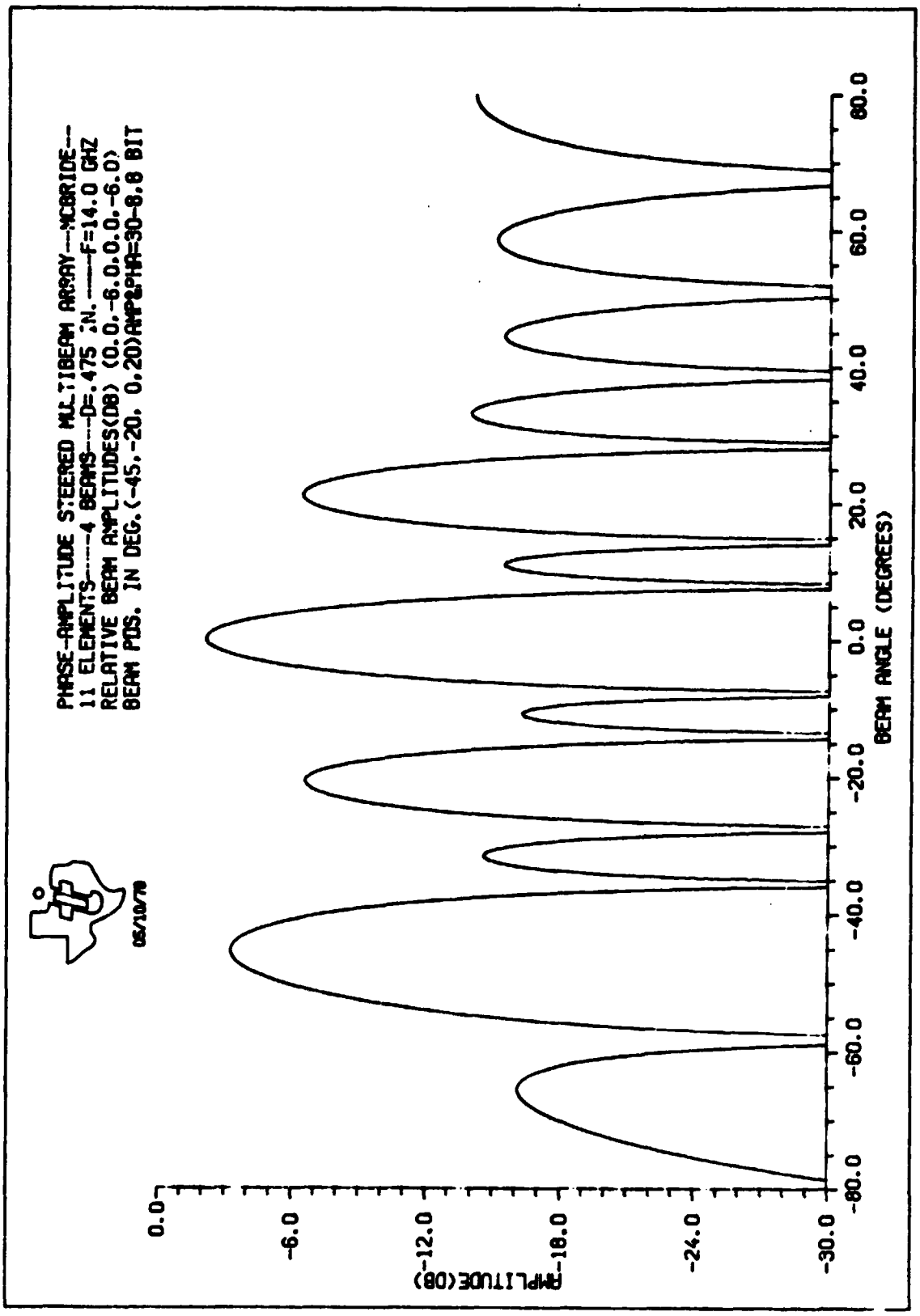

Figure 5-16. Phase-Amplitude Steered Multibeam Array Pattern Case 14

217551

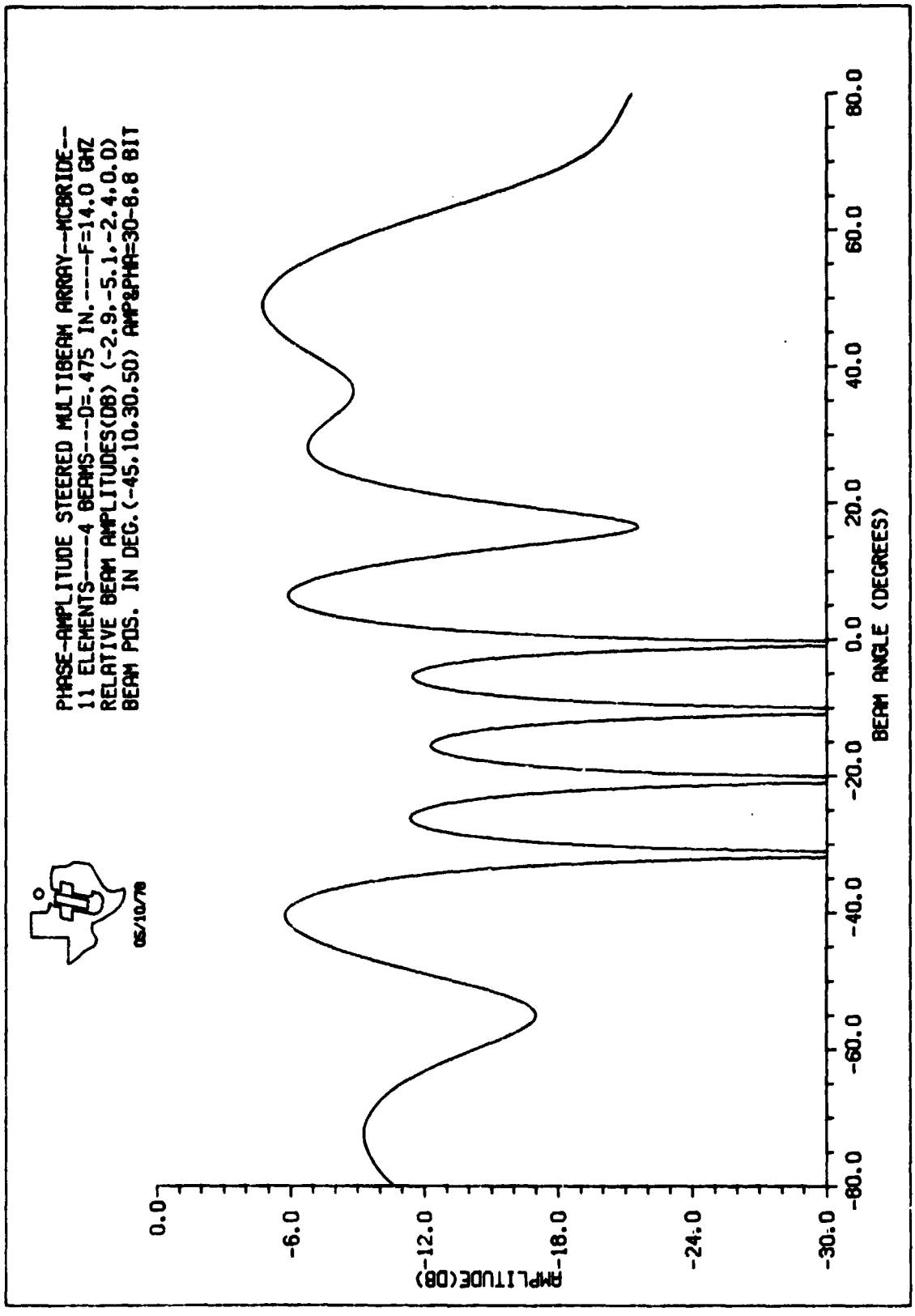

Figure 5-17. Phase-Amplitude Steered Multibeam Array Pattern Case 15

217552

5. Attenuator and Phase Shifter Bit Size

To determine the required bit size of the attenuator and phase shifter, a series of patterns was calculated with different bit sizes. The step sizes of these components affect the amplitude and pointing direction of the main beams as well as the sidelobes. Figures 5-18 through 5-21 are four-beam patterns with a 30-dB attenuator range and 2, 4, 6, and 8 bits respectively. In each of these cases the phase was ideal and not quantized.

Figures 5-22 through 5-25 are the same four-beam patterns as the previous four with 2, 3, 4, and 8 bit (phase step = 90, 45, 22.5, and 1.4 degrees) phase shifters. In each of these cases the amplitude was ideal and not quantized.

Figures 5-26 through 5-29 are patterns with a 30-dB, 6-bit attenuator and the bit size of the phase shifter is 2, 3, 4, and 8 respectively.

Figures 5-30 through 5-33 are patterns with a 30-dB, 8-bit attenuator and the bit size of the phase shifter is 2, 3, 4, and 8 respectively.

Examination of the beam shape, amplitude, and pointing of the main beams and the amplitude of the sidelobes indicates that a 30-dB, 6-bit attenuator and a 4-bit phase shifter is required for this array, but a more detailed analysis should be completed when more complete mission requirements are established.

B. BEAM STEERING COMPUTER

A beam steering computer (BSC) would be used to control the pointing of the four simultaneous beams. The computer design would be based on the requirements for controlling the beams. The primary requirements that will determine the size and complexity of the computer are as follows:

- The update rate for different beams
- The time allowed for moving from one beam position to another
- Whether beams are updated simultaneously or individually.

The above three items play a critical role in the design and implementation of the BSC. Slower update rates (i.e., time between commands to change pointing angle) allow the use of a microprocessor-based computer design, whereas fast update rates may require a discrete IC implementation. If all four beams must be updated simultaneously, the BSC will be considerably more complex than one to update the beams one at a time.

The speed at which the update must be performed also relates to power consumption. If a microprocessor based design can accomplish the updates in the required time, less power would probably be used than with a discrete implementation of the BSC. Increased speed usually relates directly to increased power consumption.

A system which updates one beam at a time will be easier to expand to more beams than the system that would update all beams simultaneously. The same computational logic can be used for expansion of the single beam update system where the simultaneous update system would require a duplication of circuitry for each additional beam to be controlled. Both systems will require additional hardware, but the simultaneous update approach will require the most additional hardware.

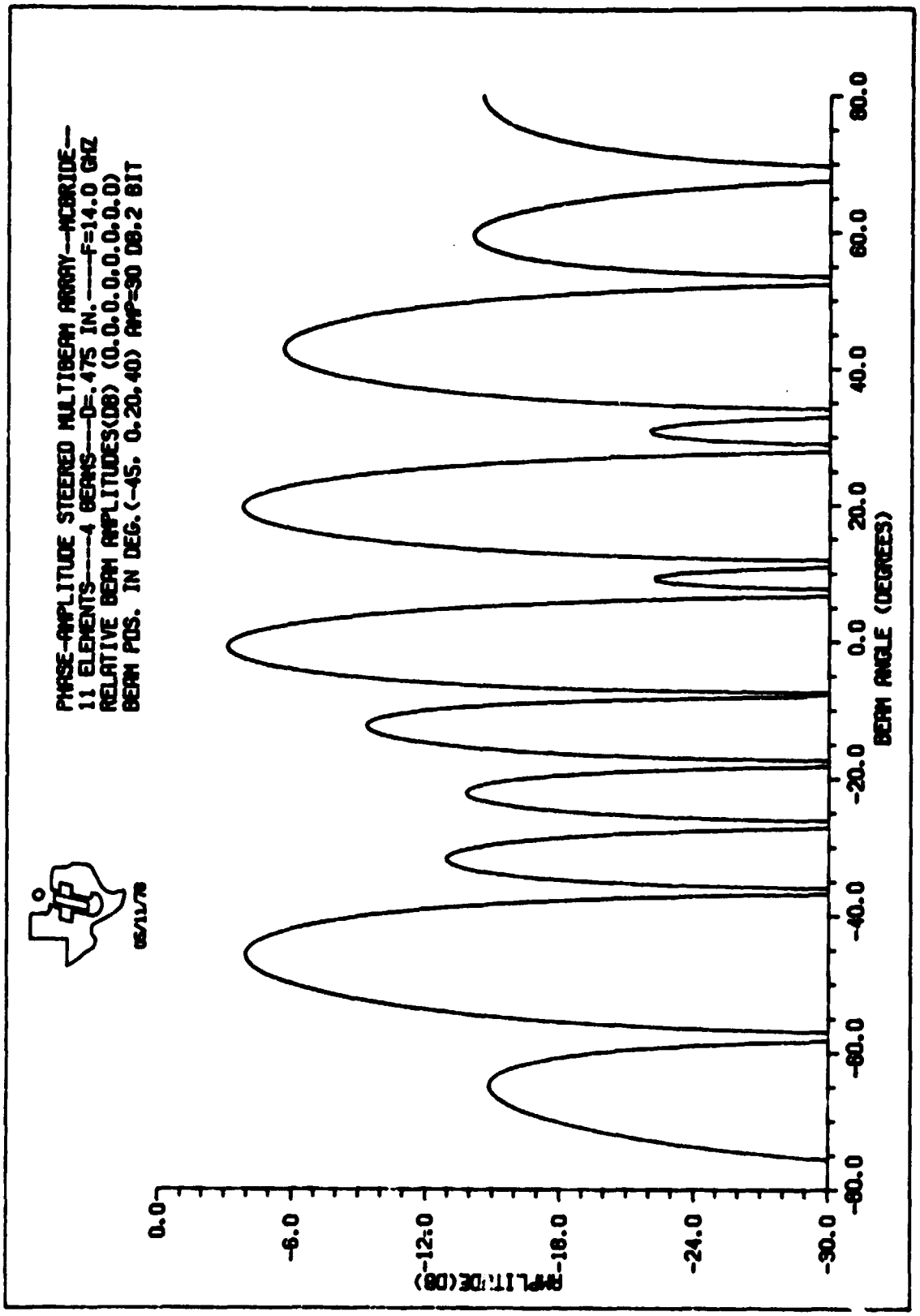

Figure 5-18. Phase-Amplitude Steered Multibeam Array Pattern Case 16

217553

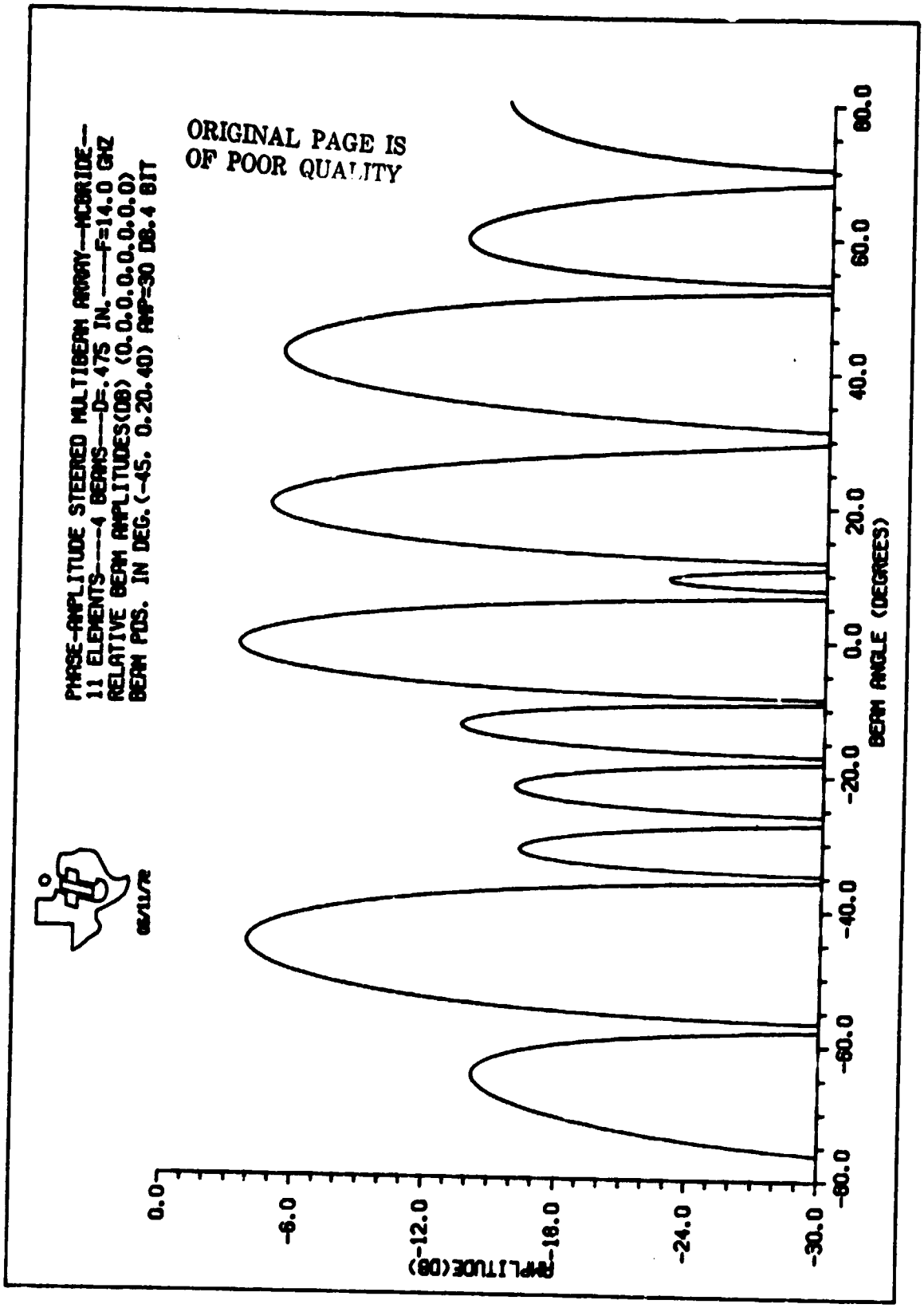

Figure 5-19. Phase-Amplitude Steered Multibeam Array Pattern Case 17

217554

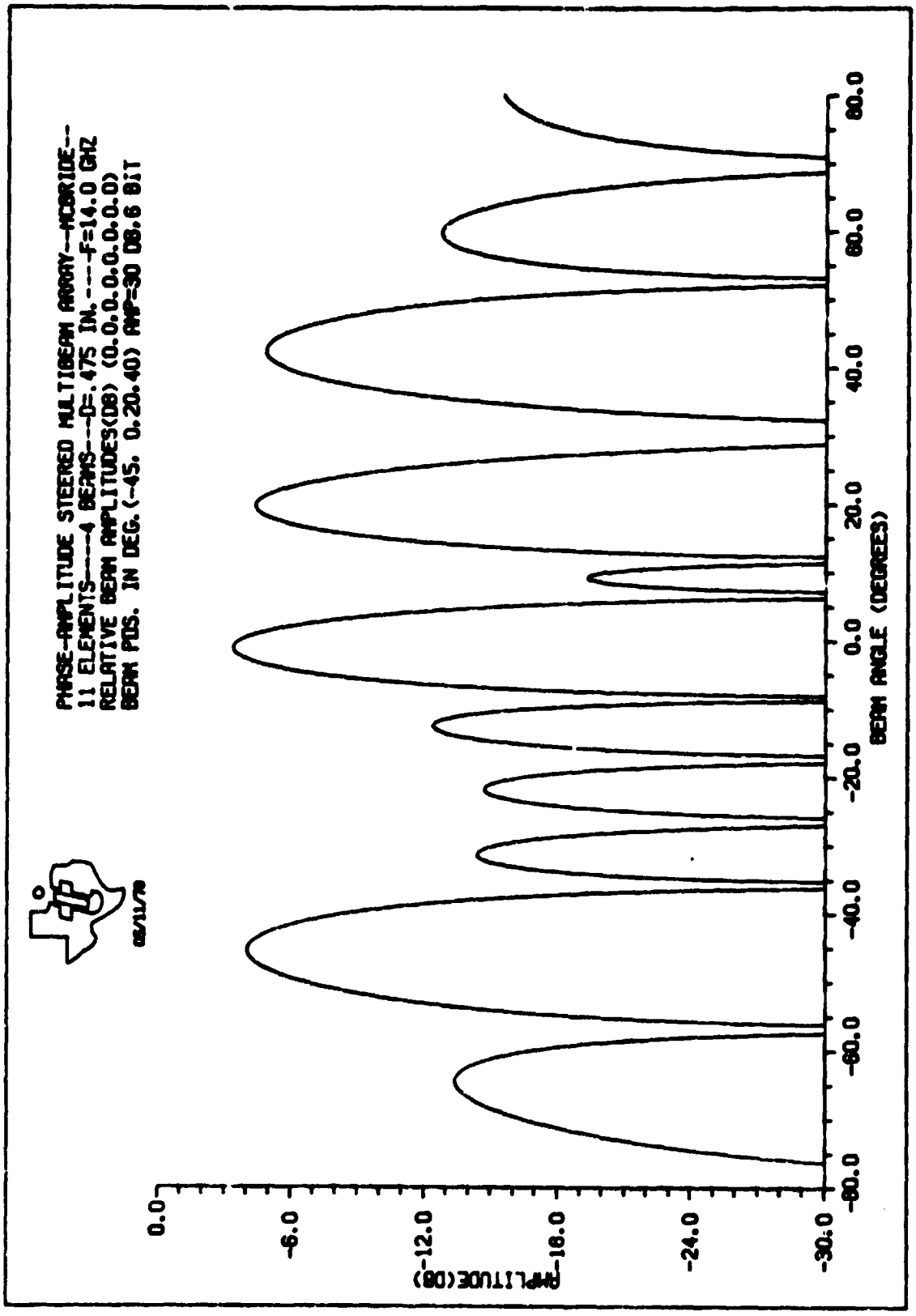

Figure 5-20. Phase-Amplitude Steered Multibeam Array Pattern Case 18

217555

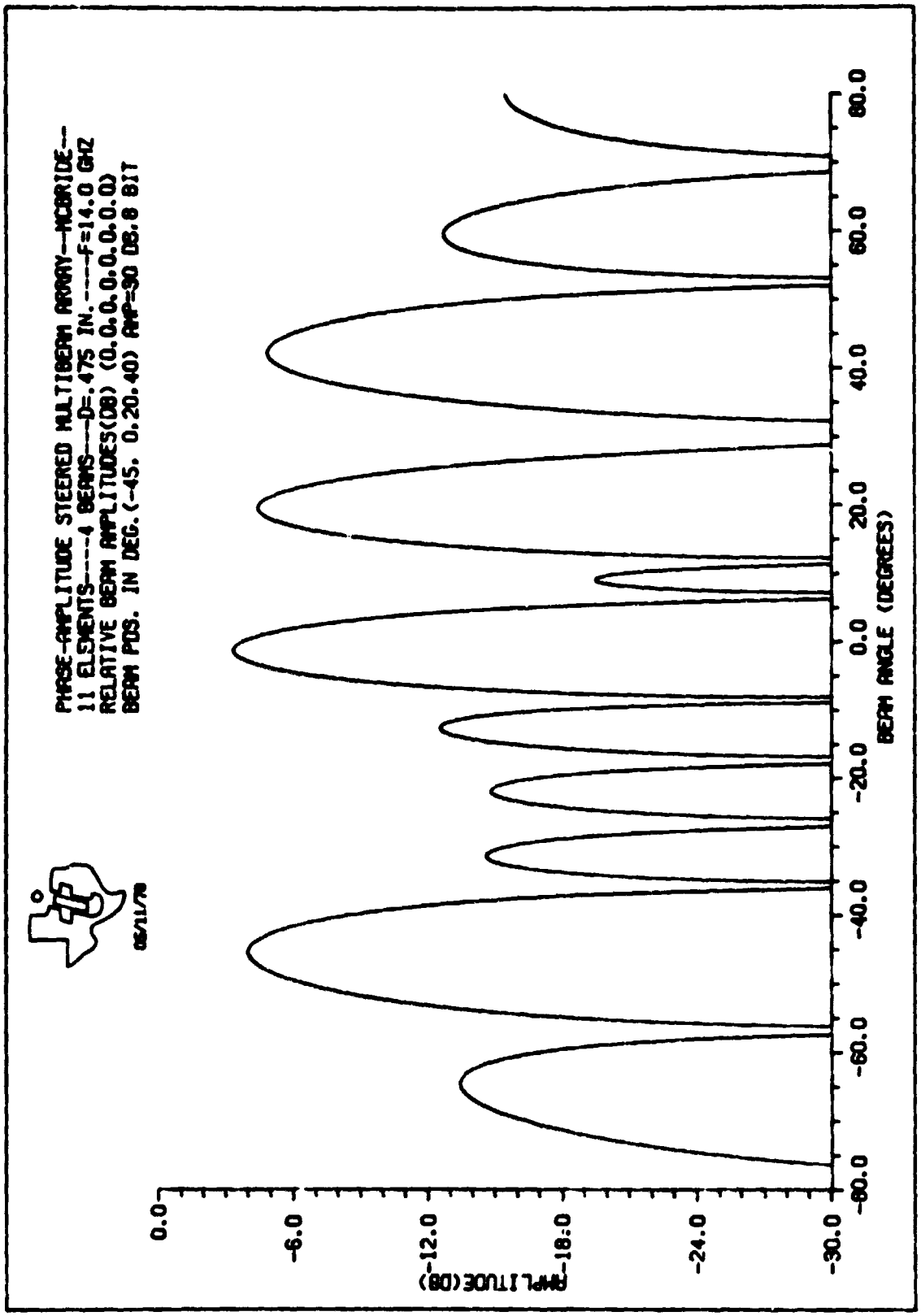

Figure 5-21. Phase-Amplitude Steered Multibeam Array Pattern Case 19

217556

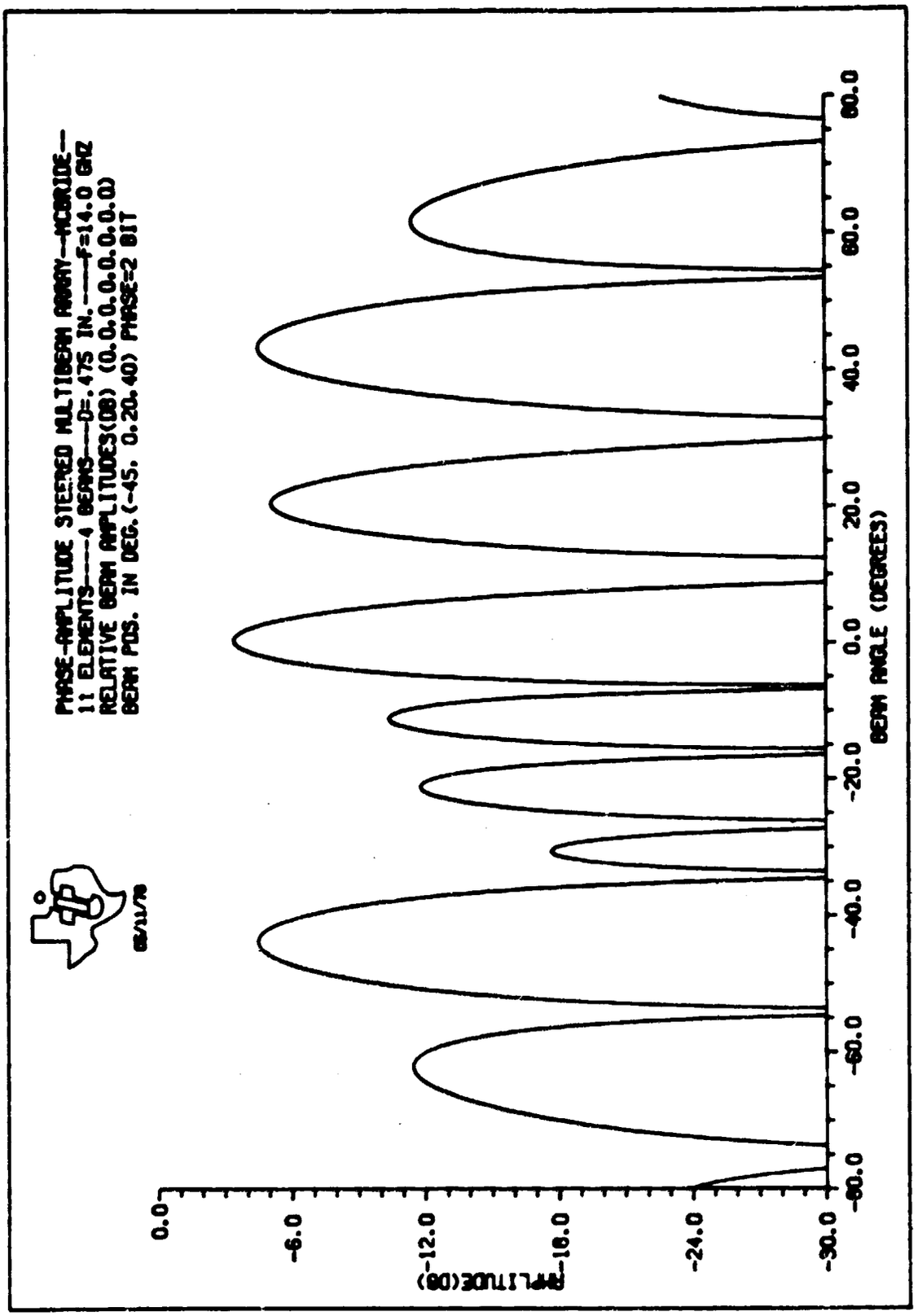

Figure 5-22. Phase-Amplitude Steered Multibeam Array Pattern Case 20

217557

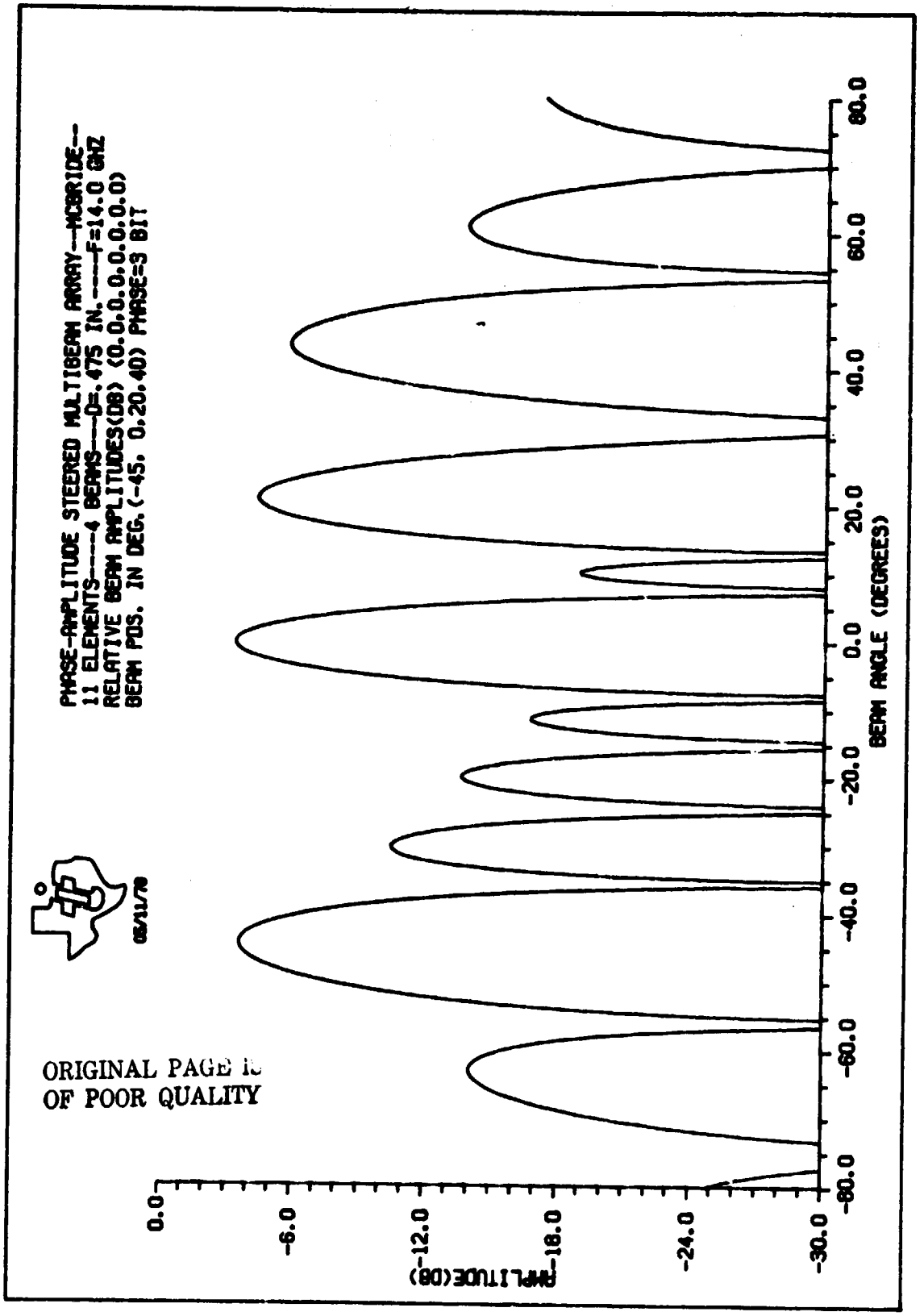

Figure 5-23. Phase-Amplitude Steered Multibeam Array Pattern Case 21

217558

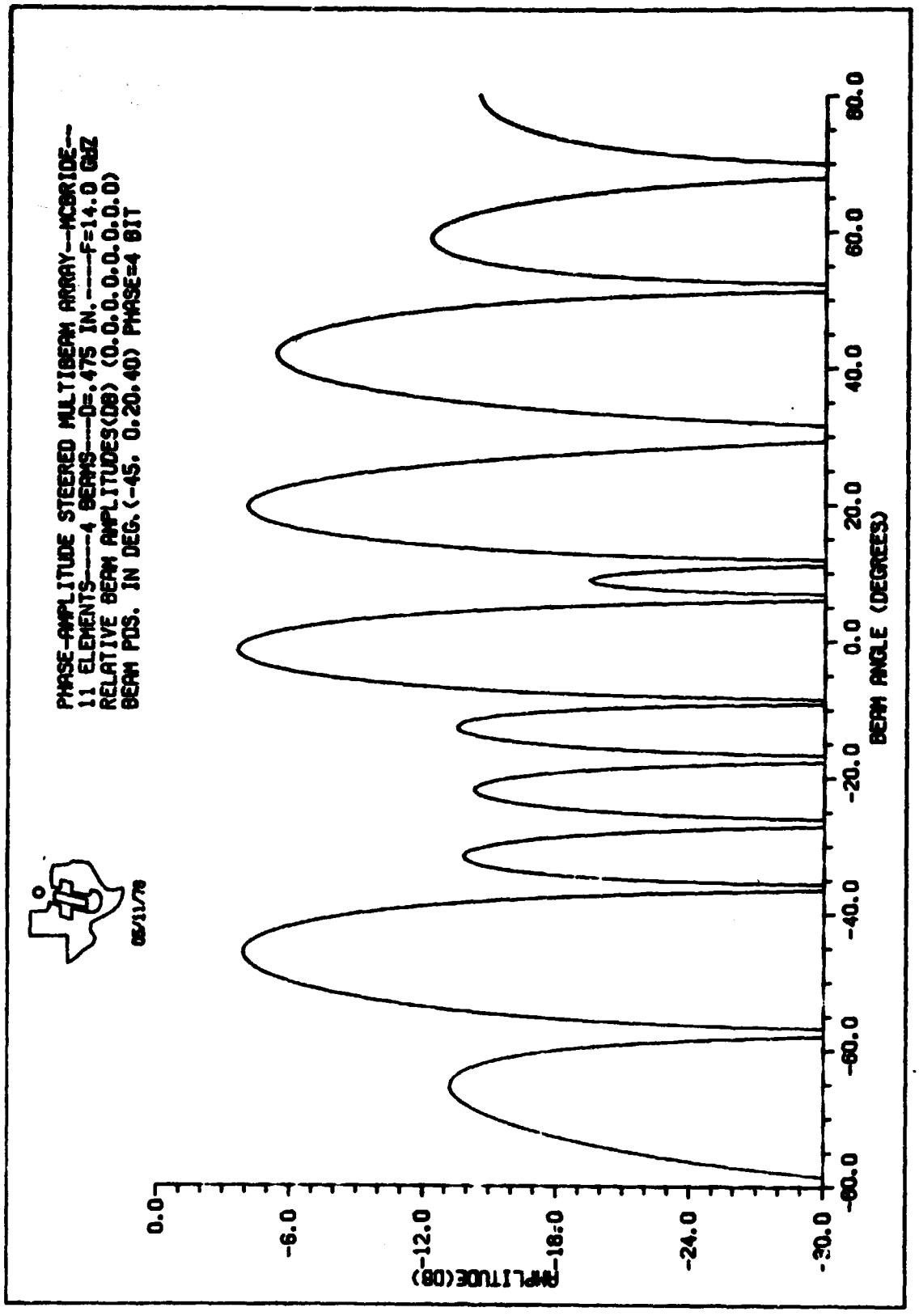

Figure 5-24. Phase-Amplitude Steered Multibeam Array Pattern Case 22

217559

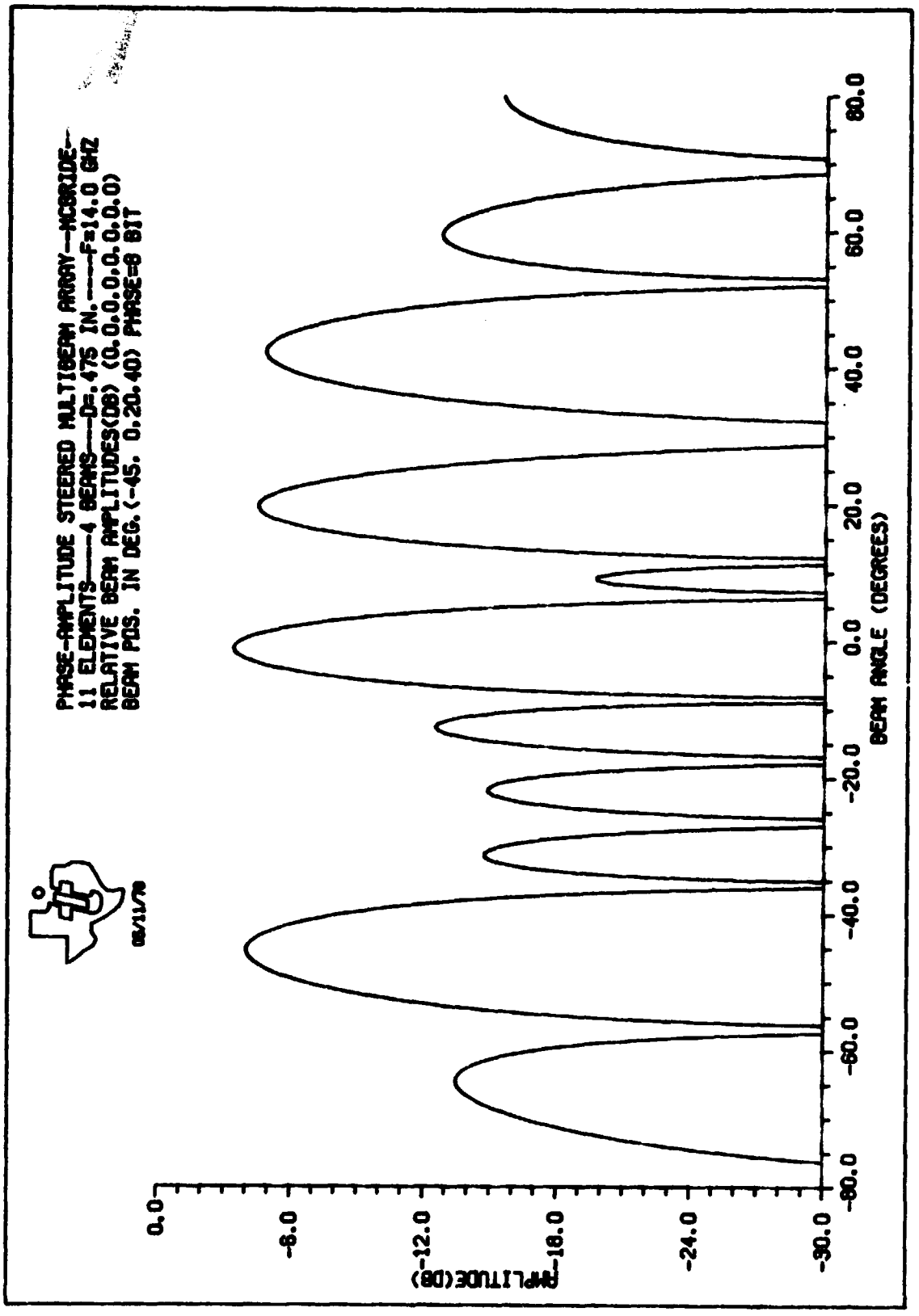

Figure 5-25. Phase-Amplitude Steered Multibeam Array Pattern Case 23

217560

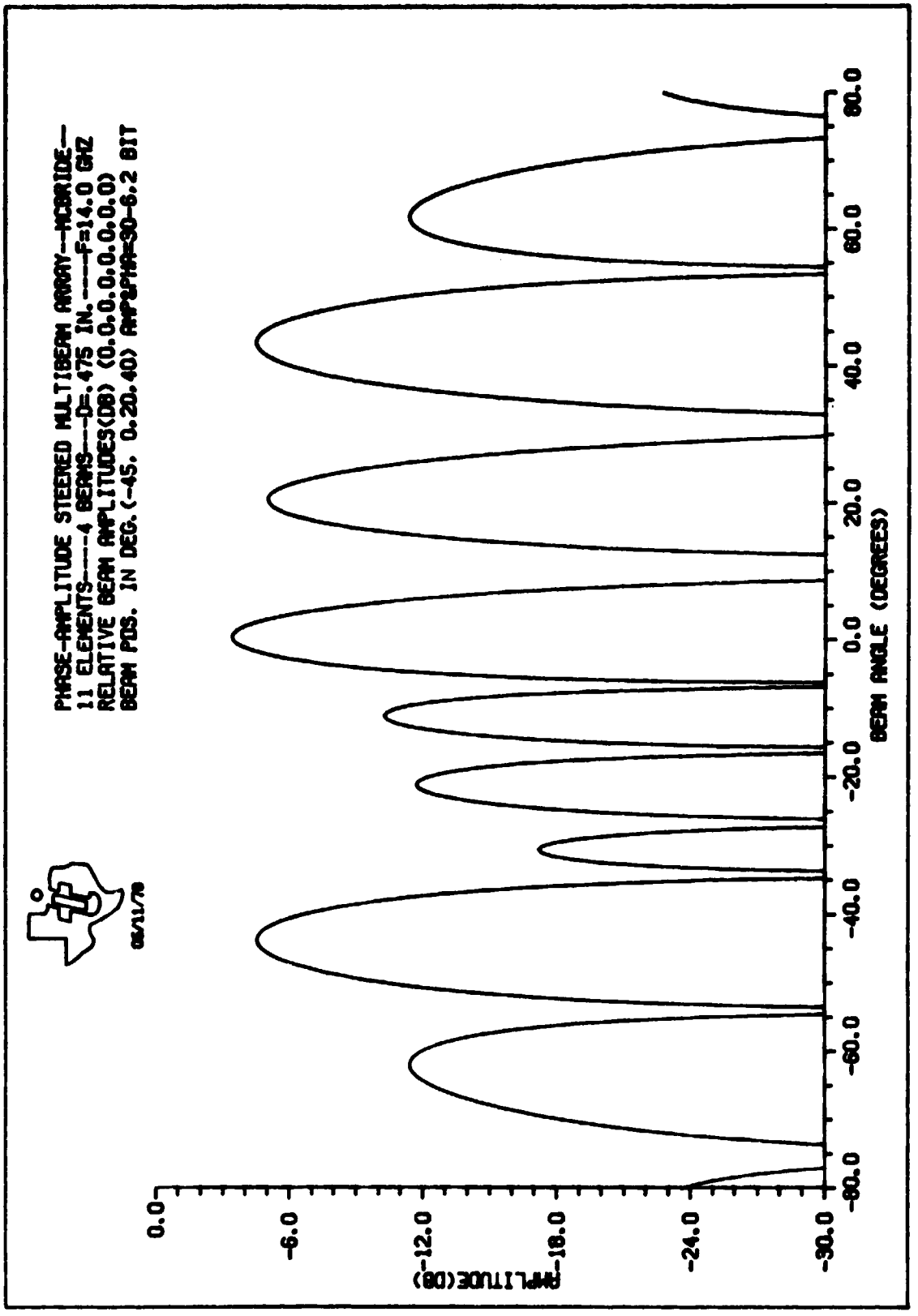

Figure 5-26. Phase-Amplitude Steered Multibeam Array Pattern Case 24

217561

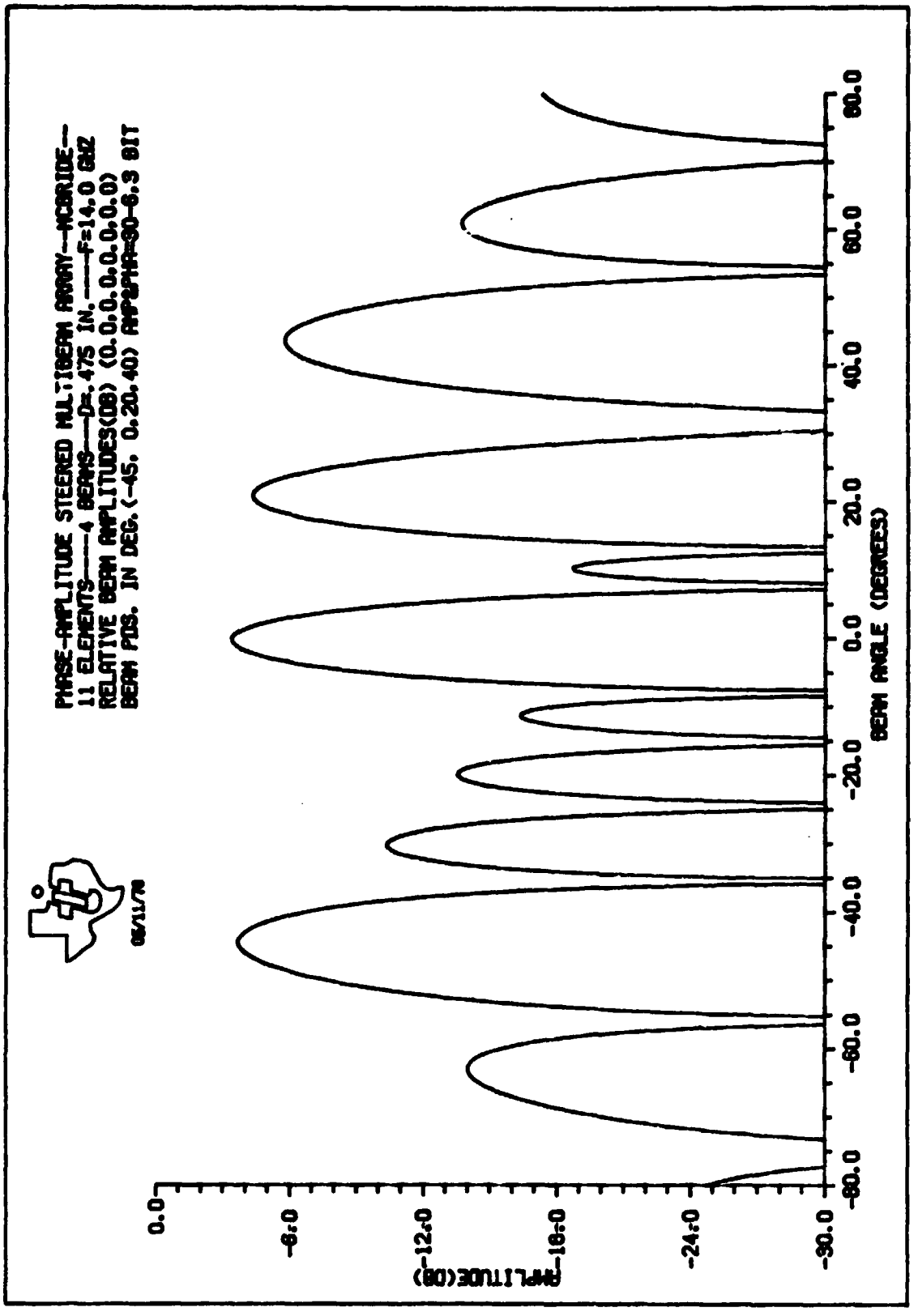

Figure 5-27. Phase-Amplitude Steered Multibeam Array Pattern Case 25

217562

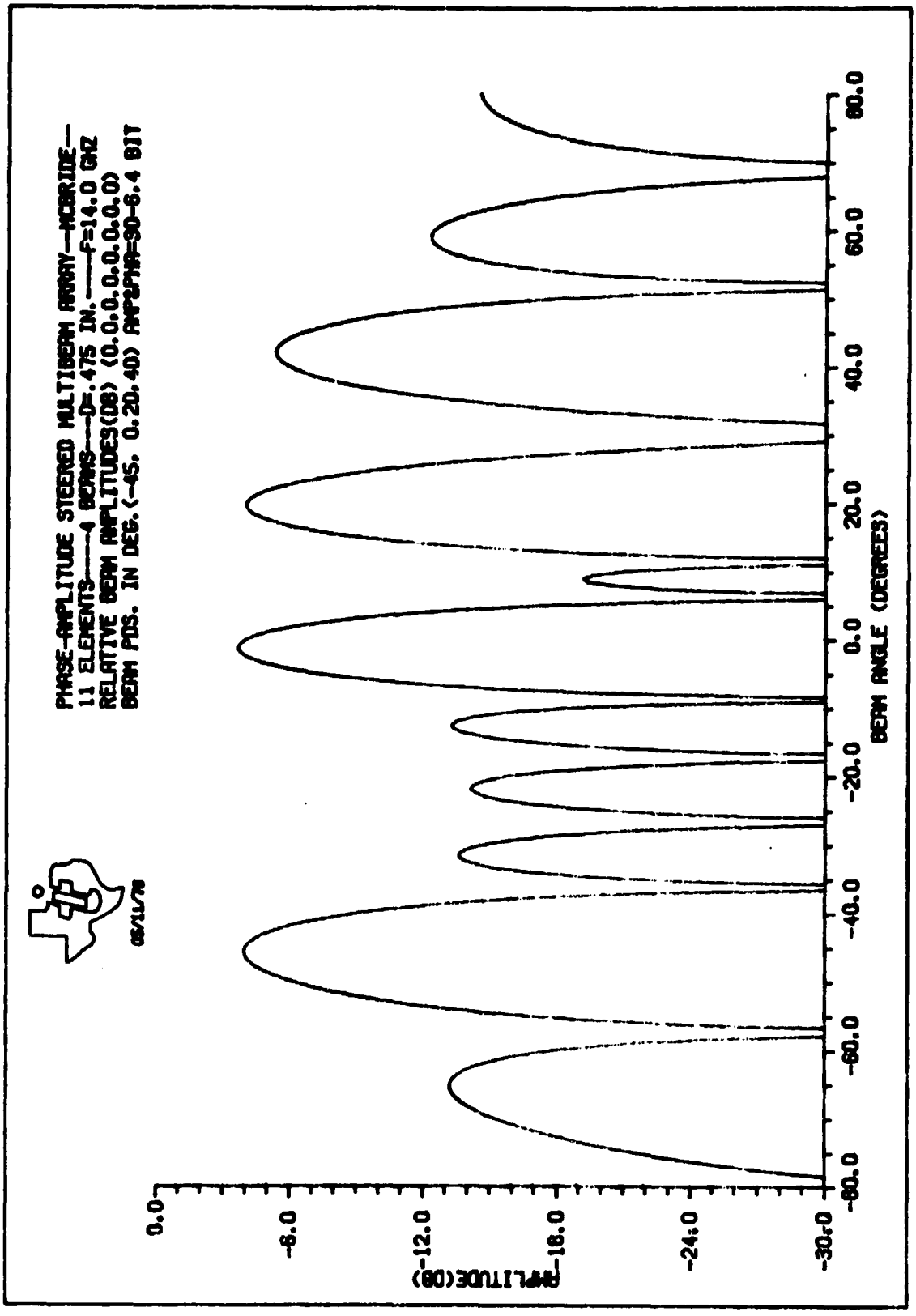

Figure 5-28. Phase-Amplitude Steered Multibeam Array Pattern Case 26

217563

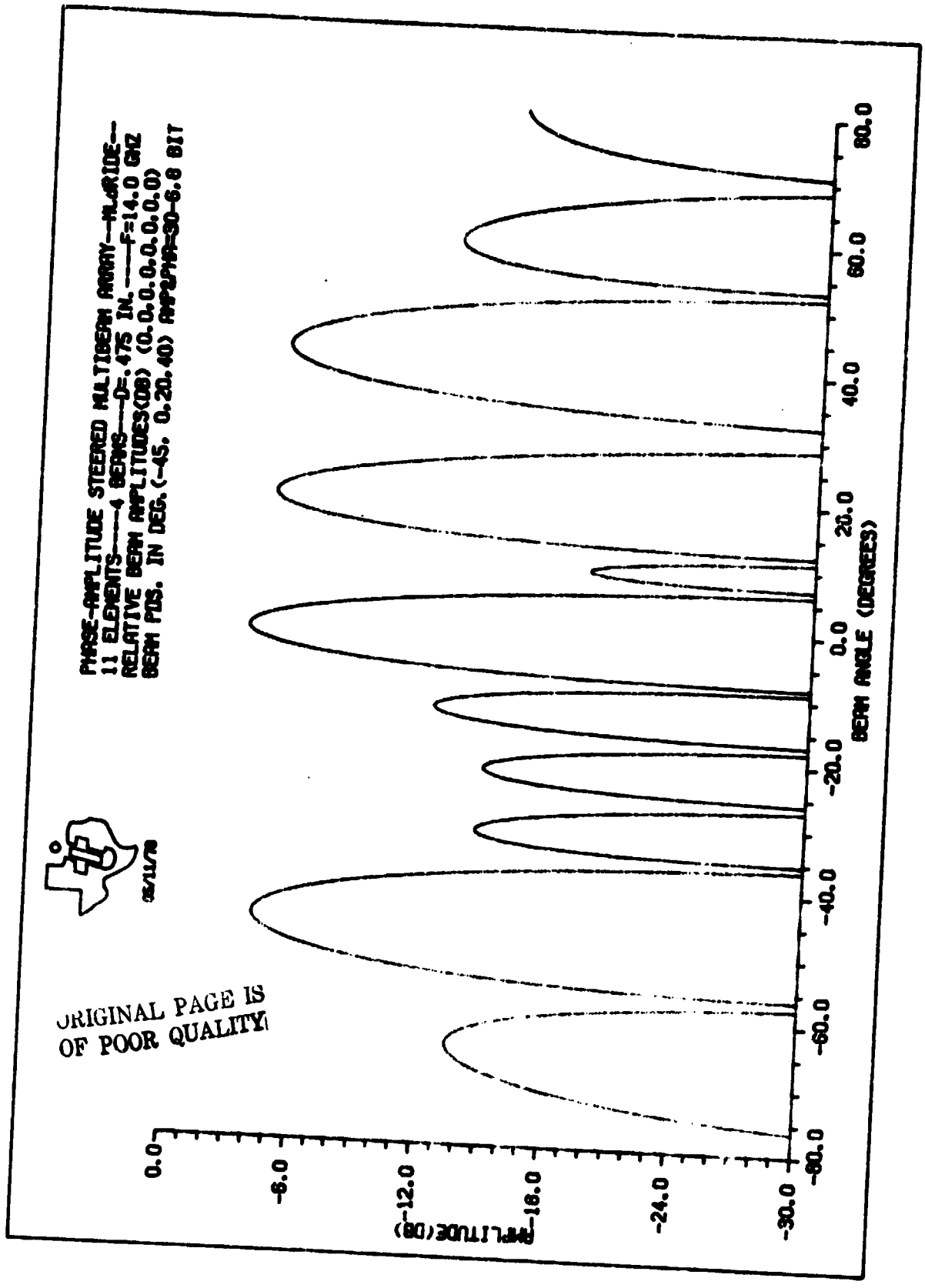

Figure 5-29. Phase-Amplitude Steered Multibeam Array Pattern Case 27

217564

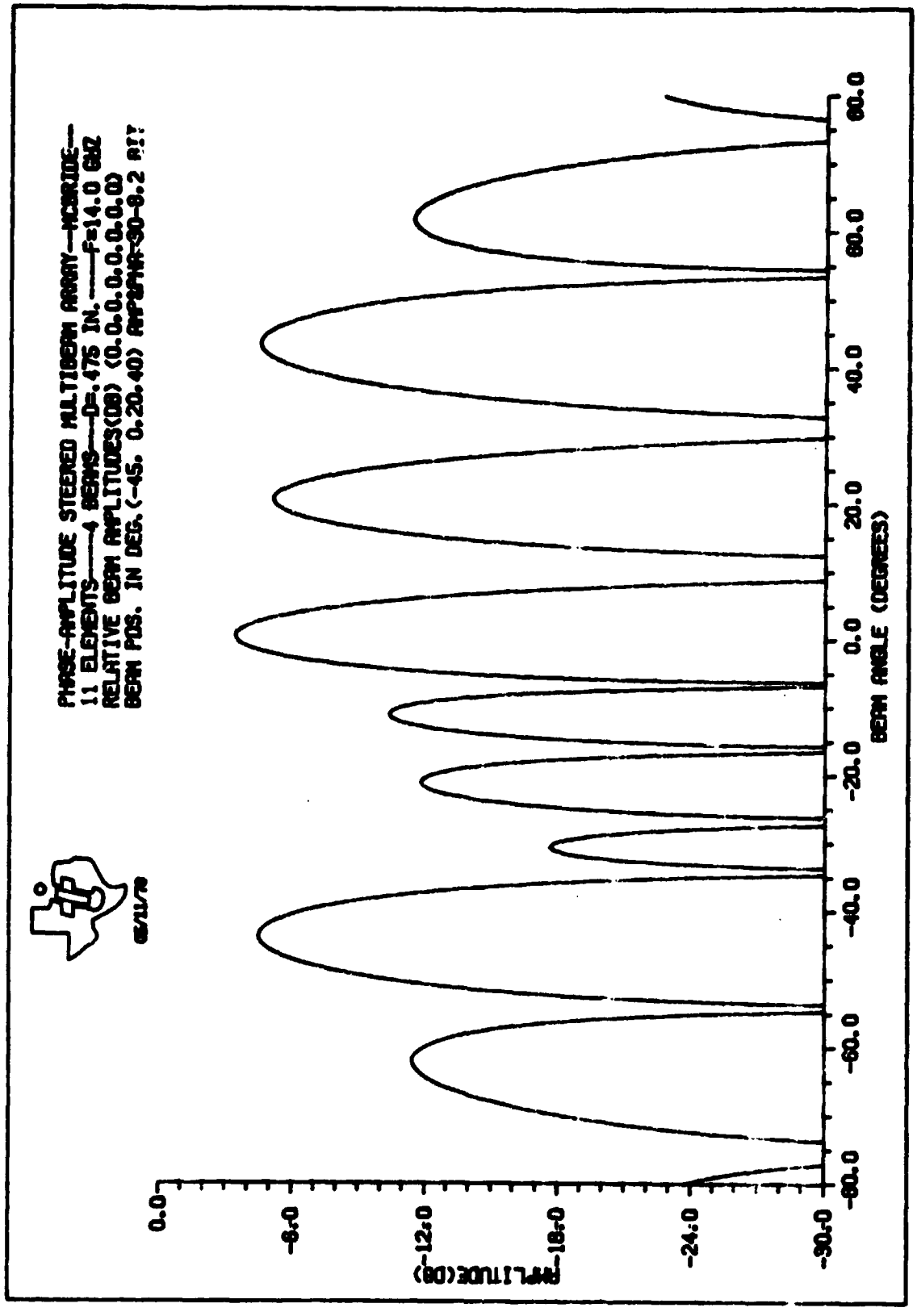

Figure 5-30. Phase-Amplitude Steered Multibeam Array Pattern Case 28

217565

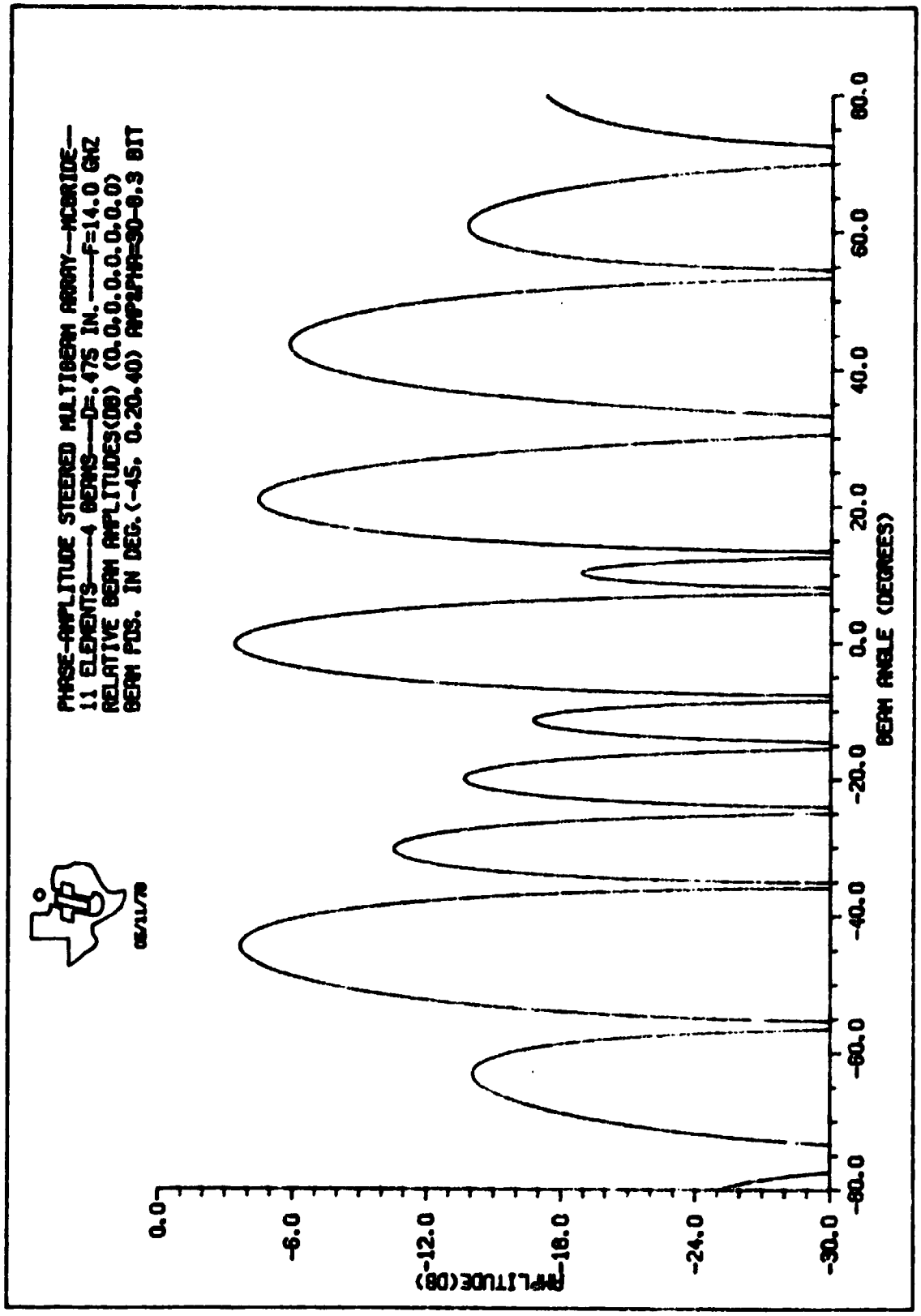

Figure 5-31. Phase-Amplitude Steered Multibeam Array Pattern Case 29

217566

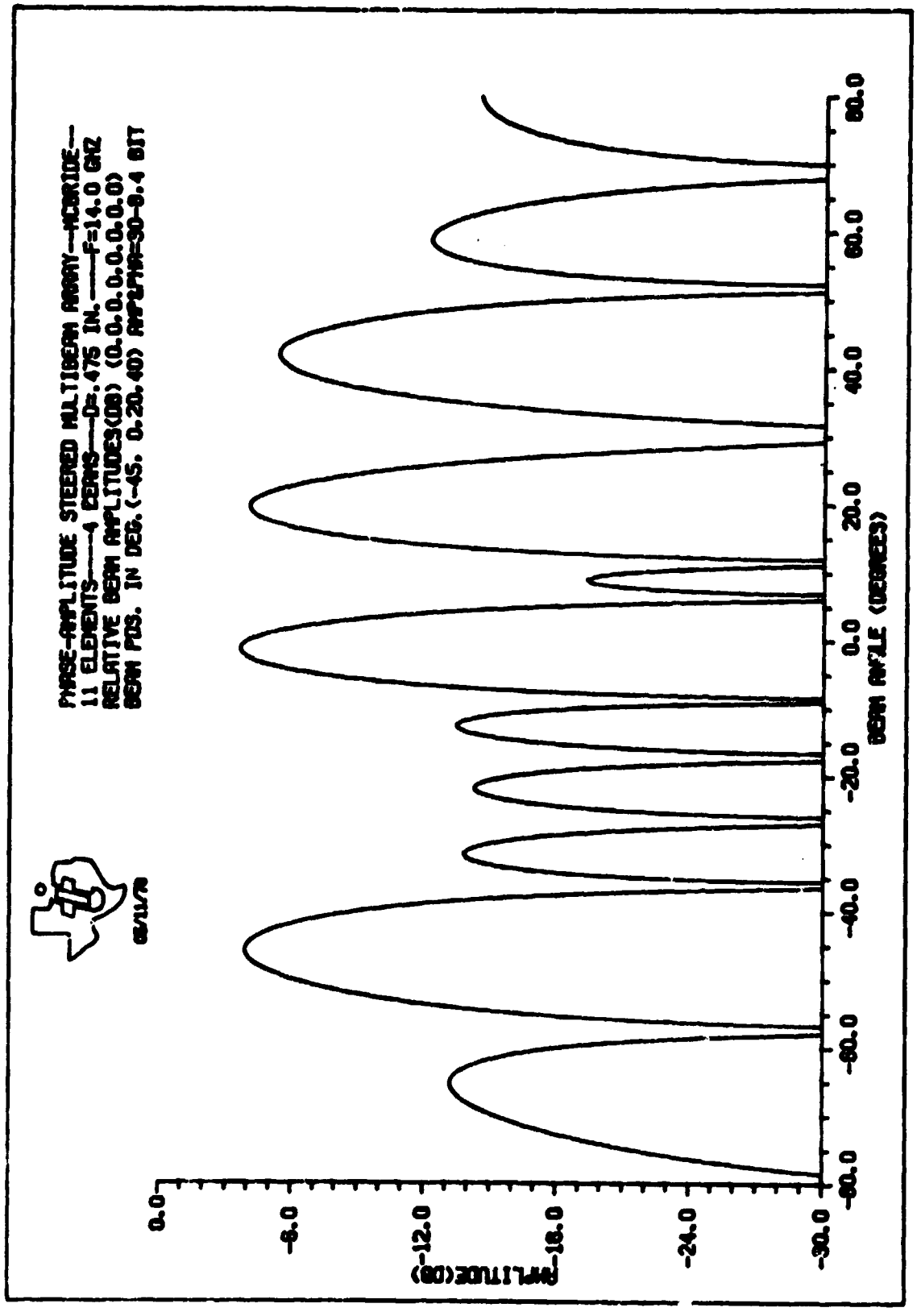

Figure 5-32. Phase-Amplitude Steered Multibeam Array Pattern Case 30

217567

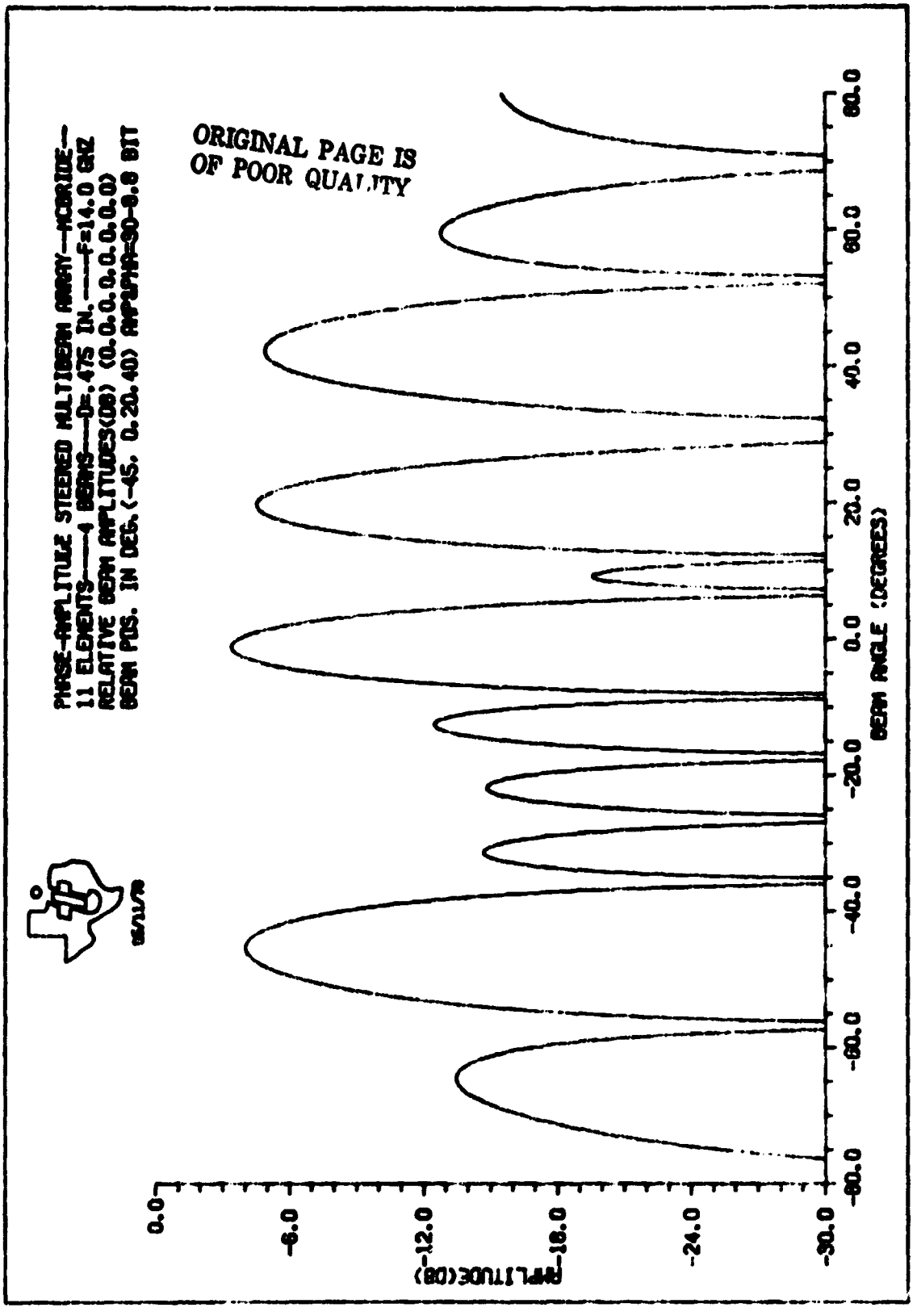

Figure 5-33. Phase-Amplitude Steered Multibeam Array Pattern Case 31

217568

Implementation of the BSC should be made with low-power IC technologies wherever possible to minimize power consumption. MSI and LSI devices could be used extensively to reduce size and complexity of the BSC.

The BSC to control the beam pointing would be required to decode the input for the selected direction and generate the necessary control signals to the switching network. Codes for the set beam directions would be stored in memory and called as necessary.

C. MECHANICAL CONFIGURATION OF PHASE-AMPLITUDE STEERED MULTIBEAM ARRAY

1. General

The phase-amplitude steered array is attractive because of its simplicity when compared to other simultaneous four-beam array concepts available to the design engineer. Most of these concepts vary little in actual aperture overall surface area, but do vary quite significantly in the volume of the active elements and supportive switching equipment. When viewed from its total system equipment volume and complexity, this multiple-beam steering concept is very attractive. A drawing of the system is shown in Figure 5-34. The complete transmit and receive array incorporates a volume of only 0.1 cubic meter and weighs 27.0 kilograms. This volume and weight include the transmit and receive functions in separate antenna apertures shown in the figure. The major difference between the transmit and receive apertures is that the modules of the receive aperture contain low-noise amplifiers in place of the power amplifiers. In addition, a low-noise amplifier is substituted for the TWT at the 1-to-4 divider antenna output. Element spacing is shown in Figure 5-35 for the receive and transmit arrays. Because of power dissipation in the power amplifiers, coupled with the closer element spacing in the transmit antenna aperture, the removal of the dissipated heat becomes a prime design consideration.

The receive and transmit antennas incorporate 96 elements each. Element interconnection is accomplished through the use of a multilayer printed circuit board (PCB) for module control functions and a 1:96 waveguide power divider for RF distribution. A cross-sectional view of the transmit antenna, depicting the interrelationship of these components, is shown in Figure 5-36. Only one of the 96 active elements is depicted. Each element is removable from the front (aperture end) of the antenna after the radome/polarizer is removed. Control and RF interconnects are aligned at assembly to allow installation and removal of the elements.

2. Array Element

The individual array aperture module or element incorporates six discrete electrical activities at the antenna "front end." The module height and width are limited by the element spacing which necessitates a long package, over 20 centimeters, to incorporate all the necessary functions in the aperture. Besides the radiating dipole, the module incorporates the power amplifier or low-noise amplifier, attenuator, phase shifter, isolator, and a cavity filter. Figure 5-37 shows the physical relationship of the functions in the module. As can be deduced from the figure, there are two microstrip packages separated by the cavity filter. The front package encloses the isolator, while the back microstrip section encloses the power amplifier or the low-noise amplifier, attenuator, and the phase shifter. Microstrip-to-waveguide transitions are designed into the module at both ends of the filter. Behind the phase shifter, the module includes an

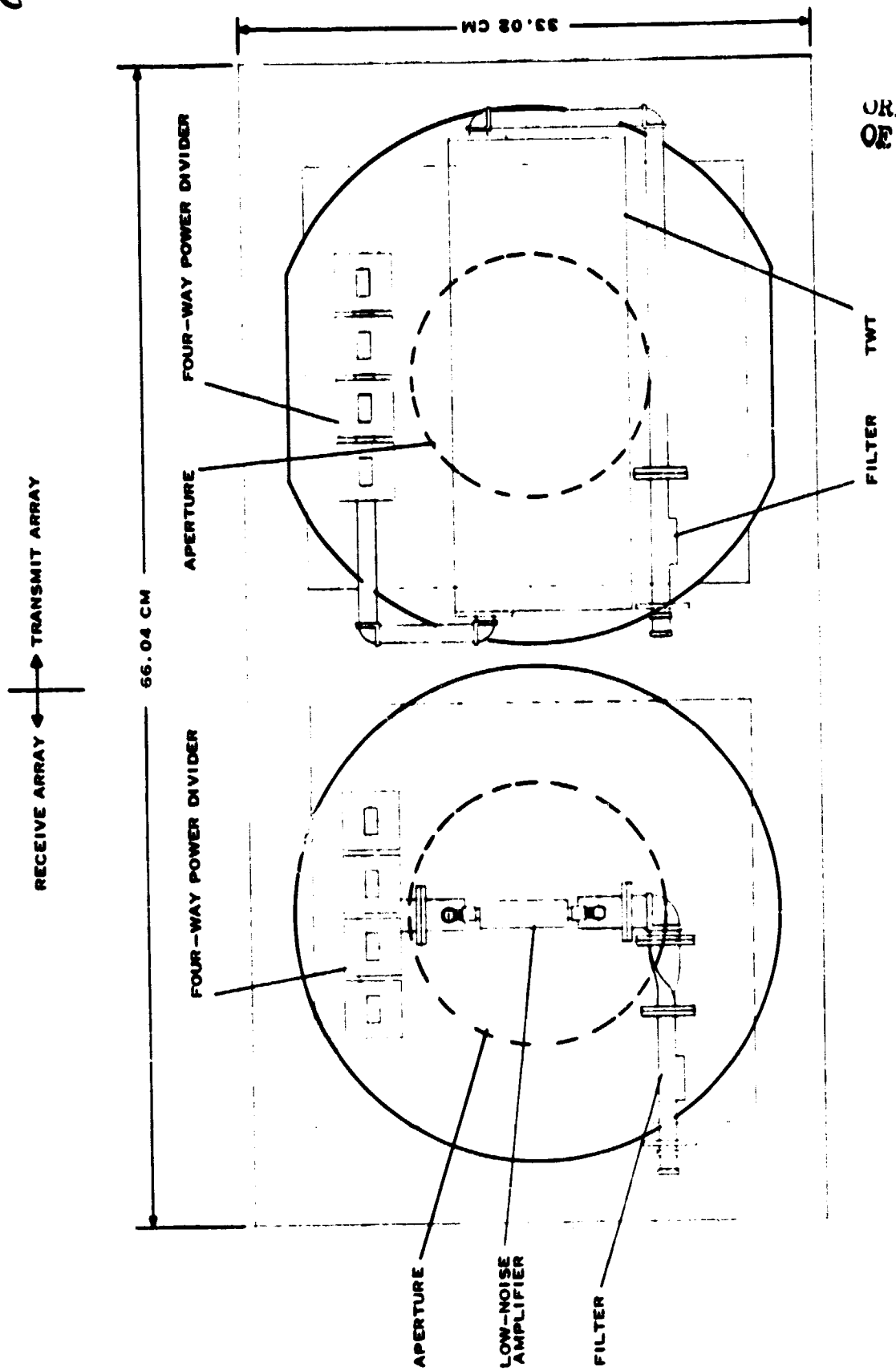

Figure 5-34. Phase-Amplitude Steered Array (Back View)

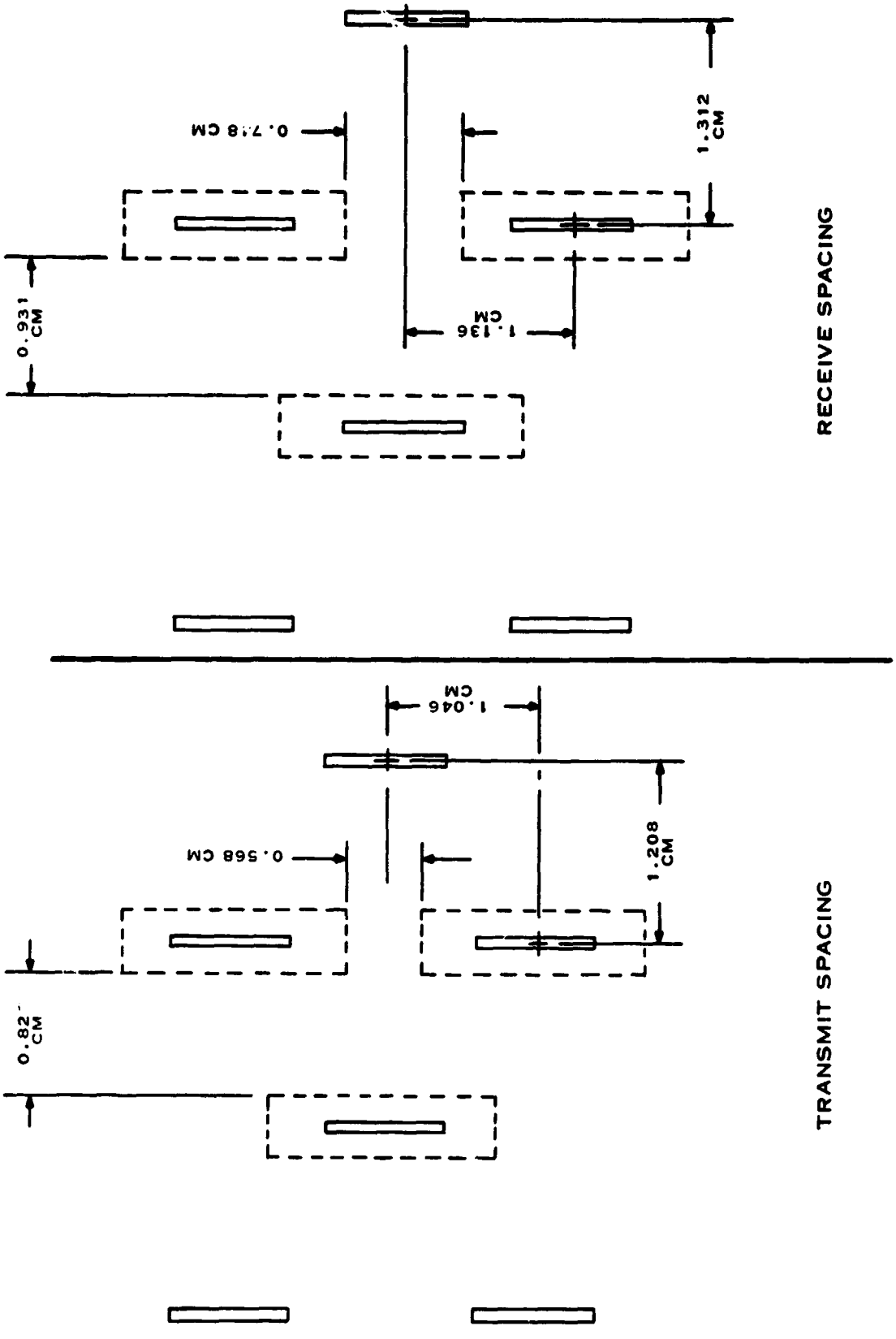

Figure 5-35. Element Spacing for Receive and Transmit Arrays

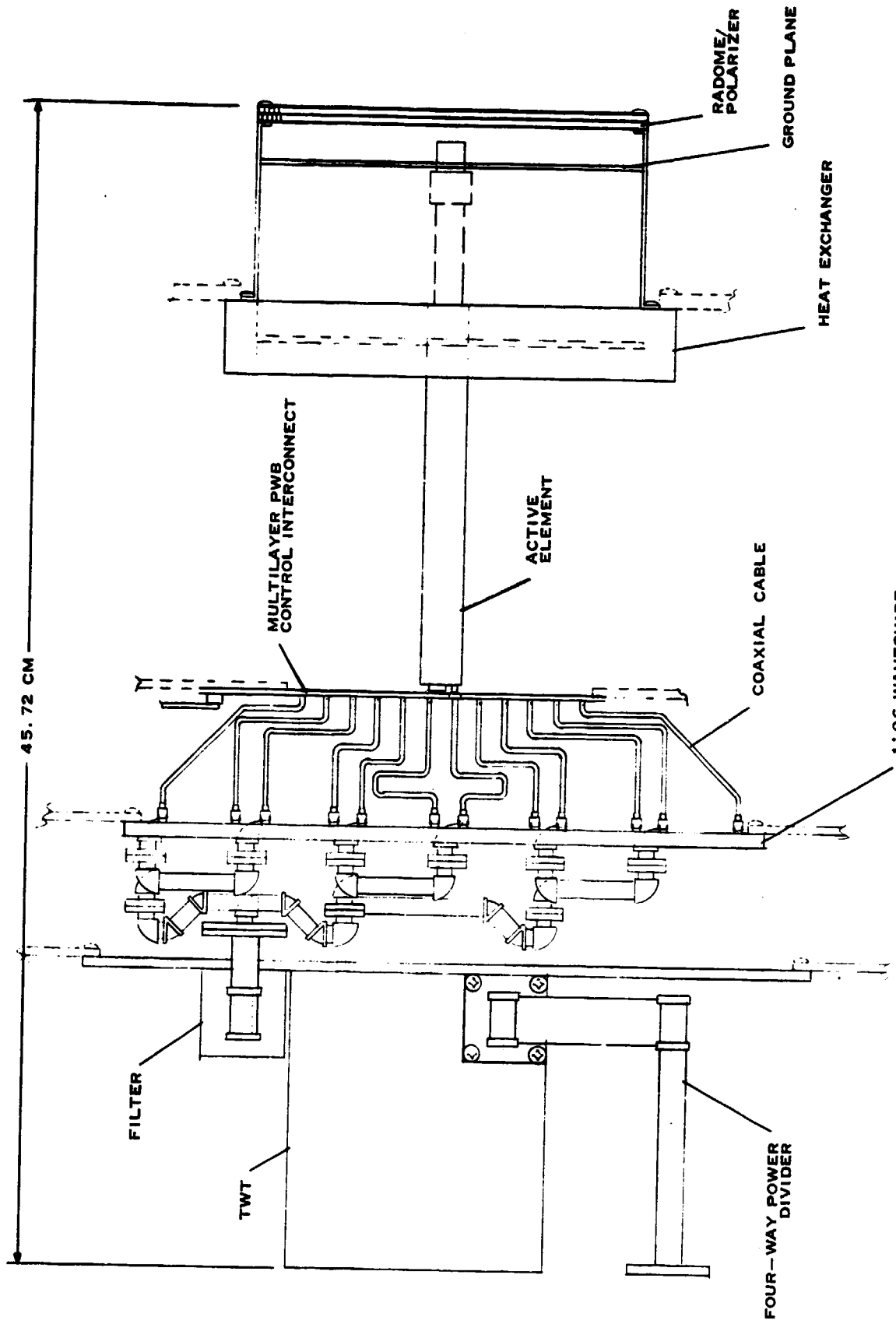

Figure 5-36. Transmit Phase-Amplitude Steered Array (Side View)

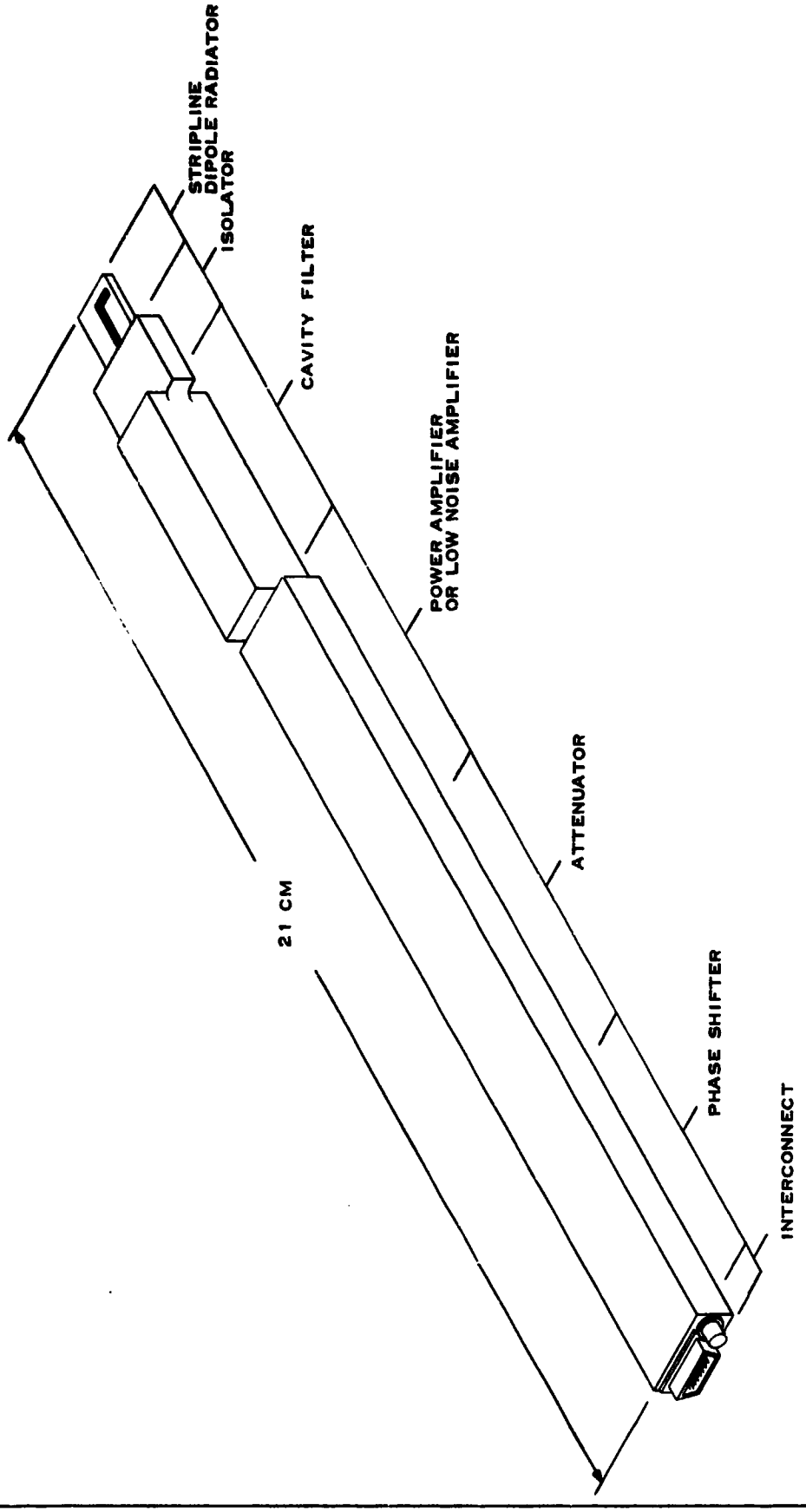

Figure 5-37. Phase-Amplitude Steered Array Element

interconnect section which includes a single plug-in RF interconnect and a power and control line multipin connector. The module is hermetically sealed to ensure reliable operation of the system. Induction soldering techniques are used to seal the individual modules after test.

3. Antenna Aperture

As stated previously, the antenna array modules are plug-in type design and can be removed after removing the faceplate. The faceplate and the modules behind the faceplate are shown in Figure 5-38. The configuration shown has a total aperture diameter of 13.7 centimeters and is the transmit antenna. The receive aperture diameter is slightly larger at 14.7 centimeters.

4. RF Interconnect

The RF interconnect of the antenna modules starts at the four-way power divider shown in Figures 5-34 and 5-35 and culminates at the individual aperture modules. The 1-to-96 power divider shown in Figure 5-39 is fabricated from dipbrazed waveguide sections and a bonded multiple four-way divider. The entire assembly is compact and weighs a little over 1 pound. Waveguide-to-coaxial transitions are designed into the assembly to form the interface for the coaxial cable used to interconnect the individual module with this power divider.

5. Cooling System

Power dissipation in the receive module is relatively low, while dissipation in the transmit module is expected to be about 3 watts. Because of this heat flux and the desire to have a relatively small temperature gradient across the aperture surface, a liquid coolant circuit would be required in the vicinity of the power amplifier function in the aperture module. The coolant circuit input flow rates and temperatures would be designed to keep the sensitive components in each module within some temperature tolerance. Because of the very close spacing, it is doubtful that convection heat transfer methods can be used to sink the heat to the outside circumference of the antenna aperture.

D. LOW-NOISE AMPLIFIER

The simultaneous multiple beam capability on receive will increase the loss prior to the receiver. This loss will decrease the signal-to-noise level at the receiver and degrade system performance. To retain the desired system performance, it will be necessary to utilize low-noise amplification at the element level.

Recent advances in device development permit the successful design of a J-band GaAs FET low-noise amplifier. New devices with 0.5 micron gate length can provide maximum available gain of 6 to 8 dB at 15 GHz. This advantage of higher available gain per transistor allows circuit design tradeoffs in favor of amplifier noise figure and reduces the number of devices necessary to construct the total amplifier. A three to four stage amplifier can be designed, using available devices, to give a nominal 20-dB gain with a noise figure of less than 5 dB. This would allow adequate signal-to-noise levels at the receiver. During the preliminary design, the amount of gain and noise figure of the amplifier can be determined. The circuit design would be carried out in microstrip to permit the necessary circuit size reduction.

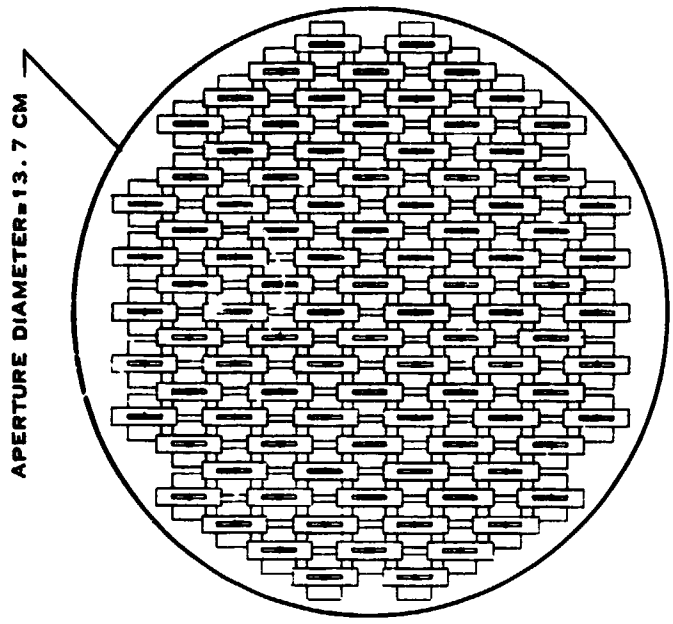

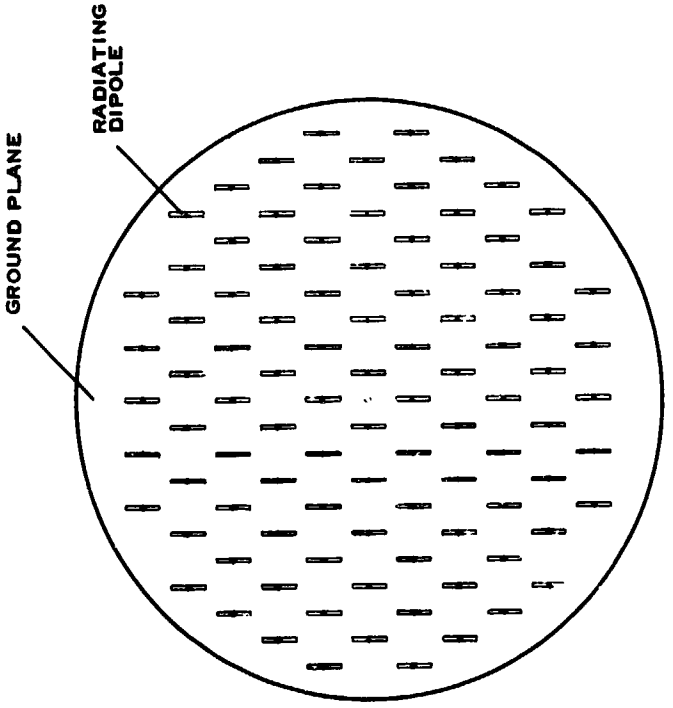

Figure 5-38. Phase-Amplitude Steered Array Transmit Aperture

217573

ORIGINAL PAGE IS
OF POOR QUALITY

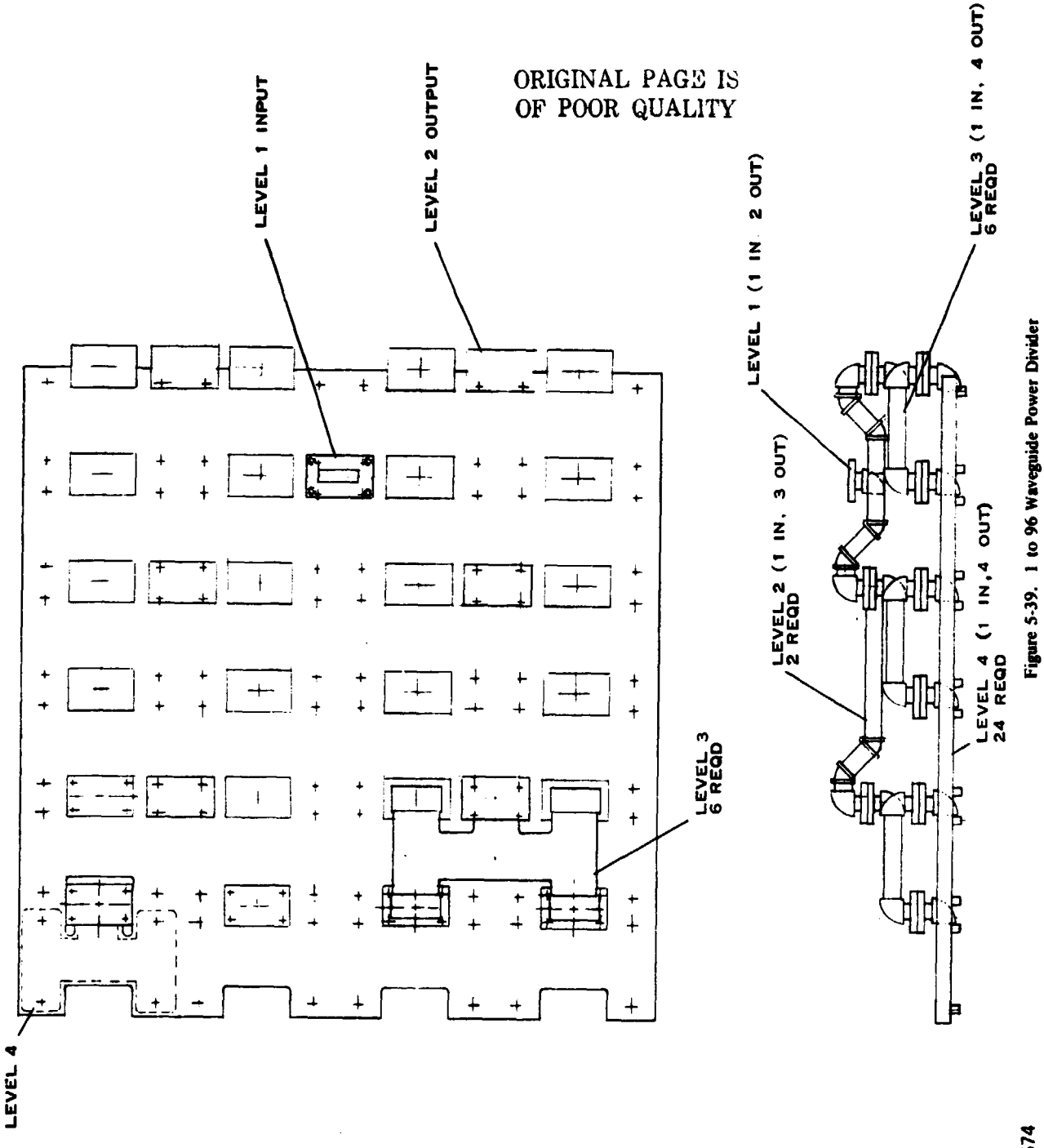

Figure 5-39. 1 to 96 Waveguide Power Divider

E. POWER AMPLIFIER

As the number of simultaneous transmit beams increases, the loss in the transmit RF feed network also increases. It is necessary to use power amplifiers in the feed network to counter this increased loss. At present, the power transistor appears to have an advantage over other approaches for this application, with the GaAs FETs showing considerable promise. Under IR&D, power FETs have been developed for J-band applications at Texas Instruments. To date, 3 watts at 15 GHz has been achieved and further work is expected to yield 5 watts.

Key to the development of GaAs FETs at Texas Instruments has been the availability of an established electron beam lithography capability. More than 10 years have been spent in developing the present Texas Instruments E-beam system, which is specifically designed for computer-controlled, direct-scanned beam lithography of semiconductor devices and is not a converted scanning electron microscope. Recently, Texas Instruments has begun development of x-ray lithography which may be important in the future development of GaAs FETs.

SECTION VI
SUMMARY AND CONCLUSIONS

This study program has addressed the design of an array to provide simultaneous, multiple beams that are independently steerable. Four transmit beams in the frequency range of 14.6 to 15.2 GHz and four receive beams in the frequency range of 13.4 to 14.0 GHz are required for this spaceborne communication application. Each beam is required to have individual gain control and be capable of achieving a 24-dB gain level.

Several multiple-beam approaches were investigated. These included phased arrays, Butler matrices, and Luneberg lenses. No active circuits were included in these configurations. All of the above approaches became large and showed no promise of meeting the size and weight requirements. This approach was abandoned for antenna configurations with active circuits.

Low-noise amplifiers were placed with every element on receive and GaAs FET power amplifiers were considered on transmit. The different approchaes analyzed were a phase array, a Butler matrix feed, and a phase-amplitude steered multibeam array. The phase-amplitude steered multibeam array was selected as the preferred approach.

This array uses an attenuator and a phase shifter with every element. The aperture excitation necessary to form the four beams is calculated and then placed across the array using these devices. Pattern analysis was performed for two-beam and four-beam cases with numerous patterns being presented. Parameter evaluation shown includes pointing accuracy and beam shape, sidelobe characteristics, gain control, and beam normalization. It was demonstrated that a 4-bit phase shifter and a 6-bit, 30-dB attenuator were sufficient to achieve adequate pattern performance. The phase-amplitude steered multibeam array offers the flexibility of 1 to 4 beams with an increase in gain of 6 dB if only one beam is selected. Since detailed system performance requirements were not available, a final phasing algorithm could not be developed for this approach. This approach has numerous advantages and appears to be a promising multibeam approach. When more complete mission requirements are established, a more detailed design and analysis should be completed on this multibeam array.

APPENDIX A
DEFINITION OF SYMBOLS

APPENDIX A
DEFINITION OF SYMBOLS

D Diameter of Luneberg lens

D_λ Diameter of Luneberg lens in wavelengths

θ_3 Lens pattern beamwidth in degrees

P Lens pattern directivity

P_{dB} Lens pattern directivity in decibels

θ_b Angle of beam separation in degrees

Ω_s Scan volume

Ω_b Beam angular volume (not 3-dB volume)

N_b Number of beams

L_s Switch matrix loss in decibels

L_o Losses other than switch matrix losses in decibels

C Beam crossover level in decibels

d_λ Distance between feeds in wavelengths

G_{dB} Lens pattern gain in decibels

APPENDIX B
LUNEBERG LENS ESTIMATES

APPENDIX B
LUNEBERG LENS ESTIMATES

In this appendix equations are formulated to perform a parametric analysis of the Luneberg lens antenna. The analysis determines the beam spacing, number of beams, feed spacing, crossover level, beamwidth, and losses for antenna configurations as a function of lens diameter. The gain is held constant at 24.0 dB. Using the notation of Appendix A the following estimates can be made. We assume that the lens aperture distribution is uniform in amplitude and phase when no blockage is present. The uniform amplitude assumption is compatible with a $\cos\theta$ feed element pattern and the lens focusing yielding a $\sec\theta$ factor. The uniform phase is a natural result of the lens.

Then,

$$\theta_3 = 59/D_\lambda \text{ (degrees)}$$

$$P = 41253/(\theta_3)^2$$

$$= 11.85\ D_\lambda{}^2$$

$$P_{dB} = 10.74 + 20 \log_{10} D_\lambda$$

$$\Omega_s = 2\pi(1-\cos 60^\circ)$$

$$\Omega_b = 2\pi[1-\cos(\theta_b/2)]$$

$$N_b = \Omega_s/\Omega_b$$

$$\cong (114.6/\theta_b)^2 \ (\theta_b \text{ in degrees})$$

A switch matrix feeding the lens represents a considerable loss of power. The switch matrix is a single pole N_b throw switch. Thus, there are approximately $\log_2 N_b$ layers of single pole double throw switches each with 0.8 dB loss. The total insertion loss for the switch matrix is approximately

$$L_s = 0.8 \log_2 N_b$$

$$= 2.66 \log_{10} N_b$$

$$L_s = 10.94 - 5.32 \log_{10} \theta_b$$

It is clear that the number of layers must be the least integer greater than or equal to $\log_2 N_b$. In the matrix implementation, if $\log_2 N_b$ is not an integer some of the feeds may involve one less switch layer than the others. Thus, the value L_s given above is a compromise or estimate to be uniformly applied to each input feed.

In addition to the switch loss which depends upon the number of beams there are additional fixed losses. The radome/polarizer, lens, mismatch, and interconnect losses are respectively 0.3, 0.7, 0.2, and 1.5 dB. Then in the case of a single receiver channel per lens antenna (case 1) the other losses are:

$$L_0 = 2.7 \text{ dB}$$

In the case of four receiver channels per lens antenna (case 2) an additional single-pole, four-throw switch is required for each beam feed element, and

$$L_o = 4.3 \text{ dB}$$

The gain for the two cases is:

$$G_{dB} = P_{dB} - L_s - L_o$$

$$= -2.9 + 20 \log_{10} D_\lambda + 5.32 \log_{10} \theta_b \quad \text{(case 1)}$$

$$= -4.5 + 20 \log_{10} D_\lambda + 5.32 \log_{10} \theta_b \quad \text{(case 2)}$$

By requiring the gain to be 24 dB the resulting relationship between θ_b and D_λ are derived.

$$\theta_b = 10^{5.06}/D_\lambda^{3.76} \quad \text{(case 1)}$$

$$\theta_b = 10^{5.36}/D_\lambda^{3.76} \quad \text{(case 2)}$$

The beam crossover as well as the feed spacing on the sphere may be approximated by the following.

$$C = -3(\theta_b/\theta_s)^2$$

$$= -3(\theta_b D_\lambda/59)^2$$

$$d_\lambda = \theta_b D_\lambda/114.6$$

The above Luneberg lens parameters as a function of lens diameter, D_λ, are given in Table B-1 for the single beam case and in Table B-2 for the four beam case. Both tables are for lenses of 24 dB gain. However, as can be seen, not all configurations are acceptable. The beam crossover levels are too low for the smaller diameter lenses. A baseline lens configuration has been selected for the single beam and four beam lens antennas. The antenna parameters for these baseline configurations are shown in Table B-3. The selected configurations have been made to compromise the crossover levels and the number of beams. It may be noted that N_b in each case is a power of two but is not necessarily constrained.

TABLE B-1. SINGLE BEAM LUNEBERG LENS PARAMETERS

D_λ	θ_3	θ_b	C	N_b	L	d_λ
11.0	5.36	13.9	-20.3	68	7.6	1.34
12.0	4.92	10 1	-12.5	130	8.3	1.05
13.0	4.54	7.4	- 8.1	237	9.0	0.84
14.0	4.21	5.6	- 5.4	414	9.7	0.69
15.0	3.93	4.3	- 3.7	696	10.3	0 *7
16.0	3.69	3.4	- 2.6	1,131	10.8	0.48
17.0	3.47	2.7	- 1.8	1,784	11.3	0.40
18.0	3.28	2.2	- 1.3	2,742	11.8	0.34

TABLE B-2. FOUR-BEAM LUNEBERG LENS PARAMETERS

D_λ	θ_3	θ_b	C	N_b	L	d_λ
14.0	4.21	11.2	21.3	104	9.7	1.37
15.0	3.93	8.7	14.6	175	10.3	1.13
16.0	3.69	6.8	10.2	284	10.8	0.95
17.0	3.47	5.4	7.3	448	11.3	0.80
18.0	3.28	4.4	5.3	689	11.8	0.69
19.0	3.11	3.6	4.0	1,034	12.3	0.59
20.0	2.95	2.9	3.0	1,521	12.8	0.51
21.0	2.81	2.4	2.3	2,195	13.2	0.45
22.0	2.68	2.1	1.8	3,114	13.6	0.39

TABLE B-3. BASELINE LUNEBERG LENS PARAMETERS

	Single Beam	Four Beams
D_λ	14.4	19.0 (wavelengths)
θ_3	4.10	3.11 (degrees)
θ_b	5.08	3.58 (degrees)
C	4.61	3.99 (dB)
N_b	512	1024
L	9.9	12.3 (dB)
d_λ	0.64	0.59 (wavelengths)